FINANCIAL AND COMPUTATIONAL MODELS IN ELECTRICITY MARKETS

A Thesis
Presented to
The Academic Faculty

by

Li Xu

In Partial Fulfillment
of the Requirements for the Degree
Doctor of Philosophy in the
School of Industrial and Systems Engineering

Georgia Institute of Technology
May, 2014

FINANCIAL AND COMPUTATIONAL MODELS IN ELECTRICITY MARKETS

Approved by:

Professor Shi-Jie Deng, Advisor
School of Industrial and Systems Engineering
Georgia Institute of Technology

Professor Andy Sun
School of Industrial and Systems Engineering
Georgia Institute of Technology

Professor Valerie M. Thomas
School of Industrial and Systems Engineering
School of Public Policy
Georgia Institute of Technology

Professor A.P. Sakis Meliopoulos
School of Electrical and Computer Engineering
Georgia Institute of Technology

Professor Steve Hackman
School of Industrial and Systems Engineering
Georgia Institute of Technology

Date Approved: March 25, 2014

ACKNOWLEDGEMENTS

I would like to express my gratitude to all individuals who have offered me generous help and insightful advice during my doctoral study at Georgia Tech.

First and foremost, I am extremely grateful to my advisor Dr. Shi-Jie Deng. He not only brought me to the journey of pursuing a Ph.D. in Industrial Engineering, but also provided me with precious opportunities to open my mind at various academic conferences and industrial workshops. I could not be more appreciative of his invaluable guidance, inspiring advice and incredible patience along the journey. Without his support and encouragement, this thesis would hardly be possible. His insights into research, attitude towards work and passion in life have influenced me signigicantly. Being his student and working with him is one of my greatest honors in my life.

Besides, I would like to thank Dr. Valerie M. Thomas, for her tremendous help and valuable suggestions to the third part of this thesis. Our research project was a memorable experience for me. I also feel fortunate to collaborate with Dr. Jingfang Huang at UNC-Chapel Hill, who motivated the first part of this thesis. I benefited a lot from his admirable deep knowledge in computational methods. Moreover, special thanks go to the other committee members: Dr. Steve Hackman, Dr. Andy Sun and Dr. A.P. Sakis Meliopoulos for their reading and comments, which make the thesis more satisfactory.

I also wish to extend my sincere thanks to Dr. Shmuel Oren and his student Dr. Anthony Papavasiliou at UC-Berkeley, for their advice and comments. I am also grateful to Dr. Aram Sogomonian at Edison Mission Energy and Dr. Sandeep Jain at UBS AG for giving me hands-on experience in electricity markets and financial markets. I am extremely thankful to the Power Systems Engineering Research Center for

its financial support during my doctoral study. I should not forget my colleagues from ISyE: Wenwei Cao, Xuefeng Gao, Jieyun Zhou, Yang Zhang, Xinyu Min, Fangfang Xiao, Zhi Han, Rensheng Zhou, Yibiao Lu, Bo Zhang and Sangho Shim. The discussions with them are essential to my thesis and research. I also wish to acknowledge my friends Mingqi Zhao, Zhenwu Shi, Xin Chen, Zhengqin Fan, Zhongyuan Yu and Mengdi Luo who always share my joy and sadness. It is a great fortune for me to have friends like them.

Finally and most importantly, my deepest appreciation goes to my parents and my girlfriend Zhen Li, for their boundless support and endless love. Thank you for giving me great confidence to succeed in my life.

TABLE OF CONTENTS

ACKNOWLEDGEMENTS . . . . . **iii**

LIST OF TABLES . . . . . **vii**

LIST OF FIGURES . . . . . **viii**

SUMMARY . . . . . **x**

I INTRODUCTION **1**

1.1 Background 1

1.2 Organization 4

II OPTIONS PRICING BY FAST TRANSFORM ALGORITHM UNDER JUMP MODELS **6**

2.1 Introduction 6

2.2 Fast Convolution Algorithm 11

2.3 Single Asset Options 15

2.3.1 Spot Price Dynamics 16

2.3.2 Barrier Options 18

2.3.3 Bermudan Options 27

2.3.4 Lookback Options 33

2.3.5 Asian Options 36

2.4 Multi-Asset Options 38

2.4.1 Fast Convolution in 2D 39

2.4.2 Bermudan Spread Options 41

2.5 Conclusion 44

III AN INCENTIVE-BASED DEMAND RESPONSE CONTRACT DESIGN FOR THERMOSTATICALLY CONTROLLED LOADS IN A SMART GRID **47**

3.1 Introduction 47

3.2 Contract Structure 52

3.3 Model Description 53

3.3.1 A Two-Stage Stochastic Programming 54
3.3.2 State-Space Representation 55
3.3.3 Model Predictive Control for TCLs 56
3.3.4 Customers' Preference and Participation 58
3.4 A Case Study 62
3.5 Conclusion 72

IV CARBON EMISSION PERMIT PRICE VOLATILITY REDUCTION VIA FINANCIAL OPTIONS 76

4.1 Introduction 76
4.2 A Two-compliance-time Model 81
4.3 Price Volatility Reduction via Different Approaches 84
4.3.1 A Safety Valve Approach 84
4.3.2 Banking and Borrowing Approach 85
4.3.3 Financial Options Approach 90
4.3.4 Financial Options in a Bankable System 98
4.4 Numerical Example 101
4.5 Conclusion 105

V CONCLUSION 107

APPENDIX A — DERIVATION OF THE CHARACTERISTIC FUNCTION OF A 2D AJD PROCESS 111

APPENDIX B — NOTATIONS AND PARAMETERS IN CHAPTER III 114

APPENDIX C — DERIVATION OF PROPOSITIONS IN CHAPTER III 119

REFERENCES 121

LIST OF TABLES

1 Comparison of Prices for a Down-and-out Put under OU Model . . . 24

2 Price of a Down-and-out Put under OU Double-Exp. Jumps 26

3 Comparison of Prices for a Bermudan Put under OU Model 30

4 Price of a Bermudan Put under Stochastic Volatility 32

5 Price of a Lookback Put under Different Lévy Models 35

6 Price of a Asian Options under Different Lévy Models 38

7 European Spread Call Option under Affine Jump Diffusion Model . . 45

8 Bermudan Spread Call Option under Affine Jump Diffusion Model . . 45

9 Thermostat Parameters 63

10 Contract Parameters 63

11 Tracking Performance (Linear) 66

12 Tracking Performance (Quadratic) 66

13 Tracking Performance (3 Contracts) 68

14 Summary of Parameters in the Numerical Example 102

15 Numerical Example of Performance of Different Price Management Approaches 103

16 A Summary Comparison of Price Management Approaches 104

LIST OF FIGURES

1 Wind Power Outputs in Western U.S. 4

2 ERCOT On Peak Electricity Prices 9

3 Changes of N_{j+1}^{-} and N_{j+1}^{+} in the Recursive Relation 14

4 Convergence of the Fast Convolution 15

5 Illustration of Fast Convolution Method for a Barrier Option in One Step 22

6 Relative Errors for a Down-and-out Put under OU Model 25

7 Relative Errors for a Down-and-out Put under OU Double-Exp. Jumps 26

8 Relative Errors for a Bermudan Put under OU Model 30

9 Relative Errors for a Bermudan Put under Stochastic Volatility . . . 32

10 Densities of the Log-returns in 1 year 34

11 Relative Errors for Lookback Options under Different Lévy Models . 35

12 Relative Errors for Asian Options 37

13 An Overview of the Model 53

14 Utility Indifference Curves 62

15 Controlled Loads v.s. Wind Power (Linear) 65

16 Controlled Loads v.s. Wind Power (Quadratic) 66

17 Controlled Loads of Two Groups 67

18 Customers Participation (Upper), Rebates to Customers/Purchasing Cost (Lower Left), and Total Cost (Lower Right) v.s. Rebate Level of Group I 70

19 Customers Participation (Upper), Rebates to Customers/Purchasing Cost (Lower Left), and Total Cost (Lower Right) v.s. Rebate Level of Group II 71

20 Customers Participation (Upper), Rebates to Customers/Purchasing Cost (Lower Left), and Total Cost (Lower Right) v.s. Set-Point Limit of Group I 73

21 Customers Participation (Upper), Rebates to Customers/Purchasing Cost (Lower Left), and Total Cost (Lower Right) v.s. Set-Point Limit of Group II 74

22 Market Equilibrium in the Base Case 83

23 Market Equilibrium in the Safety Valve Case 85

24 Market Equilibrium in the Banking Case at Time 0 (Left) and at Time 1 (Right) 87

25 Market Equilibrium in the Financial Option Case (Left) and the Combined Case (Right) 93

26 Numerical Example of Optimal Total Cost for the Entire System of Achieving Emissions Limits under Different Approaches 103

SUMMARY

The electric power industry in the United States is being transformed towards a low-carbon, clean and environmentally friendly one. The federal and state governments have been pushing forward cap-and-trade programs to reduce greenhouse gas emissions and renewable portfolio standards to increase clean energy penetration. Various types of risks associated with the newly established emission markets as well as the traditional electricity markets with emerging elements present significant new challenges to all industry participants. On the load serving entity (LSE) side, the uncertainty and intermittency of renewable energy supply resources drive the LSEs to manage customers' demand to maintain power balance in electricity markets. However, the demand itself has uncertainty (namely, volumetric risk), and this uncertainty is often positively correlated with electricity price movements (price risk). Both energy price risk and volumetric risk challenge the operational and financial success of LSEs. On the generation side, in the carbon emission markets, permit prices turn out to be volatile, bringing additional uncertainties to conventional fossil-fuel generators' operational costs. Therefore, they are seeking ways to hedge the price risks of emission permits, and for this purpose, regulators need to offer hedging mechanisms to encourage emitters' participation. In this dissertation, we contribute to the research on the design and utilization of financial contracts and pricing mechanisms for managing the demand/price risks in electricity markets and the price risks in carbon emission markets from different perspectives. This study helps to provide insights and alternatives for stakeholders to achieve financial success and to manage risks in the future electric power industry.

This dissertation contains three parts. In the first part, we study efficient computational methods for pricing complex financial options. These options include a wide variety of structured energy financial instruments such as spark-spread options, tolling contracts, and swing options, which are useful risk management tools for energy firms, such as the LSEs, to hedge against the price and demand uncertainties in electricity markets. We start with developing a generic computational framework for pricing several path-dependent options and early-exercise options under a broad class of stochastic price models. It is then extended to evaluate multi-assets options, e.g., spark-spread options, which are widely used in the electricity markets. The prices of these options are computed through evaluating a series of convolutions of a known function with the underlying price transition density function. The proposed computational scheme possesses several nice features. First, it reduces the total amount of computational work for pricing an option with multiple monitoring or exercising dates to the asymptotically optimal $\mathcal{O}(MN)$, where M is the number of monitoring or exercising dates, and N is the number of discretized sample points of the underlying price. Second, it is applicable to non-uniformly spaced grid points in computing the convolution, which provides a way to achieve exponential convergence of the option prices. We illustrate the efficiency of this algorithm via several examples covering Bermudan options, barrier options, lookback options, Asian options, and spread options under commonly assumed classes of underlying price processes.

In the second part, we present an incentive based contract design mechanism to induce demand response (DR) from thermostatically controlled loads (TCLs) as a resource to integrate intermittent power generation into a smart grid. By directly controlling customers' thermostats within their self-selected control ranges, LSEs are able to create flexible load profiles to balance the power output fluctuation of the renewable energy resources, such as wind and solar. LSEs offer an incentive compatible reward scheme specifying different levels of rebate associated with different set-point

adjustment ranges for thermostats. In the context of air-conditioning loads, we model customers' preferences on room temperature through a utility function which characterizes the reward and discomfort tradeoff of different choices of room temperature set-points. To find the optimal rebate levels under the output uncertainty of renewable generation, we propose a two-stage stochastic programming framework. A model predictive control (MPC) approach is applied to derive the second stage control strategy, which minimizes the total cost of meeting the shortage of renewable generation output. We illustrate the feasibility and effectiveness of the proposed mechanism through a case study with two- and three-contract offerings. We perform sensitivity analysis on how contract design parameters affect the customers' rebate subscription distributions, as well as the lump sum payments to customers, and the avoided costs in wholesale markets. We show that our mechanism provides a viable approach for LSEs to price customers' discomfort and achieve demand side flexibility in absorbing the variability of renewable energy supplies.

In the third part, we analyze the price volatility mitigation issue in carbon emission markets. We develop a stylized model to investigate the impact of financial options on reducing carbon permit price volatility under a cap-and-trade system. The existence of an option market provides a mechanism to hedge the uncertainty of future spot prices and is a stimulus for investment in carbon emission abatement technologies. We show that both the spot price level and the price volatility of carbon permits can be reduced via the trading of properly designed financial options, while achieving the emission reduction target. We also show that introducing carbon permit options in an environment allowing carbon permit to be banked makes more effective and economically efficient risk management in carbon permit trading.

CHAPTER I

INTRODUCTION

1.1 Background

In the process of restructuring the electric power industries, electricity markets have been established in many countries and regions around the world. In the United States, federal and state governments aim to create a clean and sustainable energy environment in the next 20 years.

Fox-Penner and Bishop [46], and Lovins [66] point out several major trends happening towards the future electricity markets in the U.S. First, global climate change drives significant transformations in the electricity markets. The regulators propose to handle the environmental issues via different approaches, including reduction of greenhouse gas emissions by cap-and-trade programs, acceleration of renewable energy integration, as well as development of plug-in hybrid electric vehicles. Regional Greenhouse Gas Initiative (RGGI) has been implemented in ten U.S. states to reduce SO_2 and NO_x [75]. In 2013, California became the first state in the U.S. to start a carbon cap-and-trade program to reduce CO_2 emissions, which provides valuable experiences to develop a model for the entire country. The design of such a cap-and-trade program remains experimental and needs investigation.

On the adoption of renewable energy, it accounts for 12% of the electricity production in the U.S. in 2012. California is a leading state and around 20% of California's electricity comes from renewable sources. The renewable energy production grew 45% from 357.65 TWh in 2005 to 520.07 TWh in 2011, and will continue to grow to reach 25% target of the total electricity production in 2025. Among renewable sources, the installed capacity of wind power grew 17% in 2011, to 47 GW and is estimated to

reach roughly 300 GW by 2030 [38]. This fast growth in renewable energy generation poses new challenges to load serving entities (LSEs) in managing the variable and intermittent resources.

Another trend is the increase of energy efficiency and the adoption of smart grid technologies. In the process of transforming the current power systems into smart grids, advanced digital control, sensoring, and communications technologies are deployed in the power grids, which enables LSEs to monitor, analyze, control, and repair the grid much more efficiently than ever before. The smart grid technologies enhance the interaction between LSEs and customers. They allow LSEs to create more sophisticated services to customers, and meanwhile they make customers aware of their own power usage and better respond to the price signals, etc. Moreover, the power generation system is shifted from a centralized one to distributed ones, called micro grids. They are cost effective and clean (usually renewable).

As more and more renewable energy generation resources are integrated in the power grids, the high variability and intermittency of the renewable energy supply have to be taken into account to ensure the reliability of the power systems. Figure 1 shows wind power outputs for 3 MW wind turbines in western U.S. We note that the wind power outputs could vary from 0 MW to the capacity during the same hours on different dates. The uncertainty in renewable generation makes LSEs to consider demand-side management instead of the supply side. There are various ways to manage the price risks and volumetric risks in electricity markets. Traditionally, price risks and demand-side (volumetric) risks are managed through trading financial derivatives [35]. A large variety of electricity derivatives are traded among market participants in over-the-counter (OTC) markets, including forwards, swaps, plain vanilla options, and exotic options such as spread options and swing options. The key to the effective utilization of the exotic financial instruments to meet the needs of LSEs lies in the ability to price these instrument fast and accurately. These exotic

options sometimes contain path-dependent or early exercise features, which impose computational challenges in pricing them under stochastic electricity price models.

Recently, due to the deployment of smart grid technologies, innovative electrity load management tools, for example, demand response (DR) programs, are designed to shift the load patterns of customers. They are graduately becoming another significant tool for managing demand risk. The fundamental of a DR program is to encourage the participation of end users in making their electricity consumption (namely, load) flexible at a low cost. This leads us to investigate the design of incentive payments in certain DR programs.

In terms of the design of a successful cap-and-trade program, one of the major challenges is to stablize the emission permit prices and control the price volatility. It is known in electricity markets and other commodity markets, trading financial derivatives, if well designed, provides information sharing and price discovery. This motivates us to study whether a properly designed option trading system can reduce the price volatility risks in emission markets.

In this dissertation, we address the issues pertaining to the efficient computational algorithms for pricing complex financial options which include many structured energy financial contracts and the design of economic mechanisms for managing the risks associated with increasing penetration of renewable energy resources and with trading emission allowance permits in the restructured electric power industry. To address the computational challenges arising from pricing exotic energy derivatives designed for various hedging purposes in electricity markets, we develop a generic computational framework based on a fast transform method, which attains asymptotically optimal computational complexity and exponential convergence. For the purpose of absorbing the variability and uncertainties of renewable energy resources in a smart grid, we propose an incentive-based contract design for thermostatically controlled loads (TCLs) to encourage end users' participation as a source of DR.

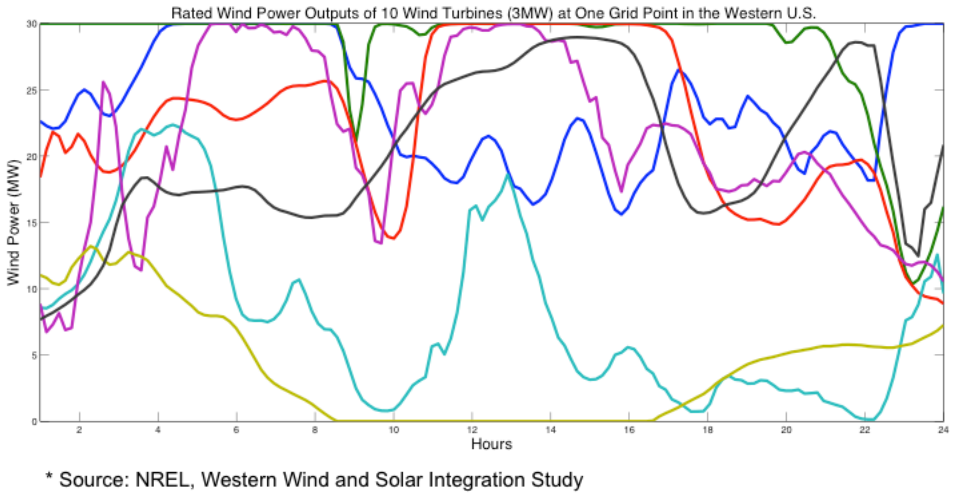

Figure 1: Wind Power Outputs in Western U.S.

Finally, we propose a market-based approach to mitigate the emission permit price risks faced by generation companies in a cap-and-trade system. Through a stylized economic model, we illustrate that the trading of properly designed financial options on emission permits reduces permit price volatility and the total emission reduction cost.

1.2 Organization

The dissertation is organized as follows. In Chapter 2, we propose a computational framework based on fast convolution for option pricing. It is applied to discretely monitored path-dependent options and discretely exercisable Bermudan options on single asset under a broad class of stochastic price models. The pricing scheme is then extended to evaluate multi-assets options with path-dependent or discretely exercisable features. We show the proposed convolution algorithm has computational complexity $\mathcal{O}(N)$, where N is the number of discretized price levels in pricing, and it works well on non-uniform grids to achieve exponential convergence.

In Chapter 3, we present an incentive based contract design mechanism to induce demand response from thermostatically controlled loads (TCLs) as a resource to integrate intermittent power generation into a smart grid. To find the optimal contract design, we propose a two-stage stochastic programming framework. A model predictive control (MPC) approach is applied to derive the second stage control strategy, which minimizes the total cost of meeting the shortage of renewable generation output. We show that our mechanism provides a viable approach for LSEs to price customers' discomfort and achieve demand side flexibility in absorbing the variability of renewable energy supplies.

In Chapter 4, we develop a stylized model to investigate the impact of financial options on reducing carbon permit price volatility under a cap-and-trade system. By analyzing the demand and supply in the cabon emission market, we show that both the spot price level and the price volatility of carbon permits can be reduced via the trading of properly designed financial options, while achieving the emission reduction target. We also compare financial options with other methods including bankable permits and safety valve in managing carbon emission permit price volatility. We conclude the dissertation in Chapter 5.

CHAPTER II

OPTIONS PRICING BY FAST TRANSFORM ALGORITHM UNDER JUMP MODELS

2.1 Introduction

Options are among the most widely traded financial derivatives across all financial markets. Option holders have the rights, but not the obligations, to buy or sell some assets on a specified date at a specified price. The asset on which an option is written is known as the underlying asset. The predetermined trading date of an option is called the maturity date or the expiry date, usually denoted by T. And the price at which the asset is delivered at the maturity is called the strike price or the delivery price, usually denoted by K.

Options are designed for hedging different types of risks. They are usually categorized by their exercising styles and payoff structures.

- European options. These options can only be exercised at the maturity date. Since European style options are the most basic, well studied and traded options, they are also named "vanilla options".

- American options. These options can be exercised by holders at any trading date before or at the maturity date.

- Bermudan options. These options allow holders to exercise at one of a set of specified dates before or at the maturity. They are intermediate between European style options and American options.

- Asian options. The option payoff depends on the average of the underlying asset over the life of the contract.

- Barrier options. The payoff for this kind of options depends on whether the underlying asset crosses the given barrier level before the maturity date.

- Lookback options. The payoff depends on the maximum or the minimum of the underlying asset's price over the life of the contract.

- Spread options. The option payoff depends on the spread of two underlying assets' prices. They are typical multi-asset options and are widely used in energy markets.

Options with complex payoff structures or exercising styles are called "exotic options".

The key issue in the theory of option pricing is to determine the price of an option. In 1973, Black and Scholes [7] first introduce an equilibrium framework for pricing an European option, which sets the foundation for the option pricing theory. They demonstrate that it is possible to construct a risk-free portfolio containing a stock and its European call option. By continuously adjusting the quantities of the stock and the option in the appropriate manner, the return of the portfolio becomes the risk-free rate. Consequently, the price of the option satisfies a partial differential equation (PDE) and an analytical pricing formula for the option is derived from the solution to the PDE (see [95]). Following the argument of no-arbitrage by Black and Scholes, a general framework, termed as the risk-neutral option pricing approach was proposed by Harrison and Pliska [49]. In short, if there exists no arbitrage in the markets, the price of an option at time t can be represented by the expectation of the discounted payoff with respect to a risk-neutral probablity measure $\mathbb{Q}$:

$$V_t(S,T) = \mathbb{E}_t^{\mathbb{Q}}[e^{-r(T-t)} f(S,K,T)], \tag{1}$$

where S is the spot price of the underlying, K is the strike price, T is the maturity date and r is the risk-free rate. $f(S,K,T)$ and $V_t(S,T)$ stand for the payoff function and the value of the option at t, respectively.

For many path-dependent options, e.g., barrier options and Asian options, their payoffs are determined by a set of prices observed on a finite set of time points called monitoring dates. Similarly, for Bermudan options, their prices depend on when to optimally exercise the options over a finite set of time points. In principle, the prices of these discrete options can be calculated by forward or backward recursion over time. For example, we compute the value of a Bermudan option at each monitoring date t by working backwards. Specifically, the option price at time t is the maximum of the exercise value and the continuation value:

$$V(S_t, t) = \max\{f(S_t, K, t), \mathbb{E}_t^{\mathbb{Q}}[e^{-r\Delta t}V(S_{t+1}, t)|S_t]\}. \tag{2}$$

In most cases, the analytical formulas for the prices of these discrete options are not available. When pricing them through numerical schemes, we discretize the price space as $\{S_{t,1}, S_{t,2}, \cdots, S_{t,N}\}$ at each monitoring date t. Then the continuation value at $(t, S_{t,i})$ is approximated by

$$\mathbb{E}^{\mathbb{Q}}[V(S_{t+1}, t+1)|S_{t,i}] \approx \sum_{j=1}^{N} w_{ij}V(S_{t+1,j}, t+1), i = 1, \cdots, N, \tag{3}$$

where w_{ij} are the quadrature weights. The computation efforts for directly evaluating the conditional expectation with the conditional price $S_{t,i}$ spanning the price space at time t in equation (3) is of order $\mathcal{O}(N^2)$. To improve the computational efficiency over the direct evaluation approach, Broadie and Yamamoto [12] propose a fast Gauss transform reducing the computational complexity to $\mathcal{O}(N)$, where the underlying asset price is modeled as a geometric Brownian motion (GBM).

However, even in equity markets, empirical studies show the GBM assumption fails to explain certain market evidences, such as the volatility smile, skewness, volatility clustering, and price jumps, etc. (see [26]). In electricity markets, the prices have some additional features, such as mean-reverison and seasonality (see [70] for empirical studies). Figure 2 shows ERCOT on-peak electricity prices from 2002-2007, in which you see spikes and mean-reversion in the price process apparently. These phenomena

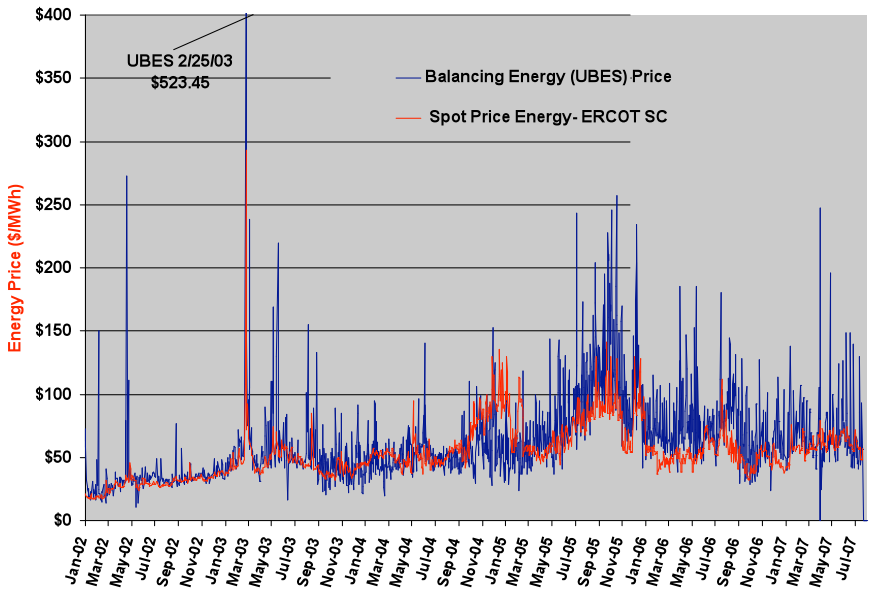

Figure 2: ERCOT On Peak Electricity Prices

prevent us using a GBM to model electricity prices. Researchers have been proposing models to capture the phenomena in price dynamics, for example, stochastic volatility models [50] and jump models [71, 31, 25]. Deng [34] introduces affine jump diffusion (AJD) processes to model the electricity price dynamics. These models bring new challenges in efficient pricing of options, especially those path-dependent and early exercise options. The underlying price distributions in the models are no longer Gaussian, which prevent the use of fast Gauss transform developed in [12]. The probability density functions of these distributions are not available in closed-forms either. In order to resolve the densities of these fat-tail distributions, we may need a large number of states in the price space, which calls for a fast numerical method in calculating prices of path-dependent options and Bermudan options. The efficiency of the numerical method becomes more essential especially when LSEs hold a very large portfolio of these types of options.

Various numerical methods have been developed in the literature for option pricing, for example, tree methods [27], Monte Carlo simulation [9, 64], finite difference method [95, 10], Fourier transform [17], etc. Recently, fast Fourier transform draws a lot of attentions to scholars in option pricing. It is very flexible to handle a wide class of processes, including Lévy processes and affine jump diffusion processes (AJD), because their density functions can be recovered from the inverse Fourier transform of the characteristic functions, which are known in closed-forms for these processes [31]. Carr and Madan [17] are among the first to use fast Fourier transform (FFT) to price European options. Benhamou [5] presents a FFT based approach to price Asian options under the Black-Scholes framework. Dempster and Hong [33], and Hurd and Zhou [54] propose two dimensional FFT to price spread options. However, these papers only focus on the pricing of a certain type of options. Some other researchers make efforts to develop more general pricing methods by means of transform analysis. Lord et. al [65] and Fang and Oosterlee [41] introduce Fourier-cosine expansion to evaluate early-exercise and barrier options under Lévy models, however, their framework does not consider mean-reversion and cannot be easily extended to other types of path-dependent options. Feng and Linetsky [43] propose an efficient method to generalize the pricing of path-dependent options and early-exercise options to any Lévy processes using Hilbert transform. Jackson et al. [57] apply Fourier space time spacing techniques to solve partial differential-integral equations for pricing various types of path-dependent and early-exercise options under Lévy processes with mean-reversion. The computational complexity of their algorithm is $\mathcal{O}(N \log N)$. One of the common problems inherent in FFT is that it is only applicable to uniform grids. This limits the use of FFT in some cases, e.g. pricing Asian options or working on non-uniform quadrature points. An alternative way is to use a nonuniform version of FFT (see [96]), but it is seen to be about 10 times slower than FFT on uniform grids.

In this chapter, we develop a fast convolution algorithm to compute the conditional expectation in (3). The algorithm avoids the direct evaluation of the Fourier sum by FFT, thus reduces the computational complexity from $\mathcal{O}(N \log N)$ to $\mathcal{O}(N)$. Another advantage of this fast algorithm is that it is applicable to nonuniform grids. It allows us to work on a nonuniform grid derived by the double-exponential formula in computing the convolution, which theoretically results in exponential convergence of the algorithm. Along the line of [11], the prices of some path-dependent options and early exercise options can be written as a series of convolutions. Thus, the proposed algorithm implies a generic pricing framework for various types of options covering path-dependent options (barrier, lookback and Asian), early-exercise options (American/Bermudan) as well as multi-asset options (spread). It also preserves the flexibility of handling a wide class of stochastic processes, as long as their characteristic functions are known analytically. This makes us easily incorporate AJD processes and Lévy processes, both of which are widely used for electricity prices modeling.

This chapter is organized as follows: in Section 2.2, we develop a fast transform algorithm to compute a general convolution. In Section 2.3, we focus on applying the fast convolution algorithm to price single asset options with path-dependent or early exercise features. We discuss the stochastic price models in Section 2.3.1. From Section 2.3.2 to 2.3.5, we cover the pricing of following options: barrier, Bermudan, lookback and Asian options. Numerical examples of these options under different price models are provided. We finally extend the algorithm to handle two-asset options, e.g., Bermudan spread options in Section 2.4. We draw the conclusion in Section 2.5.

2.2 Fast Convolution Algorithm

In this section, we propose a fast transform algorithm to calculate a probability density function convoluting with a given function. We approximate the probability density with it Fourier expansion, then a recursive relation is derived for each output,

which reduces the total computation to asymptotically $\mathcal{O}(N)$, where N is the number of grid points. In general, we would like to compute the following convolution efficiently:

$$I(x) = \int_{-\infty}^{\infty} g(y) f(x-y) dy, \tag{4}$$

where $f(\cdot)$ is a probability density function, which is smooth and decays to zero very fast at infinity.

We have an input grid y with N points: y_l, $l = 1, 2, \cdots, N$, and we compute $I(\cdot)$ at an output grid x with M points: x_j, $j = 1, 2, \cdots, M$. They are not required to be uniformly spaced. Then the discretized convolution becomes

$$I(x) \approx \sum_{l=1}^{N} q_l f(x - y_l), \tag{5}$$

where $q_l = w_l \cdot g(y_l)$, w_l are the quadrature weights. The discretization error here decreases to zero exponentially fast, given the integrand is analytic and integrable on the real line (see [94]).

As function f is a probability density, which decays to zero outside $[-L, L]$, we write f as its Fourier series expansion with period $2L$:

$$f(x) = \frac{1}{2L} \sum_{k=-\infty}^{\infty} a_k e^{-ik\frac{\pi x}{L}}, \tag{6}$$

where

$$a_k = \int_{-L}^{L} f(x) e^{ik\frac{\pi x}{L}} dx = \phi(\frac{k\pi}{L}; 0), \tag{7}$$

is the corresponding characteristic function. As a_k decays to zero fast (in the form of an exponential function), then f can be truncated and be approximated by

$$f(x) \approx \frac{1}{2L} \sum_{k=-m}^{m} a_k e^{-ik\frac{\pi x}{L}}, \tag{8}$$

where $x \in [-L, L]$. The truncation error here decays to zero exponentially fast, due to the exponential convergence of the Fourier expansion. Then for a given output

point x_j, we have

$$\begin{aligned} I(x_j) &\approx \frac{1}{2L}\sum_{l=N_j^-}^{N_j^+} q_l\Big(\sum_{k=-m}^{m} a_k e^{-ik\pi\frac{x_j-y_l}{L}}\Big) \\ &= \frac{1}{2L}\sum_{k=-m}^{m}\omega_{j,k}, \end{aligned} \tag{9}$$

where

$$\omega_{j,k} = a_k\sum_{l=N_j^-}^{N_j^+} q_l e^{-ik\pi\frac{x_j-y_l}{L}},$$

and

$$N_j^- = \min_{l\geq 0}\{x_j - y_l > -L\},$$

$$N_j^+ = \max_{l\leq N}\{x_j - y_l < L\}.$$

When we move to evaluate $I(\cdot)$ at the next point x_{j+1}, we do not need to re-calculate $\omega_{j+1,k}$ at all input points y_l, which again costs $\mathcal{O}(N)$ efforts. Instead we use the information from $\omega_{j,k}$ to compute $\omega_{j+1,k}$, which reduces the computation to $\mathcal{O}(1)$. We note that $\omega_{j+1,k}$ can be decomposed into three terms:

$$\begin{aligned} \omega_{j+1,k} &= a_k\sum_{l=N_{j+1}^-}^{N_{j+1}^+} q_l e^{-ik\pi\frac{x_{j+1}-y_l}{L}} \\ &= a_k\Big(\sum_{l=N_j^-}^{N_j^+} + \sum_{l=N_j^++1}^{N_{j+1}^+} - \sum_{l=N_j^-}^{N_{j+1}^--1}\Big) q_l e^{-ik\pi\frac{x_{j+1}-y_l}{L}} \\ &= \omega_{j+1,k}^0 + \omega_{j+1,k}^+ - \omega_{j+1,k}^-, \end{aligned} \tag{10}$$

where

$$\begin{aligned} \omega_{j+1,k}^0 &= e^{-ik\pi\frac{x_{j+1}-x_j}{L}}\omega_{j,k} \\ &= e^{-ik\pi\frac{\Delta x}{L}}\omega_{j,k}. \end{aligned} \tag{11}$$

We also notice that N_{j+1}^- and N_{j+1}^+ may not change or increase to include several terms when we move to x_{j+1}. In this way, we basically get $\omega_{j+1,k}$ by first rescaling

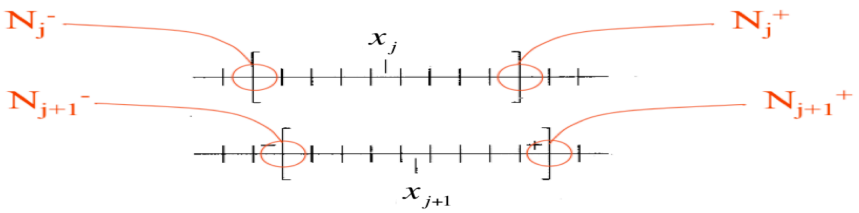

Figure 3: Changes of N_{j+1}^- and N_{j+1}^+ in the Recursive Relation

$\omega_{j,k}$ using equation (11) and then check N_{j+1}^- and N_{j+1}^+. If N_{j+1}^- and/or N_{j+1}^+ change, $\omega_{j+1,k}^+$ and/or $\omega_{j+1,k}^-$ are given as follows, otherwise, they are 0:

$$\omega_{j+1,k}^+ = a_k \sum_{l=N_j^++1}^{N_{j+1}^+} q_l e^{-ik\pi \frac{x_{j+1}-y_l}{L}}, \tag{12}$$

$$\omega_{j+1,k}^- = a_k \sum_{l=N_j^-}^{N_{j+1}^--1} q_l e^{-ik\pi \frac{x_{j+1}-y_l}{L}}. \tag{13}$$

Figure 3 illustrates the changes in N_{j+1}^- and N_{j+1}^+ when the output grid is uniform. This recursive relation (10) is the key to reduce the computational complexity.

The proposed method also possesses exponential convergence given the integrand in the convolution is C^1 continuous. To show the efficiency of the fast convolution method, we use a simple example. We consider the following convolution:

$$I(x) = \int_{-\infty}^{\infty} y f(x-y) dy,$$

where $f(z) = \frac{1}{\sqrt{2\pi}} \exp\left(-\frac{z^2}{2}\right)$ is the density of a standard normal distribution. If we let Y be a normal random variable with mean x and unit standard deviation, the value of the convolution $I(x) = E[Y] = x$, which is exact and ideal to be verified. We choose $L = 8$ and the input grid y is equally spaced on $[-L, L]$. We arbitrarily choose

$$x = [-2, -1.4, -1.26, -1.1, -0.85, -0.33, 0.02, 0.06, 0.4, 0.55, 0.68, 1.05, 1.43, 1.52, 1.7, 1.78],$$

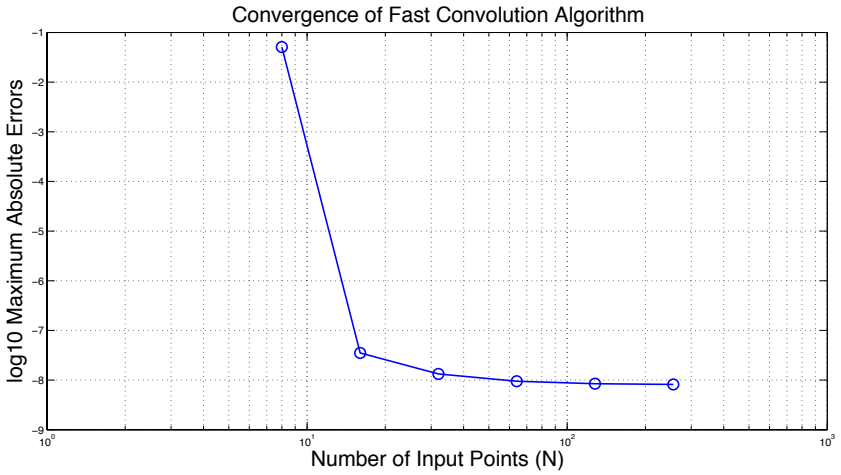

Figure 4: Convergence of the Fast Convolution

which are not equally spaced. We set $m = 16$ to truncate the Fourier series. The weights w_l are obtained from the trapezoidal rule. The use of trapezoidal rule does not bound the accuracy of the algorithm, because it converges exponentially fast provided the integrand is analytic [94]. Figure 4 shows the $\log_{10}$ maximum absolute errors with respect to the number of input points N. N is varied from 2^3 to 2^8. We find that we only need 16 points to control the errors at 10^{-8} level, which demonstrates the fast convergence of the algorithm.

2.3 Single Asset Options

According to Broadie and Yamamoto [11] and Benhamou [5], many path-dependent options and early-exercise options can be written as a series of convolutions. In this section, we discuss how to apply the proposed fast convolution algorithm in Section 2.2 to price these single asset options. We start from introducing two classes of stochastic processes to model the asset price dynamics. Then a barrier option is used as an example to show where convolution is involved in pricing. Similar approach is extended to price lookback, Asian and Bermudan options.

2.3.1 Spot Price Dynamics

In this section, we consider two classes of processes to model the asset price processes: affine jump diffusion processes (AJD) and Lévy processes. Both classes belong to the jump processes and are capable of capturing certain features of the electricity prices, such as stochastic volatility, mean-reversion, jumps and spikes, etc.

Let S_t denote the underlying asset price, for instance, the electricity price. We denote the log-return of the asset price by X_t, where $X_t = \log S_t/S_0$. The asset price is then modeled as an exponential process $S_t = S_0 e^{X_t}$. The definitions of the two classes of processes are given below.

AJD processes are jump-diffusion processes in which the drift, covariance and jump intensities are all affine functions. Specifically, they are defined as follows:

Definition 2.1. *A Markov process $X_t \in D \subset \mathbb{R}_n$ on a filtered probability space $(\Omega, \mathcal{F}, \mathbb{P})$ is an AJD process if it satisfies the following dynamics*

$$dX_t = \mu(X_t)dt + \sigma(X_t)dW_t + dZ_t$$

where

1. *the drift vector $\mu(X_t) :\to D \to \mathbb{R}_n$ is an affine function of X;*
2. *the covariance matrix $\sigma(X_t)\sigma^\intercal(X_t)$ is an affine function of X;*
3. *W_t is a n-dimensional $\mathcal{F}_t$-Brownian motion;*
4. *Z_t is a pure jump process whose jumps have a fixed probability distribution ν on $\mathbb{R}_n$ and arrive with intensity $\lambda(X_t) : t \geq 0$ for some affine function $\lambda : D \to [0, \infty)$.*

A Lévy process is a Brownian motion with drift combined with a jump process. It is defined as follows:

Definition 2.2. *A càdlàg, real valued stochastic process $(X_t)_{t\geq 0}$ on a filtered probability space $(\Omega, \mathcal{F}, \mathbb{P})$ with $X_0 = 0$ is called a Lévy process if it satisfies the following conditions:*

1. *Independent increments: for any $0 \leq s < t \leq T$, the increment $X_t - X_s$ is independent of $\mathcal{F}_s$.*

2. *Stationary increments: for any $s, t \geq 0$, the distribution of $X_{t+s} - X_t$ does not depend on t.*

3. *Stochastic continuity: for any $t \geq 0$ and $\varepsilon > 0$, $\lim_{s\to t} \mathbb{P}(|X_t - X_s| > \varepsilon) = 0$.*

The conditional characteristic functions (CCFs) of both families are known in closed-forms. From equation (6), we know the characteristic function a_k is an essential input argument to the fast convolution algorithm. This is why the pricing framework is applicable to both price models without any modification.

For example, we consider the following AJD process:

$$dX_t = \kappa(\theta - X_t)dt + \sigma dW_t + \sum_{i=1}^{2} \Delta Z_t^i, \tag{14}$$

where κ is the mean-reverting coefficient, θ is the long-term mean, σ is the volatility, Z^j is a compound Poisson process with arrival intensity λ_j and mean of jump size μ_j, $j = 1, 2$. The CCF of this AJD process given x_t is defined as

$$\begin{aligned} \phi(u; x_t) &= \mathbb{E}^Q[e^{iuX_{t+1}}|x_t] \\ &= \int_{-\infty}^{\infty} e^{iux_{t+1}} f(x_{t+1}|x_t)dx_{t+1}, \end{aligned} \tag{15}$$

where $f(y|x)$ denotes the transition probability density function. By Duffie et. al [31], the CCF has the following form:

$$\begin{aligned} \phi(u; x_t) &= e^{-Au^2+iDu+H(u)} \\ &= (\frac{1 - iH_1u}{1 - iH_2u})^{\frac{\lambda_1}{\kappa}} (\frac{1 - iH_3u}{1 - iH_4u})^{\frac{\lambda_2}{\kappa}} e^{-Au^2+iDu}, \end{aligned} \tag{16}$$

where

$$A = \frac{\sigma^2}{4\kappa} - \frac{\sigma^2}{4\kappa} e^{-2\kappa\Delta t},$$

$$D = \theta + (x_t - \theta)e^{-\kappa\Delta t},$$

$$H_1 = \mu_1 e^{-\kappa\Delta t}, H_2 = \mu_1, H_3 = \mu_2 e^{-\kappa\Delta t}, H_2 = \mu_2.$$

The CCFs of Lévy processes are also known in analytical forms through Lévy-Khinchine representation. Let X'_t be a Lévy process, the asset price is modeled as

$$S_t = S_0 e^{rt+\omega t+X'_t}, \tag{17}$$

where ω is determined by setting $\exp(-\omega t) = \phi_X(-i, t)$ or equivalently $\mathbb{E}^{\mathbb{Q}}[e^{X'_t}] = \exp(-\omega t)$. If such ω is chosen, the discounted asset price $\exp(-rt)S_t = S_0 \exp(\omega t + X'_t)$ is definitely a martingale, i.e. it is under risk-neutral probability measure $\mathbb{Q}$. In this setting, we have $X_t = rt + \omega t + X'_t$. The CCFs $\phi_X(u, t)$ of some widely used Lévy processes are listed as follows:

- Log-normal model: $\phi_{\mathrm{LN}}(u, t) = \exp(-\frac{\sigma^2 u^2}{2} t)$.
- Merton's jump diffusion model: $\phi_{\mathrm{MJD}}(u, t) = \exp\left[-\frac{\sigma^2 u^2}{2} t + \lambda t\big(e^{iu\alpha - \delta^2 u^2/2} - 1\big)\right]$.
- Variance-Gamma model: $\phi_{\mathrm{VG}}(u, t) = \left(\frac{1}{1 - i\theta\nu u + (\sigma^2\nu/2)u^2}\right)^{t/\nu}$.
- Normal Inverse Gaussian model: $\phi_{\mathrm{NIG}}(u, t) = \exp[t\delta(\sqrt{\alpha^2 - \beta^2} - \sqrt{\alpha^2 - (\beta + iu)^2})]$.
- CGMY model: $\phi_{\mathrm{CGMY}}(u, t) = \exp\{tC\Gamma(-Y)[(M - iu)^Y - M^Y + (G + iu)^Y - G^Y]\}$, where $\Gamma(\cdot)$ is a gamma function.

2.3.2 Barrier Options

2.3.2.1 The Pricing Problem

In this section, we set up a framework for pricing an European barrier option with discrete monitoring dates. We assume the log return of asset price x_t follows an affine jump diffusion (14) or a Lévy process. The asset price is modeled by $S_t = S_0 e^{x_t}$.

We now consider a set of time points $t = 0, 1, \cdots, T$. A discrete down-and-out call option with maturity T, monitoring dates t, barrier B and strike K pays $(S_T - K)^+$ if $S_t > B$ for all t, $1 \leq t \leq T$ and zero otherwise. This payoff is equivalent to

$$h(x_t) = \begin{cases} (S_0 e^{x_t} - K)^+ & x_t > b, \\ 0 & x_t \leq b, \end{cases}$$

where $b = \log B/S_0$. We introduce a sequence of probability density functions $f_t(x_t)$, $0 \leq t \leq T$ under the risk-neutral measure such that $f_t(x)dx$ is the probability that $x_s > b$ for $1 \leq s \leq t$ and $x \leq x_t \leq x + dx$. Then the price of such a down-and-out call at time 0 is given by

$$V_0(S_0, K, B) = e^{-rT} \int_{\log K/S_0}^{\infty} f_T(x_T)(S_0 e^{x_T} - K) dx_T. \tag{18}$$

We go along with Broadie's [11] formulation, the probability density functions f_t can be obtained by the following recursive formula:

$$f_1(x_1) = \begin{cases} f(x_1|x_0) & x_1 > b, \\ 0 & x_1 \leq b, \end{cases}$$

$$f_{t+1}(x_{t+1}) = \begin{cases} \int_b^{\infty} f(x_{t+1}|x_t) f_t(x_t) dx_t & x_{t+1} > b, \\ 0 & x_{t+1} \leq b, \end{cases}$$

where $f(x_{t+1}|x_t)$ is the transition probability density of x_t. For a Lévy process, the increments are independent and stationary, which follows $f(x_{t+1}|x_t) = f(x_{t+1} - x_t|0)$. Thus

$$f_{t+1}(x_{t+1}) = \int_b^{\infty} f(x_{t+1}|x_t) f_t(x_t) dx_t, \tag{19}$$

which is a convolution on the half line $[b, \infty]$. For a AJD process, the CCF in (16) implies $f(x_{t+1}|x_t) = f(x_{t+1} - x_t e^{-\kappa \Delta t}|0)$. Let $y_t = x_t e^{-\kappa \Delta t}$, and $g_t(y_t) = f_t(y_t e^{\kappa \Delta t}) e^{\kappa \Delta t}$, then $f_{t+1}(x_{t+1})$ becomes

$$f_{t+1}(x_{t+1}) = \int_{be^{-\kappa \Delta t}}^{\infty} f(x_{t+1} - y_t|0) g_t(y_t) dy_t, \tag{20}$$

which is again a convolution along the half line $[be^{-\kappa\Delta t}, \infty]$. In principle, we could pad 0's on $[-\infty, b]$ or $[-\infty, be^{-\kappa\Delta t}]$ and apply any convolution methods, e.g., FFT based algorithm, to compute $f_{t+1}(x_{t+1})$ directly. But the corner point at b or $be^{-\kappa\Delta t}$ reduces the accuracy of the algorithm. Takahasi and Mori [88], Mori [74] and Ooura and Mori [77] introduce a double-exponential (DE) formula to transform such an integral on a half line to the entire real line. It is known that the discretization error decreases to zero exponentially fast as the number of points increases. This preserves the exponential convergence of the convolution algorithm. Additionally, the DE grid is non-uniform, which can be properly handled by the proposed fast convolution method.

2.3.2.2 The Double-Exponential Formula

Given the following integral:

$$I = \int_c^\infty f(x)dx,$$

we would like to compute it efficiently. We apply the following change of variable, so called DE formula to transform the integral from a half line to the whole real line:

$$x = c + \exp\big(\frac{\pi}{2}\sinh(u)\big). \tag{21}$$

Then the integral becomes

$$I = \int_{-\infty}^\infty f\big(c + \exp\big(\frac{\pi}{2}\sinh(u)\big)\big)\exp\big(\frac{\pi}{2}\sinh(u)\big)\frac{\pi}{2}\cosh(u)du. \tag{22}$$

The advantage of DE transform is that if the integral I converges, the integrand in (22) decays at least as fast as the double-exponential function at $\pm\infty$. Then trapezoidal rule is optimal to discretize the integral to attain the exponential convergence. When the integrand f itself decays to zero very fast at ∞, for example, a multiplication of two probability density functions in the barrier options pricing, the DE formula gives another factor approaching zero double-exponentially. In this case, the benefit is that we can truncate the integration region at a small range, but the drawback is that we

need a finer grid to resolve the integrand. Some numerical experiments suggest that the drawback is more obvious. To improve the efficiency of computing convolutions in the barrier option pricing, Broadie and Yamamoto [11] suggest a modified formula, which mimics the DE transform at $-\infty$ and approaches an identity at ∞ to take advantage of the rapid decay of the integrand $f(x_{t+1}|x_t)f_t(x_t)$.

The modified DE formula for the integral I is given as:

$$x = \ln\{e^c + \exp(\frac{\pi}{2}(1 + u - e^{-u}))\}.$$

In the barrier option pricing formula (20), the modified DE formula implies the input grid points and the corresponding weights are:

$$y_i = \ln\{e^{be^{-\kappa\Delta t}} + \exp(\frac{\pi}{2}(1 + ih - e^{-ih}))\}, \tag{23}$$

and

$$w_i = h\frac{\exp(\frac{\pi}{2}(1 + ih - e^{-ih}))\frac{\pi}{2}(1 + e^{-ih})}{e^{be^{-\kappa\Delta t}} + \exp(\frac{\pi}{2}(1 + ih - e^{-ih}))}. \tag{24}$$

2.3.2.3 Fast Convolution for Barriers Options

In this section, we put CCF of the underlying spot process, DE formula and the fast convolution method together to price an European barrier option efficiently. For the down-and-out call under AJD, we compute $f_t(x_t)$ at each monitoring date t. We discretize $f_{t+1}(x_{t+1})$ by the modified DE formula, which gives:

$$f_{t+1}(x_{t+1}) \approx \sum_{i=1}^{N} q_i f(x_{t+1} - y_i), \tag{25}$$

where $q_i = w_i \cdot g(y_i)$, y_i and w_i are DE points and weights given in (23) and (24). Then we apply the fast convolution algorithm to this finite sum. For the output grid x_j, $j = 1, 2, \cdots, M$, we have

$$f_{t+1}(x_j) \approx \frac{1}{2L}\sum_{k=-m}^{m} \omega_{j,k}, \tag{26}$$

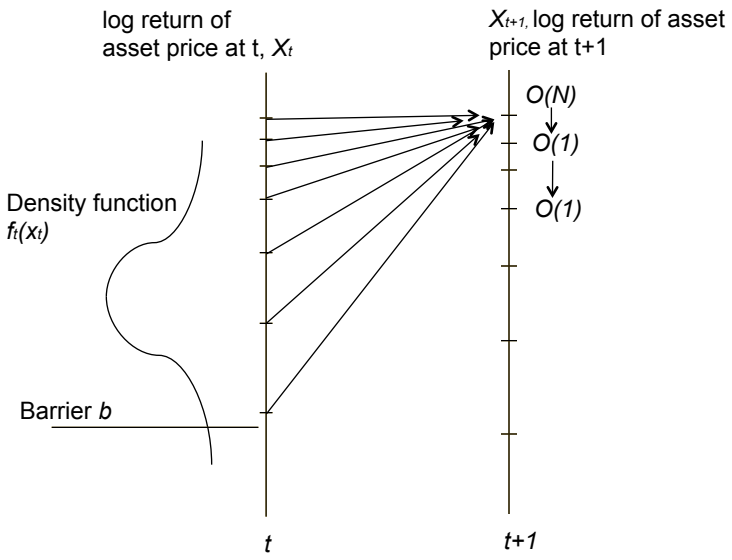

Figure 5: Illustration of Fast Convolution Method for a Barrier Option in One Step

where

$$\omega_{j,k} = a_k \sum_{i=N^-}^{N^+} q_i e^{-ik\pi(x_j - y_i)/L}, \tag{27}$$

$$a_k = \phi(\frac{k\pi}{L}; 0). \tag{28}$$

The algorithm for a barrier option under Lévy processes is the same. The computational complexity of the above algorithm for a convolution in pricing a barrier option is $\mathcal{O}(M + N)$. Figure 5 shows how fast convolution method is applied at each step in pricing a barrier option from source points x_t to target points x_{t+1}. As it does not require uniformly spaced grid for inputs and outputs, we can rely on the double-exponential transform to retain the exponential convergence. Moreover, a non-uniform grid enable us to compute the option price at the final step in equation (18) more efficiently by high accurate quadratures. For example, we can simply output f_T at a Gaussian grid and use Gaussian quadrature to compute (18).

The algorithm for barrier options pricing is summarized as follows:

1. Choose a uniform grid $[-U, U]$ with N points.

2. Derive a non-uniform grid y_i and weights w_i by the modified DE formula (23-24). $x_i = y_i e^{\kappa \Delta t}$.

3. Compute $f_1(x_i)$ by Fourier expansion.

4. Loop $t = 2$ to $T - 1$. **Input:** $f_t(x_i)$.

   - Compute $f_{t+1}(x_i)$ by the fast convolution algorithm.

   End Loop. **Output:** $f_{t+1}(x_i)$.

5. Derive a Gaussian grid on $[\log K/S_0, Bound]$ for a call and $[b, \log K/S_0]$ for a put.

6. Output f_T at the Gaussian grid by the fast convolution algorithm.

7. Compute the option price by (18).

2.3.2.4 Numerical Examples

We provide an example of pricing a down-and-out put when the price log return is modeled by an Ornstein-Uhlenbeck (OU) process

$$dx_t = \kappa(x_t - \theta)dt + \sigma dW_t,$$

where the mean-reverting rate $\kappa = 0.5$, long-term mean $\theta = 0.4$, and instantaneous volatility $\sigma = 0.1$. We assume the risk-free rate $r = 0.1$, maturity $T = 1$, barrier $B = 95$, initial asset price $S_0 = 100$, and strike price $K = 110$. Number of monitoring dates $M = 50$. An OU process has an analytic formula for transition density which allows us for an easy check.

Table 1: Comparison of Prices for a Down-and-out Put under OU Model

N	M	DE+Conv+Gaussian quad	Uniform Grid via FFT
2^7	50	0.728657	0.630441
2^8	50	0.608877	0.585485
2^9	50	0.608872	0.604733
2^{10}	50	0.608872	0.607901
2^{11}	50	0.608872	0.609543
2^{12}	50	0.608872	0.610379

The conditional characteristic function of an OU process is

$$\phi(u; x_t) = e^{-Au^2+iDu}, \tag{29}$$

where

$$A = \frac{\sigma^2}{4\kappa} - \frac{\sigma^2}{4\kappa}e^{-2\kappa\Delta t},$$
$$D = \theta + (x_t - \theta)e^{-\kappa\Delta t},$$

a special case of (16).

We choose the support of density $L = 0.12$, the uniform grid $u \in [-3, 3]$ to deduce a DE grid, and $2m = 64$ be the number of terms in the Fourier expansion to ensure that the errors of Fourier expansion and fast convolution stay at 10^{-14} level. We compare the results obtained by fast convoluton algorithm plus DE formula with FFT in Figure 6 and Table 1. We keep 6 decimal places here and note that our fast convolution algorithm converges much faster than FFT. This is because FFT has to be on a uniform grid which prevents the use of DE formula to enhance the convergence.

In the second example of a barrier option, we consider that the log price x_t follows an OU process with Kou's double-exponential jumps [61]:

$$dX_t = \kappa(\theta - X_t)dt + \sigma dW_t + \Delta Z_t, \tag{30}$$

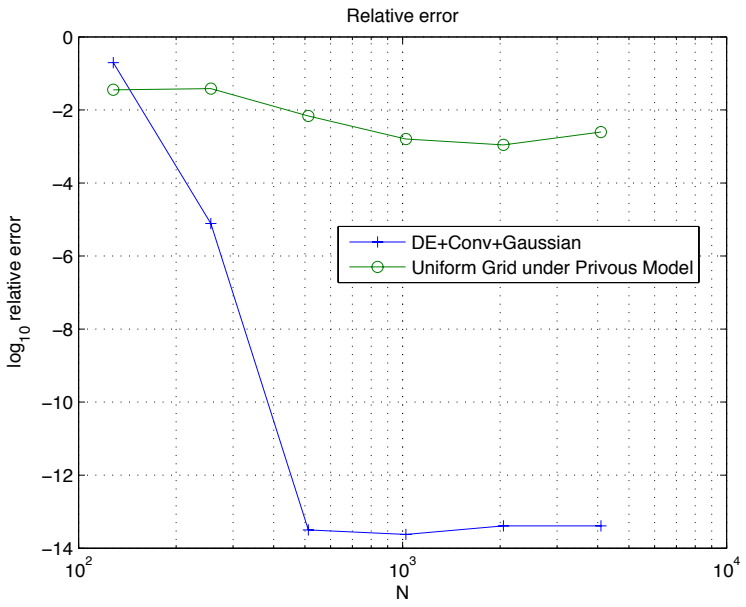

Figure 6: Relative Errors for a Down-and-out Put under OU Model

where Z_t is a compound Poisson process with arrival rate λ, and the jumps are i.i.d. double-exponential distributed with parameter p, η^+, η^-, where η^+ and η^- stand for the mean of positive jump size and negative jump size. The rest parameters have the same meaning as in an OU process.

The conditional characteristic function is derived as:

$$\phi(u; x_t) = (\frac{1 - iH_1u}{1 - iH_2u})^{\frac{\lambda p}{\kappa}} (\frac{1 + iH_3u}{1 + iH_4u})^{\frac{\lambda(1-p)}{\kappa}} e^{-Au^2 + iDu}, \tag{31}$$

where

$$A = \frac{\sigma^2}{4\kappa} - \frac{\sigma^2}{4\kappa} e^{-2\kappa\Delta t},$$

$$D = \theta + (x_t - \theta)e^{-\kappa\Delta t},$$

$$H_1 = \eta^+ e^{-\kappa\Delta t}, H_2 = \eta^+, H_3 = \eta^- e^{-\kappa\Delta t}, H_2 = \eta^-.$$

We price a down-and-out put under the OU mean-reverting double-exponential process with mean-reverting rate $\kappa = 0.5$, long-term $\theta = 0.4$, instantaneous volatility $\sigma = 0.25$, mean of positive jump $\eta^+ = 0.45$, mean of negative jump $\eta^- = 0.35$, $p =$

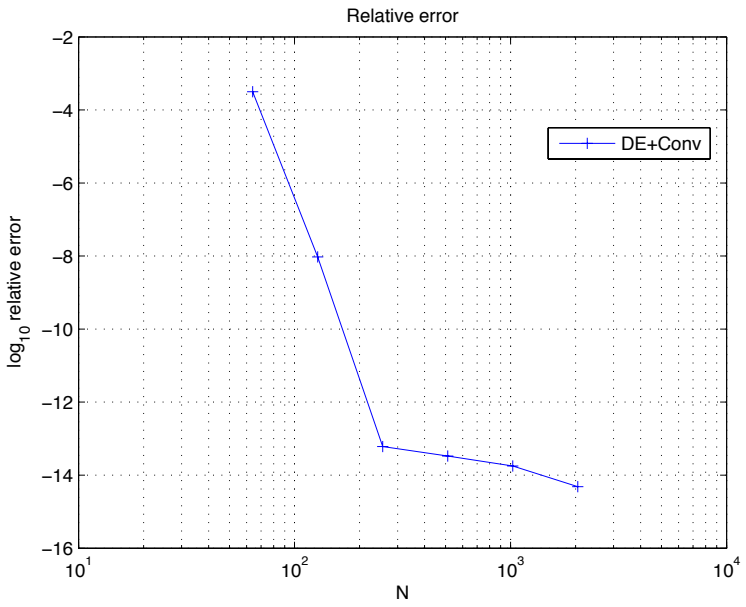

Figure 7: Relative Errors for a Down-and-out Put under OU Double-Exp. Jumps

Table 2: Price of a Down-and-out Put under OU Double-Exp. Jumps

N	M	DE+Conv+Gaussian quad	CPU time
2^6	12	0.287459	0.155
2^7	12	0.287368	0.301
2^8	12	0.287368	0.608
2^9	12	0.287368	1.335

0.96, and jump intensity $\lambda = 0.6$. Let risk-free rate $r = 0.1$, maturity $T = 1$, barrier $B = 95$, initial price $S_0 = 100$, and strike price $K = 110$. Number of monitoring dates $M = 12$ (monthly). We choose support $L = 6$ (heavier tail than OU process), uniform grid $u \in [-3, 3]$, and $m = 256$ in the Fourier expansion. In Figure 7 and Table 2, we find again the price converges fairly fast. We only need 128 points to achieve 6 correct digits within 0.3 seconds.

2.3.3 Bermudan Options

Similar to barrier options, the fast convolution method is applicable to Bermudan options as well. We consider a Bermudan option with exercise dates t. At each exercise date, the price of a Bermudan option is the maximum of its continuation value and the instant payoff. Specifically, a Bermudan option can be priced by the following backward induction:

$$\begin{aligned}
&1. \quad v(T, x_T) = h(T, x_T) \\
&2. \quad p(t, x_t) = e^{-r\Delta t} \int_{-\infty}^{\infty} v(t+1, x_{t+1}) f(x_{t+1}|x_t) dx_{t+1} \\
&3. \quad v(t, x_t) = \max\{p(t, x_t), h(t, x_t)\}
\end{aligned}$$

where $h(t, x_t)$ is the payoff at time t and $t = 1, 2, \cdots, T$.

For a Bermudan put, whose payoff is $h(T, x_T) = (K - S_0 e^{x_T})^+$, it has an optimal exercise price $S_0 e^{x_t^c}$ at each time t. When $x_t < x_t^c$, $h(t, x_t) > p(t, x_t)$, and when $x_t \geq x_t^c$, $h(t, x_t) \leq p(t, x_t)$. Basically, the above backward induction can be re-written as:

$$\begin{aligned}
p(t, x_t) &= e^{-r\Delta t} \Big\{ \int_{-\infty}^{x_{t+1}^c} h(t+1, x_{t+1}) f(x_{t+1}|x_t) dx_{t+1} \\
&+ \int_{x_{t+1}^c}^{\infty} p(t+1, x_{t+1}) f(x_{t+1}|x_t) dx_{t+1} \Big\}, \qquad (32)
\end{aligned}$$

with terminal conditions $x_T^c = \log(K/S_0)$, $h(T, x_T) = (K - S_0 e^{x_T})$, and $p(T, x_T) = 0$.

Under an AJD process, we let $y_t = x_t e^{-\kappa \Delta t}$, and $g_t(x) = f_t(-x)$, then equation (32) becomes

$$\begin{aligned}
p(t, y_t) &= e^{-r\Delta t} \Big\{ \int_{-\infty}^{x_{t+1}^c} h(t+1, x_{t+1}) g(y_t - x_{t+1}) dx_{t+1} \\
&+ \int_{x_{t+1}^c}^{\infty} p(t+1, x_{t+1}) g(y_t - x_{t+1}) dx_{t+1} \Big\}, \qquad (33)
\end{aligned}$$

containing two convolution type of integrals on a half line.

In the first step, we apply the DE formula to transform the integration on $(-\infty, x_t^c]$ and $[x_t^c, \infty)$ into $(-\infty, \infty)$, then the integrand shows double-exponential decay, so that

we can take advantage of the trapezoidal rule to compute the integration after the change of variables. For $(-\infty, x_t^c]$, we discretize the integral with grid points $x_{t,i}$ and weights $w_{t,i}$:

$$x_{t,i} = -\ln\{e^{-x_{t+1}^c} + \exp(\frac{\pi}{2}(1 + ih - e^{-ih}))\} \tag{34}$$

$$w_{t,i} = h\frac{\exp(\frac{\pi}{2}(1 + ih - e^{-ih}))\frac{\pi}{2}(1 + e^{-ih})}{e^{-x_{t+1}^c} + \exp(\frac{\pi}{2}(1 + ih - e^{-ih}))}, \tag{35}$$

and for $[x_t^c, \infty)$, we use

$$x_{t,i} = \ln\{e^{x_{t+1}^c} + \exp(\frac{\pi}{2}(1 + ih - e^{-ih}))\} \tag{36}$$

$$w_{t,i} = h\frac{\exp(\frac{\pi}{2}(1 + ih - e^{-ih}))\frac{\pi}{2}(1 + e^{-ih})}{e^{x_{t+1}^c} + \exp(\frac{\pi}{2}(1 + ih - e^{-ih}))}. \tag{37}$$

As noted, the grid and the weights change at every time step t because of the change of x_t^c. We locate x_t^c by finding the root of $p(t, x_t) - h(t, x_t)$ at each step via secant method. (Because the first order derivative is not available, Newton's method is not applicable here). We specify the bounds of the root, $x_{t,L}$ and $x_{t,U}$, and compute the corresponding $p(t, x_{t,L})$ and $p(t, x_{t,U})$ (the computational complexity is $\mathcal{O}(N)$). In the iteration of secant method, we take advantage of the fast convolution method again to compute the value of $p(t, x_t)$ by only 1 operation instead of N. Therefore, at $t+1$, given x_{t+1}^c, grid $x_{t+1,i}$, weights $w_{t+1,i}$ and $p(t+1, x_{t+1})$ on $[x_{t+1}^c, \infty)$, we compute $p(t, x_t)$ in equation (32) and apply secant search until the root x_t^c of $p(t, x_t) - h(t, x_t)$ is located within a given tolerance. Once x_t^c is obtained, we derive the grid and weights by equation (33-37). Finally, $p(t, x_t)$ on this grid $[x_t^c, \infty)$ can be computed via the fast convolution.

The algorithm for Bermudan options pricing is summarized as follows:

1. Choose a uniform grid $[-U, U]$ with N points.

2. Given $x_T^c = k$, derive a non-uniform grid $x_{T,i}$ and weights $w_{T,i}$ by equation (33-37).

3. Given $p(T, x_T) = 0$ on $[x_T^c, \infty)$.

4. Loop $t = T - 1$ to 2. **Input:** $x_{t+1}^c = k$ and $p(t+1, x_{t+1})$.

   - Specify the bounds, $x_{t,L}$ and $x_{t,U}$.
   - Locate $x_t^c = k$ by secant method, $p(t, x_t)$ in the iteration is calculated by fast convolution in equation (32).
   - Derive the DE grid $x_{t,i}$ and weights $w_{t,i}$ by equation (33-37) given x_t^c.
   - Compute $p(t, x_t)$ on $[x_t^c, \infty)$.

   End Loop. **Output:** $x_t^c = k$ and $p(t, x_t)$.

5. Compute price $P = p(0, 0)$.

2.3.3.1 Numerical Examples

We first price a Bermudan put when log price is modeled by an OU process with mean-reverting rate $\kappa = 0.5$, long-term mean $\theta = 0.4$, and instantaneous volatility $\sigma = 0.1$. We assume the risk-free rate $r = 0.1$, maturity $T = 1$, initial asset price $S_0 = 100$, and strike price $K = 110$. Number of monitoring dates $M = 50$. Again, an OU process has an analytic formula for transition density which allows us for an easy check. We choose the support of density $L = 0.12$, the uniform grid $u \in [-3, 3]$ to deduce a DE grid, and $2m = 64$ be the number of terms in the Fourier expansion to ensure that the errors of Fourier expansion and fast convolution stay at 10^{-14} level. Monte Carlo simulation gives a reference price at 9.585234 with standard error

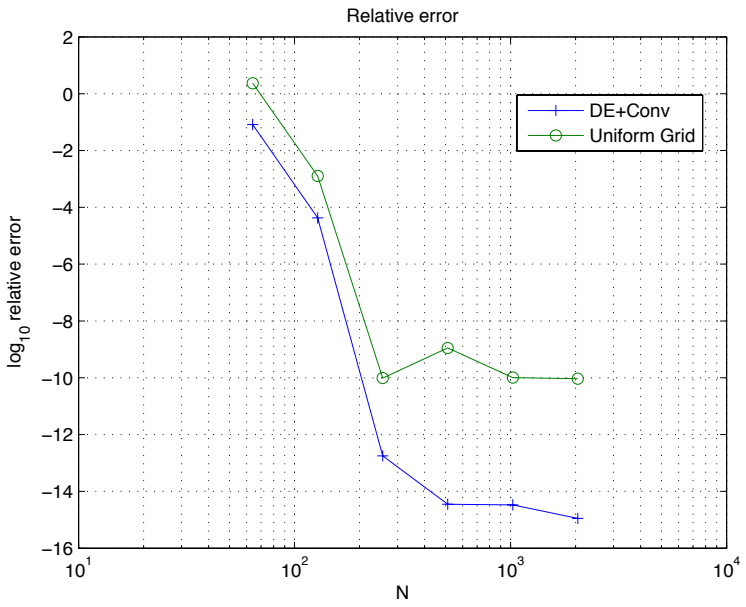

Figure 8: Relative Errors for a Bermudan Put under OU Model

Table 3: Comparison of Prices for a Bermudan Put under OU Model

N	M	DE+Conv	Uniform Grid
2^6	50	10.353984	31.986766
2^7	50	9.572504	9.560004
2^8	50	9.572096	9.572096
2^9	50	9.572096	9.572096
2^{10}	50	9.572096	9.572096

0.013943 within 1.286 seconds (10,000 paths). In Figure 8 and Table 3, we find the fast convolution method for pricing Bermudan option still converges faster than using FFT. The CPU time of using 2^7 grid points is 0.664 seconds, which gives 4 correct digits and is 2 times faster than the Monte Carlo method.

Next, we consider the following stochastic volatility model for the log return x_t and stochastic volatility v_t:

$$d\begin{bmatrix} x_t \\ v_t \end{bmatrix} = \begin{bmatrix} \kappa_1(\theta_1 - x_t) \\ \kappa_2(\theta_2 - v_t) \end{bmatrix} dt + \begin{bmatrix} \sqrt{v_t} & 0 \\ \rho\sigma\sqrt{v_t} & \sqrt{1-\rho^2}\sigma\sqrt{v_t} \end{bmatrix} dW_t + \sum_{i=1}^{2} \Delta Z_t^i, \quad (38)$$

where κ_1 is the mean-reverting rate of the log return, θ_1 is the long-term mean of the log return, κ_2 is the mean-reverting rate of the volatility, θ_1 is the long-term mean of the volatility, σ is the volatility of volatility, W_t is a $\mathcal{F}_t$-adapted standard Brownian motion under $\mathbb{Q}$ in $\mathbb{R}^2$ with correlation ρ, Z_t^i is a compound Poisson process in $\mathbb{R}^2$ with the Poisson arrival intensity being $\lambda_i, i = 1, 2$, and ΔZ_t^i denotes the random jump size in $\mathbb{R}^2$ with mean jump size being $\mu_i, i = 1, 2$. This is again an affine jump duffusion process, and its conditional characteristic function is in the form of (see [31]):

$$\phi(u, v; x_t, v_t) = \exp[A(u, v, t, T)x_t + B(u, v, t, T)v_t + C(u, v, t, T)] \quad (39)$$

where $A(\cdot), B(\cdot), C(\cdot)$ satisfy the Riccati equations:

$$\begin{aligned} \frac{dA(\cdot)}{dt} &= \kappa_1 A(\cdot) \\ \frac{dB(\cdot)}{dt} &= \kappa_2 B(\cdot) - \frac{1}{2}A(\cdot)(A(\cdot) + \rho\sigma B(\cdot)) - \frac{1}{2}B(\cdot)(A(\cdot)\rho\sigma + B(\cdot)\sigma^2)) \\ \frac{dC(\cdot)}{dt} &= -\kappa_1\theta_1 A(\cdot) - \kappa_2\theta_2 B(\cdot) - \lambda_1(\frac{1}{1 - A(\cdot)\mu_1} - 1) - \lambda_2(\frac{1}{1 - A(\cdot)\mu_2} - 1), \end{aligned}$$

with terminal conditions $A(u, v, T, T) = iu$, $B(u, v, T, T) = iv$ and $C(u, v, T, T) = 0$. We can solve for $A(\cdot) = iue^{-\kappa_1(T-t)}$. We only need to find $\phi(\frac{k\pi}{L} - i\epsilon, 0; 0, 0) = \exp[C(\frac{k\pi}{L} - i\epsilon, 0, t, t + \Delta t; 0, 0)]$. As $B(\cdot)$ and $C(\cdot)$ cannot be solved analytically, we do it numerically. By change of variable, $s = T - t$, we solve $B(\frac{k\pi}{L} - i\epsilon, 0, \Delta t)$ and $C(\frac{k\pi}{L} - i\epsilon, 0, \Delta t)$ by Runge-Kutta method with the initial conditions $B(\frac{k\pi}{L}, 0, 0) = 0$ and $C(\frac{k\pi}{L}, 0, 0) = 0$.

We price a Bermudan put under such a mean-reverting stochastic volatility model with the following parameters: $\kappa_1 = 0.5$, $\theta_1 = 0.03$, $\kappa_2 = 1$, $\theta_2 = 0.4$, $\sigma = 0.3$, $\rho = 0.8$, $\lambda_1 = 0.5$, $\lambda_2 = 0.3$, $\mu_1 = 0.15$, $\mu_2 = 0.1$, risk-free rate $r = 0.1$, maturity $T = 1$, initial

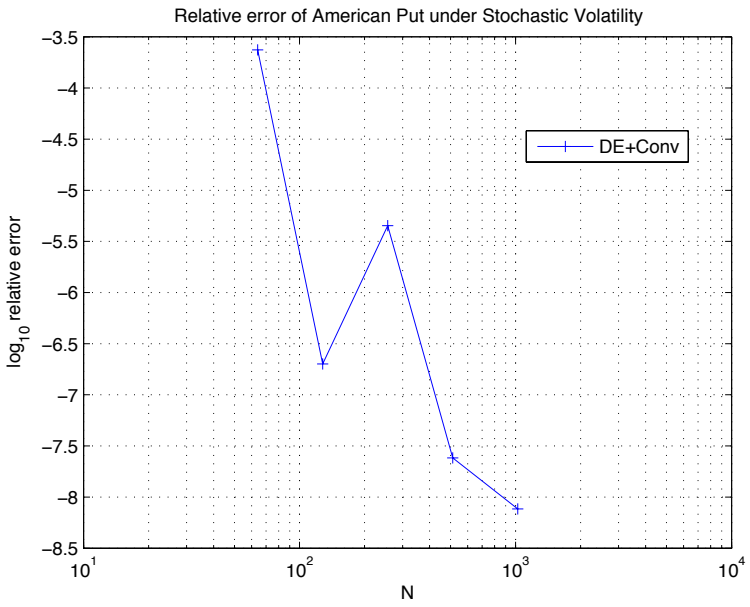

Figure 9: Relative Errors for a Bermudan Put under Stochastic Volatility

Table 4: Price of a Bermudan Put under Stochastic Volatility

N	M	DE+Conv	CPU time
2^6	12	10.547933	0.416
2^7	12	10.550425	0.860
2^8	12	10.550474	1.565
2^9	12	10.550427	3.148
2^{10}	12	10.550427	5.801
2^{11}	12	10.550427	14.596

asset price $S_0 = 100$, and strike price $K = 110$. Number of monitoring dates $M = 12$. We choose density support $L = 3$, uniform grid $u \in [-3, 3]$, and $m = 128$ in the Fourier expansion. We list the price of the put under the stochastic volatility model in Figure 9 and Table 4. We achieve 4 digits within 0.86 seconds.

2.3.4 Lookback Options

We can also price lookback options using the proposed fast convolution algorithm, and it works for any exponential Lévy models.

Following [11], the price of a lookback put option is given by

$$P(S_0, K) = e^{-rT} S_0 \mathbb{E}[e^{m_T - x_T} - 1] \tag{40}$$

where $x_T = \log(S_T/S_0)$, $m_T = \log(M_T/S_0)$, and $M_t = \max S_s$, $0 \leq s \leq t$. The probability density of $y_t = m_t - x_t$ can be written as $c_t\delta(x) + g_t(x)$, where $\delta(x)$ is a Dirac function. We have the following relation:

$$m_t - x_t = \max(0, (m_{t-1} - x_{t-1}) + (x_{t-1} - x_t)).$$

Then given c_{t-1} and $g_{t-1}(x)$, we calculate c_t and $g_t(x)$ by the following recursive formula with $c_0 = 1$, $g_0(x) = 0$.

$$\bar{g}_t(x) = c_{t-1} f(x) + \int_0^\infty g_{t-1}(y) f(x-y) dy, \tag{41}$$

$$c_t = \int_{-\infty}^0 \bar{g}_t(x) dx, g_t(x) = \bar{g}_t(x), \tag{42}$$

where f is the density of $x_{t+1} - x_t$, i.e. the transition density function $f(x_{t+1}|x_t)$ as $f(x_{t+1}|x_t) = f(x_{t+1} - x_t)$ for any Lévy processes, which again gives a series of convolutions. We deduce a double-exponential grid for $[0, \infty)$ and $(-\infty, 0]$, and at the final step, the expectation is a integral on $[0, \infty)$, double exponential grid and trapezoidal rule is applied again to get the price.

2.3.4.1 Numerical Example

We price a one year lookback put when the log return follows log-normal model, Merton's jump diffusion model, NIG model and CGMY model. In order to facilitate a comparison, the model parameters are calibrated form the market data of S&P 500 European options in [82]. Also the initial price $S_0 = 100$, and risk-free rate $r = 0.0367$.

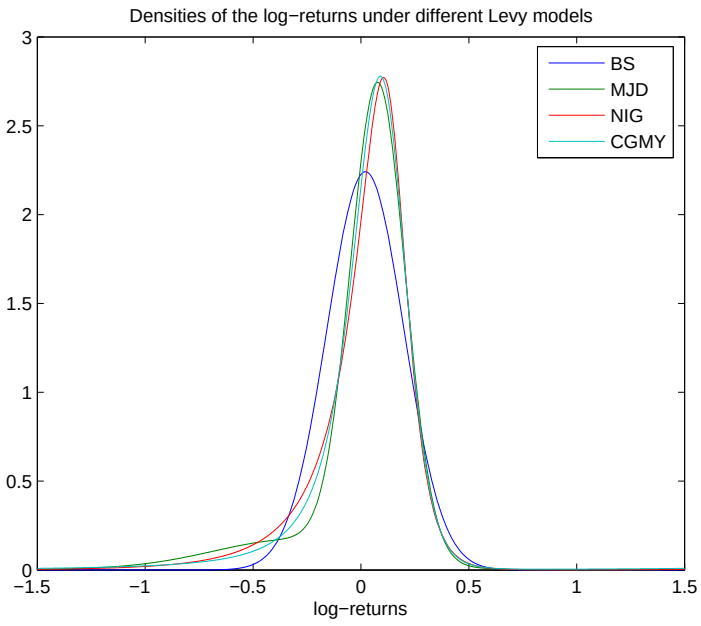

Figure 10: Densities of the Log-returns in 1 year

The calibrated volatility parameter for the log-normal model is $\sigma = 0.17801$.

The calibrated parameters for the Merton's jump diffusion model are $\sigma = 0.126349$, $\alpha = -0.390078$, $\lambda = 0.174814$ and $\delta = 0.338796$.

The calibrated parameters for the NIG model are $\alpha = 6.1882$, $\beta = -3.8941$ and $\delta = 0.1622$.

The calibrated parameters for the CGMY model are $C = 0.0244$, $G = 0.0765$, $M = 7.5515$ and $Y = 1.2945$.

The densities of the log-returns modeled by these Lévy processes in the risk-neutral world are plotted in Figure 10.

The comparison of lookback put prices under different Lévy models are presented in Table 5. In the LN model, the price converges very fast. However, for other Lévy models, it converges a bit slow due to the fat tail behavior in the transition densities. The relative errors are given in Figure 11.

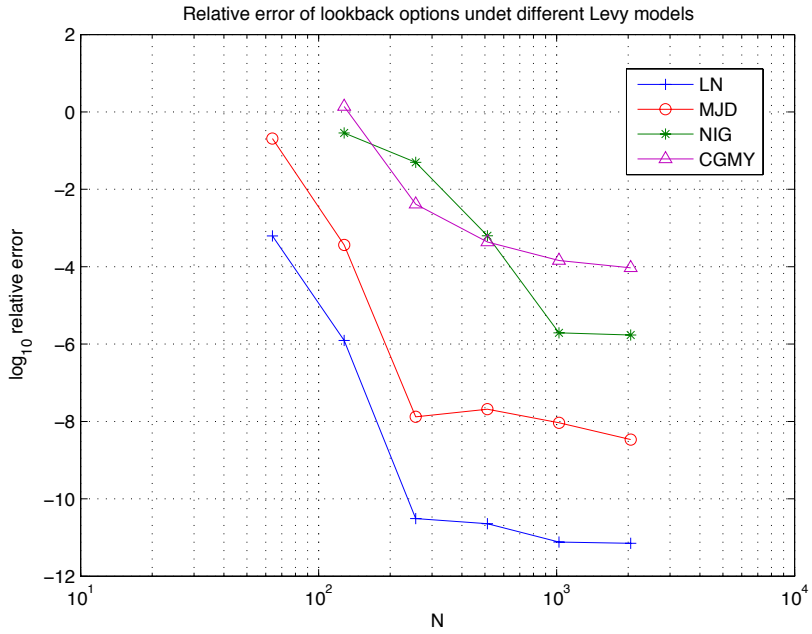

Figure 11: Relative Errors for Lookback Options under Different Lévy Models

Table 5: Price of a Lookback Put under Different Lévy Models

N	M	LN	MJD
2^6	12	13.622075	15.763815
2^7	12	13.630574	13.077226
2^8	12	13.630591	13.072445
2^9	12	13.630591	13.072445
2^{10}	12	13.630591	13.072446
2^{11}	12	13.630591	13.072446
N	M	NIG	CGMY
2^7	12	9.204032	41.277875
2^8	12	12.265347	17.298511
2^9	12	12.914692	17.362650
2^{10}	12	12.906571	17.372705
2^{11}	12	12.906524	17.368559

2.3.5 Asian Options

The price of a discretely monitored Asian option is given by

$$P(S_0, K) = e^{-rT}\mathbb{E}[(A - K)^+], \tag{43}$$

where the average price $A = \frac{1}{T}\sum_{i=0}^{T} S_i$. Let $r_t = x_t - x_{t-1}$ and the mean of r_t be μ_t. Benhamou [5] introduces a recursive formula for sequences A_t and m_t:

$$m_t = \mu_{T+1-t} + \log(1 + \exp m_{t-1}), \tag{44}$$

$$A_t = r_{T+1-t} + \log(1 + \exp(A_{t-1} + m_{t-1})) - m_t, \tag{45}$$

with $m_1 = \mu_T$ and $A_1 = r_T - m_1$. Then $A = \frac{S_0}{T+1}(1 + e^{A_T + m_T})$, so that the price of a Asian option is computable upon knowing the density of A_T. The probability density of A_t is a convolution of r_{T+1-t} and the density of $\log(1 + e^{A_{t-1}+m_{t-1}}) - m_t$.

Denote the density function of A_t as $f_t^A(x)$, the density of r_t as $f^r(x)$ (time independent due to independent increments of any Lévy processes), and the density of $y_t = \log(1 + e^{A_{t-1}+m_{t-1}}) - m_t$ as $g_t(y)$. The following steps summarize the Asian option pricing via fast convolutions.

- At each time t, deduce a double-exponential grid on $[-m_{t+1}, \infty)$ for y.
- Find a grid x by $x = \log(\exp(y + m_{t+1}) - 1) - m_t$.
- Evaluate f_t^A on x.
- Find $g_t(y) = \frac{e^{y+m_{t+1}}}{e^{y+m_{t+1}}-1} f_t^A(x)$.
- Deduce a double-exponential grid on $[-m_{t+2}, \infty)$ for y.
- Find a grid x by $x = \log(\exp(y + m_{t+2}) - 1) - m_{t+1}$.
- Output $f_{t+1}^A(x) = \int_{-m_{t+1}}^{\infty} g_t(y) f(x - y) dy$.

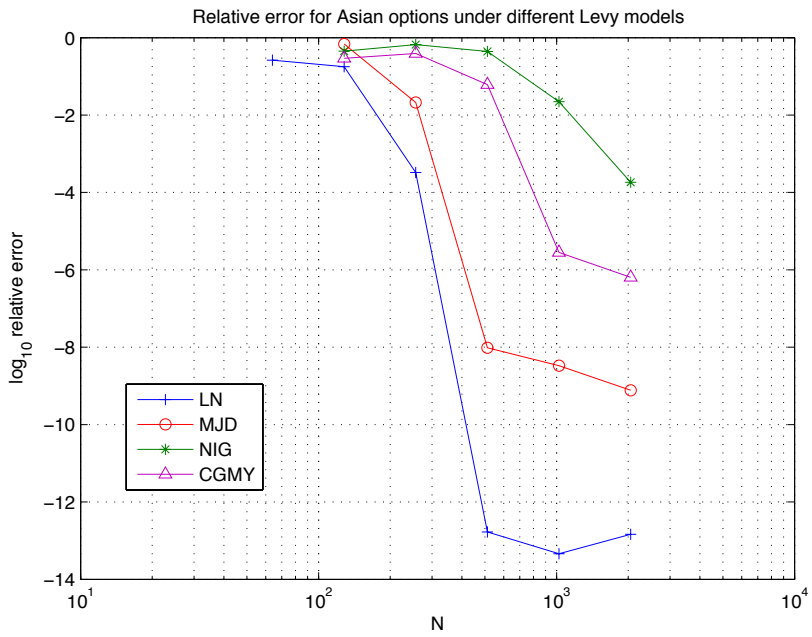

Figure 12: Relative Errors for Asian Options

f_{t+1}^A can be computed by the proposed fast convolution method with a double-exponential transform. At each step, the grid is shifted because of the introduction of the sequence m_t to center the density function of the average A_t.

2.3.5.1 Numerical Example

We price an Asian call option using the same set of parameters for the Lévy processes in Section 2.3.4.1. The comparison of Asian call prices when the asset price is modeled by different Lévy models are presented in Table 6. In the LN model and MJD model, the option price converges very fast. However, for other Lévy models, it converges a bit slow again due to the fat tail behavior in the transition densities. The relative errors are given in Figure 12.

Table 6: Price of a Asian Options under Different Lévy Models

N	M	LN	MJD
2^7	12	9.792488	3.962091
2^8	12	11.908814	12.442391
2^9	12	11.904916	12.710676
2^{10}	12	11.904916	12.710676
2^{11}	12	11.904916	12.710676
N	M	NIG	CGMY
2^7	12	18.302354	10.486487
2^8	12	14.249799	9.029223
2^9	12	13.077276	13.914945
2^{10}	12	12.909521	14.826061
2^{11}	12	12.626188	14.827052

2.4 Multi-Asset Options

The fast convolution algorithm can be extended to handle multi-asset options with path-dependent or early exercise features, e.g., a Bermudan spread option. Spread options are commonly used in energy markets to hedge the spreads in fuel prices or hedge the price spreads at different delivery dates of certain fuel. For example, there are two assets, electricity and natural gas. Let x_t and y_t be the logarithm of electricity and natural gas spot price respectively: $x_t = \log S_t^e$ and $y_t = \log S_t^g$, where S_t^e and S_t^g is the spot electricity and natural gas price at time t. The difference $S_t^e - HS_t^g$ is called spark-spread, where H is the heat rate. A call spark-spread option is an European call option on the spark-spread, whose payoff is

$$h(x_T, y_T) = (e^{x_T} - He^{y_T} - K)_+,$$

and a Bermudan spread option can be exercised on a set of dates t before and on the maturity T. To price a Bermudan spread option, we compare its continuation value with the instant payoff at each exercise date, and the continuation values involve computation of a series of convolutions in 2 dimensions:

$$\int\int_{R^2} v(t+1, x_{t+1}, y_{t+1}) f(x_{t+1}, y_{t+1}|x_t, y_t) dx_{t+1} dy_{t+1}.$$

This 2D convolution cannot be simply calculated by two 1D convolutions. In the next section, we show how the fast convolution algorithm can be extended to 2D with computational complexity $\mathcal{O}(N^2)$, where N is the number of points in each dimension. In Section 2.4.2, we apply 2D convolution to price a Bermudan spread put. Numerical examples are also provided.

2.4.1 Fast Convolution in 2D

We consider the following convolution in 2D:

$$I(u,v) = \int\int_{R^2} g(x,y) f(u-x, v-y) dxdy, \tag{46}$$

where $f(\cdot,\cdot)$ is a joint probability density function, which is smooth and vanishes to zero fast. We choose an input grid with N^2 points (x_s, y_t), $s,t = 1,2,\cdots,N$ and an output grid with M^2 points (u_i, v_j), $i,j = 1,2,\cdots,M$. They need not be uniformly spaced. Then

$$I(u_i,v_j) = \sum_{s,t=1}^{N} q_{s,t} f(u_i - x_s, v_j - y_t),$$

where $q_{s,t} = w_{s,t} \cdot g(x_s, y_t)$, $w_{s,t}$ are the quadrature weights.

As f is a joint probability density, we expand it using Fourier series:

$$f(x,y) = \frac{1}{2L}\frac{1}{2R} \sum_{k=-\infty}^{\infty} \sum_{l=-\infty}^{\infty} a_{k,l} e^{-i\pi(\frac{kx}{L} + \frac{ly}{R})}. \tag{47}$$

where

$$\begin{aligned} a_{k,l} &= \int_{-R}^{R}\int_{-L}^{L} f(x,y) e^{-i\pi(\frac{kx}{L}+\frac{ly}{R})} dxdy. \\ &= \phi(\frac{k\pi}{L}, \frac{l\pi}{R}) \end{aligned} \tag{48}$$

is the corresponding characteristic function. So

$$\begin{aligned} I(u_i,v_j) &= \frac{1}{4LR} \sum_{s=N_i^-}^{N_i^+} \sum_{t=N_j^-}^{N_j^+} q_{s,t} \Big(\sum_{k=-m}^{m} \sum_{l=-n}^{n} a_{k,l} e^{-i\pi[\frac{k(u_i-x_s)}{L} + \frac{l(v_j-y_t)}{R}]} \Big) \\ &= \frac{1}{4LR} \sum_{k=-m}^{m} \sum_{l=-n}^{n} \omega_{i,j,k,l} \end{aligned} \tag{49}$$

$$\omega_{i,j,k,l} = a_{k,l} \sum_{s=N_i^-}^{N_i^+} \sum_{t=N_j^-}^{N_j^+} q_{s,t} e^{-i\pi[\frac{k(u_i - x_s)}{L} + \frac{l(v_j - y_t)}{R}]}, \tag{50}$$

where

$$N_i^- = \min_{s \geq 0}\{u_i - x_s > -L\}, N_i^+ = \max_{s \leq N}\{u_i - x_s < L\},$$

$$N_j^- = \min_{t \geq 0}\{v_j - y_t > -R\}, N_j^+ = \max_{t \leq N}\{v_j - y_t < R\}.$$

Let

$$\beta_{t,i,k} = \sum_{s=N_i^-}^{N_i^+} q_{s,t} e^{-i\pi \frac{k(u_i - x_s)}{L}}, \tag{51}$$

then

$$\omega_{i,j,k,l} = a_{k,l} \sum_{t=N_j^-}^{N_j^+} \beta_{t,i,k} e^{-i\pi \frac{l(v_j - y_t)}{R}}. \tag{52}$$

For a given v_j, when we move to u_{i+1}, we have

$$\omega_{i+1,j,k,l} = a_{k,l} \sum_{t=N_j^-}^{N_j^+} \beta_{t,i+1,k} e^{-i\pi \frac{l(v_j - y_t)}{R}},$$

and

$$\beta_{t,i+1,k} = \beta^0_{t,i+1,k} + \beta^+_{t,i+1,k} - \beta^-_{t,i+1,k},$$

where

$$\beta^0_{t,i+1,k} = e^{ik\pi \frac{\Delta u}{L}} \beta_{t,i,k},$$

and when two ends of x_s change, then

$$\beta^+_{t,i+1,k} = q_{N_i^+ + 1,t} e^{-i\pi \frac{k(u_{N_i^+ + 1} - u_{i+1})}{L}},$$

$$\beta^-_{t,i+1,k} = q_{N_i^-,t} e^{-i\pi \frac{k(u_{N_i^-} - u_{i+1})}{L}}.$$

For a given u_i, when we move to v_{j+1}, we have

$$\omega_{i,j+1,k,l} = \omega^0_{i,j+1,k,l} + \omega^+_{i,j+1,k,l} - \omega^-_{i,j+1,k,l},$$

where

$$\omega^0_{i,j+1,k,l} = e^{il\pi \frac{\Delta v}{R}} \omega_{i,j,k,l},$$

and when two ends of y_t change, then

$$\omega^{+}_{i,j+1,k,l} = a_{k,l}\beta_{N^{+}_{j}+1,i,k}e^{-i\pi\frac{l(v_{N^{+}_{j}+1}-v_{j+1})}{R}}$$

$$\omega^{-}_{i,j+1,k,l} = a_{k,l}\beta_{N^{-}_{j},i,k}e^{-i\pi\frac{l(v_{N^{-}_{j}}-v_{j+1})}{R}}.$$

Now the computational complexity has been reduced to $\mathcal{O}(N^2) + \mathcal{O}(M^2)$.

2.4.2 Bermudan Spread Options

In this section, we apply the 2D fast convolution algorithm to a Bermudan spread option under the following two dimensional mean-reverting model:

$$d\begin{bmatrix} x_t \\ y_t \end{bmatrix} = \begin{bmatrix} \kappa_1(\theta_1 - x_t) \\ \kappa_2(\theta_2 - y_t) \end{bmatrix} dt + \begin{bmatrix} \sigma_1 & 0 \\ \rho\sigma_2 & \sqrt{1-\rho^2}\sigma_2 \end{bmatrix} dW_t + \sum_{i=1}^{2} \Delta Z^i_t, \tag{53}$$

where κ_1 and κ_2 are the mean-reverting coefficients, θ_1 and θ_2 are the long term means, σ_1 and σ_2 are instantaneous volatilities of x_t and y_t, W_t is a $\mathcal{F}_t$-adapted standard Brownian motion under $\mathbb{Q}$ in $\mathbb{R}^2$ with correlation ρ, Z^i_t is a compound Poisson process in $\mathbb{R}^2$ with the Poisson arrival intensity being $\lambda_i, i = 1, 2$, and ΔZ^i_t denotes the random jump size in $\mathbb{R}^2$ with mean jump size being $\mu_i, i = 1, 2$.

Its conditional characteristic function has the following formation (see Appendix A for derivation):

$$\begin{aligned} \phi(u, v; x_t, y_t) &= e^{-Au^2 - Bv^2 - Cuv + iDu + iEv + H(u)} \\ &= \left(\frac{1 - iH_1u}{1 - iH_2u}\right)^{\frac{\lambda_1}{\kappa_1}} \left(\frac{1 - iH_3u}{1 - iH_4u}\right)^{\frac{\lambda_2}{\kappa_1}} e^{-Au^2 - Bv^2 - Cuv + iDu + iEv}, \end{aligned} \tag{54}$$

where

$$A = \frac{\sigma_1^2}{4\kappa_1} - \frac{\sigma_1^2}{4\kappa_1}e^{-2\kappa_1\Delta t},$$

$$B = \frac{\sigma_2^2}{4\kappa_2} - \frac{\sigma_2^2}{4\kappa_2}e^{-2\kappa_2\Delta t},$$

$$C = \frac{\rho\sigma_1\sigma_2}{\kappa_1+\kappa_2}(1-e^{-(\kappa_1+\kappa_2)\Delta t})$$

$$D = \theta_1 + (x_t-\theta_1)e^{-\kappa_1\Delta t},$$

$$E = \theta_2 + (y_t-\theta_2)e^{-\kappa_2\Delta t},$$

$$H_1 = \mu_1 e^{-\kappa_1\Delta t}, H_2 = \mu_1, H_3 = \mu_2 e^{-\kappa_1\Delta t}, H_4 = \mu_2.$$

For a Bermudan spread put, as an analog to the 1D case, the option value at each exercise date can be written as

$$\begin{aligned} p(t,x_t,y_t) &= e^{-r\Delta t}\Big\{\int\int_{D^2_{t+1}} v(t+1,x_{t+1},y_{t+1})f(x_{t+1},y_{t+1}|x_t,y_t)dx_{t+1}dy_{t+1} \\ &+ \int\int_{\bar{D}^2_{t+1}} p(t+1,x_{t+1},y_{t+1})f(x_{t+1},y_{t+1}|x_t,y_t)dx_{t+1}dy_{t+1}\Big\}, \\ &= \Big\{\int\int_{D^2_{t+1}} v(t+1,x_{t+1},y_{t+1})f(x_{t+1}-x_te^{-\kappa_1\Delta t},y_{t+1}-y_te^{-\kappa_2\Delta t}|0,0)dx_{t+1}dy_{t+1} \\ &+ \int\int_{\bar{D}^2_{t+1}} p(t+1,x_{t+1},y_{t+1})f(x_{t+1}-x_te^{-\kappa_1\Delta t},y_{t+1}-y_te^{-\kappa_2\Delta t}|0,0)dx_{t+1}dy_{t+1}\Big\}. \end{aligned}$$

It is again a series of 2D convolutions and the algorithm proposed in the above section can be applied.

The algorithm for Bermudan spread options pricing is summarized as follows:

1. Choose a uniform grid $[-U, U]$ with N points.

2. Fix a uniform grid $[-Y, Y]$ with N points for y_t, $t = 1, 2, \cdots, T$.

3. Given y_T^j, $j = 1, \cdots, N$, compute $x_T^{c,j} = \log(K + He^{y_T^j})$, which is the exercise boundary at T, denoted as ∂D_T^2.

4. Derive a non-uniform grid $x_{T,i}^j$ and weights $w_{T,i}^j$ by equation (33-37).

5. Given $p(T, x_T, y_T) = 0$ on $\bar{D}_T^2$.

6. Loop $t = T - 1$ to 2. **Input:** ∂D_{t+1}^2 and $p(t+1, x_{t+1}, y_{t+1})$.

   - Locate ∂D_t^2 by repeating secant method N times looping y_t. $p(t, x_t, y_t)$ in the iteration is calculated by 2D fast convolution in equation (55).
   - Derive the DE grid $x_{t,i}^j$ and weights $w_{t,i}^j$ by equation (33-37) given $x_t^{c,j}$ on the ∂D_t^2.
   - Compute $p(t, x_t, y_t)$ on $\bar{D}_t^2$ by 2D fast convolution.

   End Loop. **Output:** ∂D_t^2 and $p(t, x_t, y_t)$.

7. Compute price $P = p(0, 0, 0)$.

We price European and Bermudan call spread options under the affine jump dissusion model (53) with the parameters: $\kappa_1 = 1.7$, $\theta_1 = 3.4$, $\kappa_2 = 1.8$, $\theta_2 = 0.87$, $\sigma_1 = 0.74$, $\sigma_2 = 0.34$, $\rho = 0.2$, $\lambda_1 = 6.08$, $\lambda_2 = 7$, $\mu_1 = 0.19$, $\mu_2 = -0.11$, risk-free rate $r = 0.04$, maturity $T = 1$, initial electricity price $S_0^e = 24.63$, initial gas price $S_0^g = 2.105$, heat rate $H = 9.5$, and strike price $K = 5$. European spread call is priced first and it can be valued by one convolution. But in order to check whether the values produced by our algorithm are correct, we can still use some intermediate steps for European options. We set the support of the transition probability

function to be $[-8, 8] \times [-2, 2]$, and the payoff function decays to zero outside region $[0, 12] \times [-10, 8]$. An semi-analytical form of an European spread under an affine jump diffusion is available via inverse FFT. It gives a benchmark value of the European call spread at 15.771749. The value of such an European call spread option by our convolution method as well as the error compared with the benchmark value are given in Table 7. It shows the fast convolution method does converge to the exact value as expected. For Bermudan spread call options with different number of exercise dates, we compute their prices in Table 8. The Monte Carlo simulation gives a reference value for the 2 exercise dates Bermudan spread call at 18.867930 with standard error of 0.251212 in 29.56 seconds (10,000 paths). We note the computational time of Bermudan spread options under 2D fast convolution is not faster than the Monte Carlo. This is because the major computation burden comes from searching the exercise boundary in 2D, though theoritically the computational complexity is $\mathcal{O}(N^2)$. However, the convolution based algorithm is still superior to Monte Carlo simulation, especially for path-dependent options. Kou and Wang [61] point out that Monte Carlo simulation has systematic discretization bias in pricing path-dependent options. This bias is difficult to be reduced because for an example of lookback options, simulation approximates the maximum of a coutinuous process by the maximum of a discrete process. The same reason applies to barrier options and Asian options. Asmussen et al. [3] show that the discretization error decays at an order of $1/2$ with respect to the number of paths, which is much slower than the convolution method.

2.5 Conclusion

Energy firms commonly utilize exotic derivatives for hedging their exposure to the price and volumetic risks in electricity markets. The complex contract provisions

Table 7: European Spread Call Option under Affine Jump Diffusion Model

N	M	Value	Absolute Error	Time (sec)
$2^6 \times 2^7$	1	15.780483	0.0087	0.13
$2^7 \times 2^8$	1	15.771763	1.4E-5	0.43
$2^8 \times 2^9$	1	15.771741	8.0E-6	0.89
$2^6 \times 2^7$	2	15.786538	0.0148	6.28
$2^7 \times 2^8$	2	15.771787	3.8E-5	23.56
$2^7 \times 2^8$	4	15.771772	2.3E-5	67.98

Table 8: Bermudan Spread Call Option under Affine Jump Diffusion Model

N	M	Value	Time (sec)
$2^6 \times 2^7$	2	18.667381	33.50
$2^7 \times 2^8$	2	18.632833	131.88
$2^8 \times 2^9$	2	18.632941	509.47
$2^6 \times 2^7$	3	19.744085	64.04
$2^7 \times 2^8$	3	19.670257	260.51
$2^6 \times 2^7$	4	20.308621	101.38
$2^7 \times 2^8$	4	20.192349	410.06

of these derivatives, such as path-dependency and early-exercising, make their pricing time consuming. The prices of these path-dependent options and early-exercise options, which include barrier, Bermudan, lookback and Asian options, can be evaluated through a series of convolutions of a given function against the transition density of the underlying electricity prices. In this chapter, we propose a fast algorithm to compute a convolution which reduces the computational complexity from $\mathcal{O}(N \log N)$ to asymptotically $\mathcal{O}(N)$, where N is the number of discretized price levels in computing the convolution. The computational complexity of our method in pricing path-dependent options and Bermudan options is $\mathcal{O}(MN)$, where M is the number of monitoring/exercise dates. The algorithm is general to a broad class of stochastic electricity price models, including AJD processes and Lévy processes, because it takes the characteristic function of the underlying electricity price distribution as an input,

which is known in closed-form for such price models.

The proposed fast convolution algorithm is applicable to non-uniform grids instead of uniform grids in FFT. This feature allows us to take advantage of the double-exponential integration formula to speed up the rate of convergence in option pricing. Theoretically, the error of our method decreases faster than any negative power of N. Our computational framework can also handle lookback and Asian options due to the use of non-uniform grids.

We also extend the fast convolution algorithm to two dimensions in order to price spread options with path-dependent and early exercise features. Numerical examples show the fast convolution method is flexible and efficient pricing different types of exotic options in electricity markets.

CHAPTER III

AN INCENTIVE-BASED DEMAND RESPONSE CONTRACT DESIGN FOR THERMOSTATICALLY CONTROLLED LOADS IN A SMART GRID

3.1 Introduction

A smart grid is being developed rapidly in the United States to potentially resolve many challenges faced by the future electric power industry. It uses information and communication technology to improve the efficiency, reliability, economics, and sustainability of the production and distribution of electricity in an automated manner [37]. For example, the sophisticated control capability of a smart grid facilitates the integration of intermittent and variable renewable energy resources, and smart meter technology enables many possibilities in demand side management. Renewable energy capacity in the United States nearly doubled from 43.5GW in 2008 to 85.7GW in 2012. In particular, wind power installed capacity reached 48 GW in 2012, and the electricity production from wind power grows 10 times to 120 billion kWh in the past ten years. The growth in renewable energy helps reduce the carbon emission by 13% and reduce the energy consumption by 6.4% from 2007 [39]. However, renewable energy resources are costly to integrate into the current power grid due to some of their different features from the conventional coal and gas generation ones. On the one hand, renewables are highly variable and intermittent. It is hard to accurately predict the renewable energy production; even during the same hours on two different dates, the patterns of renewables might behave dramatically different. The increasing uncertainty in the supply side requires fast responsive generators as additional reserves when load serving entities (LSEs) are short of renewable energy supply. On the

other hand, renewable energy is limited dispachable. For example, when wind power resources are excessive, operators cannot ramp up or ramp down the wind generators as they can conventional ones in order to adjust the outputs. It is feasible to curtail some wind turbines, but it might waste this cheap and clean energy.

High uncertainty in renewable energy supply turns system operators and LSEs to managing demand instead of managing supply. Demand response contracts are tools designed to create demand flexibility (see [36] for a detailed survey of demand response mechanisms). In addition to traditional demand response programs offered by system operators, researchers are looking for other sources of flexible loads as demand responses. For example, Papavasiliou and Oren [78] study directly coupling deferrable loads, such as plug-in electric vehicles charging, laundry, etc., with renewable energy resources to mitigate the inherent intermittency and variability. Husen et al. [55] address the control of multiple lighting systems in a building to provide demand response services. Among sources of energy consumption, the Department of Energy in 2007 reported that thermostatically controlled loads (TCLs) including cooling, air conditioning and refrigerating, account for 60%-70% of U.S. household energy consumption. In the smart grid environment, LSEs are able to communicate with commercial/residential thermostat devices remotely via programmable thermostats. In practice, a variety of pilot demand response programs on curtailing and controlling TCLs have been deployed in several states. In Texas, Austin Energy successfully recruited 2,000 customers to participant in its "Rush Hour Rewards" program last summer. Austin Energy gives participants one-time $85 rebate toward the purchase of a smart thermostat, like "Nest". When a period of high demand is expected, they send an alert to the programmable thermostats to notify participants that their thermostats will be set higher during that period so they use less air-conditioning. ERCORT has been implementing such polit programs since 2007. According to their

experience, an average demand reduction of 0.6 kW is estimated for each participating household, and wholesale prices could be reduced by over 60% during the peak-periods. The total value saved from controlling customers' thermostats during peak-periods is estimated to be $160 million (see [45]). In California, Southern California Edison and San Diego Gas & Electric partnered with major thermostat makers to leverage smart thermostats in 2013. They offer participants $1.25 credit per kWh saved during peak days. For customers enrolling with "EnergyHub" brand thermostats, the set-points may be adjusted by up to 6°F, although EnergyHub usually precools homes to avoid discomfort. These programs illustrate that peak-period loads can be reduced by controlling TCLs, however, the potential of TCLs has not been fully explored. The rebate plan and the set-point control range can be designed in a more flexible and customer-friendly way to encourage participation. By directly controlling customers' thermostats within their self-selected control ranges, LSEs achieve flexible load profiles to balance the power output fluctuation from intermittent and variable renewable energy resources, such as wind and solar.

Modeling of TCLs is well documented in the literatures. Ihara and Schweppe [56] start to model the dynamics of a single thermostat in the population from a physical view. Malhame and Chong [69] describe the dynamics of aggregated TCLs by using Fokker-Planck equation. Ucak and Dokuyucu [91] use Monte Carlo simulation to study TCLs as a direct control method. Lu et al. [67] discuss the modeling of uncertainties in aggregated TCLs using a state queueing model. Recently, researchers have been exploring the potentials of TCLs as demand response in tracking an exogenous renewable generation signal. Callaway [14] proposes a minimum variance controller of manipulating thermostat set-points of a homogeneous group to track a wind power generation signal. Kundu et al. [62] derive a transfer function relating the aggregate response of a homogeneous group of TCLs to uniform variation of thermostat set-points, and present a linear quadratic regulator for tracking purposes. Both works

assume a known reference signal. However, a long-term forecast, even in hour ahead, is far from accurate. Using forecasted values as a whole trajectory to get a close loop control signal will produce large control errors in the real time operations. Koch et al. [60] extend the idea to a heterogeneous group of TCLs, and apply the model predictive control (MPC) technique to solve for a control rule, which only requires one step ahead forecast of wind power as a model input. However, their paper assumes the central control cannot override customers' settings and cannot cause any discomfort to customers. This means the room temperature must always stay inside the set-point dead band, and LSEs can only shift the operating cycles of thermostat devices. This limits the availability of TCLs, especially during some extreme events, e.g. wind production is extremely low. LSEs do not have sufficient amount of flexible loads for control, which prevents matching the demand to the wind profile. In order to maintain the system reliability in such situations, costly additional reserves have to come in places of renewables, or LSEs have to purchase electricity in the wholesale market at very high prices.

In this chapter, we would like to expolit the potential of TCLs as a source of demand response for renewable energy integration. We assume customers are willing to bear some discomfort by allowing the temperature to be outside of the set-point dead band in exchange for some rewards. LSEs offer an incentive-compatible reward scheme to compensate the discomfort that customers endure as a result of rendering the control of their loads to LSEs. In this way, LSEs gain more flexible control of customers' thermostat-related loads to absorb the variability of renewable energy outputs. By offering different levels of rebate associated with different set-point adjustment ranges, LSEs are able to differentiate customers into several control groups according to their preference types. Customers decide whether to participate and which rebate/temperature set-point range to subscribe to based on their preferences. We model customers' preferences on room-temperature through a utility function

which characterizes the reward and discomfort tradeoff of different choices of room temperature set-point by a customer. As long as the contracts are designed to be incentive compatible and individually rational, LSEs can vary the rebate offering levels to induce different degrees of customers' participation and get different contract-subscription distributions. LSEs then come up with a control law for each group optimizing their performance metrics. Two examples of performance metrics are considered. The first one minimizes the opportunity costs of purchasing in the wholesale electricity market when LSEs lack concerned renewable power outputs, and the second one minimizes the weighted sum of squared errors of tracking an output level of renewable resources. We apply MPC to handle the control problem. MPC is attractive here for two reasons. First, it is easily applicable to both linear and quadratic control problem with inequality constraints (ranges of set-point adjustment). Second, as an input of MPC, the reference signal is updated according to the short-term 10 minutes forecasting at each step. However, LSEs have to offer the reward/discomfort scheme to customers before the uncertainties in the renewable production and the electricity wholesale spot prices are realized. In order to obtain an optimal contract parameters design, we present a two-stage stochastic programming, in which LSEs minimize the expected total costs among different scenarios.

The rest of the chapter is organized as follows: in Section 3.2 we provide an overview of the contract structure and key contract parameters. A two-stage stochastic programming framework addressing the optimal contract design is proposed in Section 3.3. We also discuss the dynamics of TCLs, the solution to LSEs' control problem by MPC, and customers' choices in this section. In Section 3.4 we provide a case study which includes comparisons of control strategies under two performance metrics, and under different rebate level offerings. We also analyze the sensitivity of contract parameters to customer subscription distributions, the lump sum payments to customers, and the total costs of this mechanism. We conclude in Section 3.5.

3.2 Contract Structure

In the context of air-conditioning or heating, we assume LSEs own renewable energy resources which are designated to serve a load from N customers. LSEs offer a reward scheme $(\mathbf{s}, \bar{\mathbf{u}})$ containing m different levels of reward and temperature set-point range to customers. $\mathbf{s}_{m\times 1} = (s_1, s_2, \cdots, s_m)^T$, where s_j is the bill savings to the customers who choose contract j, $j = 1, 2, \cdots m$ (from LSEs' prespective, it is the rebate they pay to the customers). $\mathbf{u}_{m\times 1}$ is the controller (the change of temperature set point). An upper bound $\bar{\mathbf{u}}$ and a lower bound $-\bar{\mathbf{u}}$ for the controller specify the ranges of the controller for each group. Under cooling environments, LSEs need to raise the temperature set-point in order to reduce the power consumption, i.e. they exercise control $0 < \mathbf{u} < \bar{\mathbf{u}}$, then the participating customers will receive rebates $\mathbf{s}$ on their utility bills.

LSEs can change the key contract parameters $(\mathbf{s}, \bar{\mathbf{u}})$ to get a different subscription from customers, which follows different dynamics of TCLs. For example, increasing the rebate levels of every group will definitely get more customer subscription, and as a result, will increase the loads available to release. Increase the rebate level of a single group will increase the subscription of that group and change the distribution of control groups as well. LSEs need to find the optimal levels of rebate and associated subscription, which achieve certain targets, such as minimizing the total costs or the tracking errors. Figure 13 gives a simple illustration of the entire process. There are two stages in the process. At stage 1, an LSE offers two contracts, \$2 monthly rebate for 0.2°C adjustment and \$5 monthly rebate for 0.5°C adjustment. We assume there are 10 target customers. Based on their own preferences, 5 of them choose contract I, 3 of them choose contract II and the rest 2 do not participate. In this case, the LSE will pay $\$2*5+\$5*3 = \$25$ per month to gain access to TCLs. At stage 2, the LSE starts to control the thermostats of the 8 subscribers. When there is renewable shortage, it lowers the loads from the subscribers to prevent high purchasing costs in the wholesale

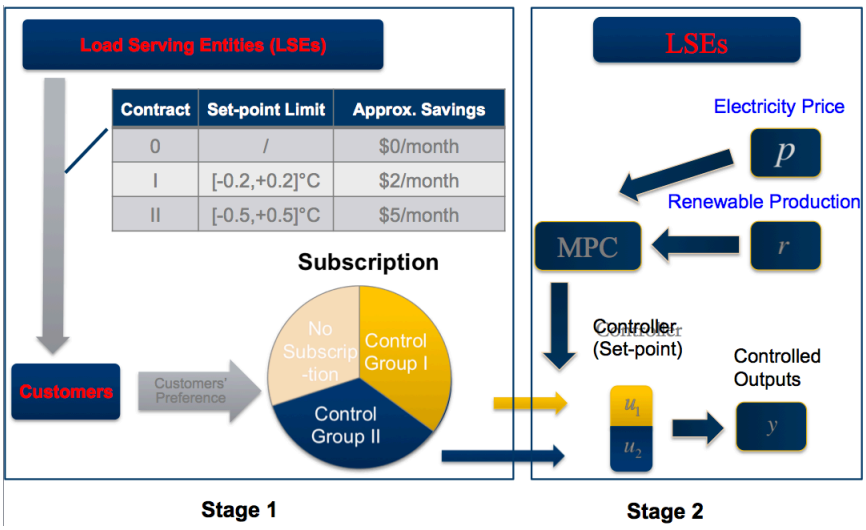

Figure 13: An Overview of the Model

market. The LSE will implement an optimal strategy which minimizes the purchasing costs. Since the renewable energy production and the electricity wholesale price are random and unknown at stage 1, the LSE estimates an expected purchasing cost and choose an optimal contract design to minimize its lump sum payment plus the expected purchasing cost.

3.3 Model Description

In this section, we describe how to design optimal rebate levels $\mathbf{s}$ to minimize LSEs' cost of integrating uncertain renewable energy resources via controlling TCLs. We formulate it as a two-stage stochastic programming in Section 3.3.1. By working backward, we then discuss if LSEs were given a scenario, how can they develop a control strategy under contract design parameters $(\mathbf{s}, \bar{\mathbf{u}})$ and customers' subscription $\mathbf{N}$? In Section 3.3.2 we utilize a state-space form of a linear system to describe the dynamics of TCLs in terms of the customers' subscription. At the second stage, we define an optimal control problem subject to the linear system with inequality constraints. We solve it by MPC in Section 3.3.3. At the first stage, we need to answer

whether customers participate and how they choose which contract to subscribe to. We study customer preferences in Section 3.3.4. All the notations appearing in the following text are listed in Appendix B.1.

3.3.1 A Two-Stage Stochastic Programming

Due to high uncertainties in renewable energy resources and load profiles, when LSEs make decisions on the levels of rebate paid to customers, they do not have much information about which scenario is going to be realized for the renewable energy outputs and the wholesale spot prices. There are two stages in the decision process. At the first stage, LSEs need to determine the contract design parameters without the realization of uncertainties (the here and now stage), customers observe the contracts and decide a subscription, which has an impact on the dynamics of the TCLs (though it does not have an impact on the realization of uncertainties). At the second stage, the LSEs solve a control problem minimizing the control costs based on the observations of renewable energy outputs and wholesale spot prices (the wait and see stage).

The stochastic programming can be formulated as follows:

$$\min_{\mathbf{s}} \quad \mathbf{N^T s} + \mathbb{E}[J(y_t(\mathbf{N}(\mathbf{s}, \bar{\mathbf{u}}), p_t, r_t)] \tag{55}$$

$$s.t. \quad \mathbf{s} > \mathbf{0}. \tag{56}$$

$\mathbf{N^T s}$ is the lump sum payment to the customers who participate in the contract offerings. $J(y_t(\mathbf{N}(\mathbf{s}, \bar{\mathbf{u}}), p_t, r_t)$ is the control cost for each scenario, where $y_t(\mathbf{N}(\mathbf{s}))$ is the TCLs under control at time t depending on the subscription $\mathbf{N}$. And the subscription $\mathbf{N}$ is a function of the rebate level $\mathbf{s}$. We optimize the expected costs among all possible scenarios. In order to solve this two-stage problem, we need to construct different scenarios and associated probabilities. A simple and popular way to handle this is by means of Monte Carlo sampling and approximating the expectation by the sample average. This needs a stochastic model to describe the

joint distribution of renewable energy outputs and electricity prices, for example, [78]. It requires a process of calibrating the model parameters from renewable energy and price data sets. Although, this takes extra computation, the resulting distribution may not well describe the variable renewable outputs. Bootstrap sampling method is an alternative here, which is model-free and preserves the seasonality patterns in renewable energy and price processes. After solving the two-stage problem by the bootstrapped sample average given a set of rebate levels, we apply a random search to find the optimal rebate levels.

3.3.2 State-Space Representation

Kundu et al. [62] proposed a state-space model for a homogeneous group of TCLs as follows:

$$\dot{x} = Ax + Bu \tag{57}$$

$$y = Cx + Du \tag{58}$$

where the model output y is the change of total power outputs from the steady-state, and the input u is the shift in thermostat set-points.

We extend this model to homogeneous TCLs (with the same characteristics of thermostats) with different initial temperature set-points and contract subscriptions. We assume there is an initial distribution of customers' temperature set-point θ_0 with n possible values θ_0^i, $i = 1, 2, \cdots, n$. Each possible set-point has an equal probability. As we have m different contract offerings, there are in total mn groups of customers. The dynamics of TCLs for each group follow the model (57)-(58). For $i = 1, 2, \cdots, n$ and $j = 1, 2, \cdots, m$, we have

$$\dot{\mathbf{x}}_{\mathbf{ij}} = \mathbf{A_i x_{ij}} + \mathbf{B_{ij}} u_j \tag{59}$$

$$y_{ij} = \mathbf{C_0 x_{ij}} + D_j u_j, \tag{60}$$

where $\mathbf{A_i}, \mathbf{B_{ij}}, \mathbf{C_0}, D_j$ depend on thermostats parameters, given in Appendix B.2.

We combine the states of group ij into one state vector $\mathbf{x}$ and derive the aggregated power outputs $y = \sum_{i,j} y_{ij}$ in a new state-space form as follows:

$$\dot{\mathbf{x}} = \mathbf{A}\mathbf{x} + \mathbf{B}\mathbf{u} \tag{61}$$

$$y = \mathbf{C}\mathbf{x} + \mathbf{D}\mathbf{u} \tag{62}$$

where $\mathbf{A}, \mathbf{B}, \mathbf{C}, \mathbf{D}$ are also given in Appendix B.2. This is the model we will use in the subsequent control problem.

3.3.3 Model Predictive Control for TCLs

Given design parameters $(\mathbf{s}, \bar{\mathbf{u}})$ and customers' subscription $\mathbf{N}$, we propose two objectives for the control problem in the second stage. The first one minimizes the purchasing cost in the wholesale market due to wind power shortage [1]:

$$J = \min_{\mathbf{u}} \int_0^T p_t (y_t - r_t)^+ dt \tag{63}$$

$$s.t. \quad -\bar{\mathbf{u}} \leq \mathbf{u} \leq \bar{\mathbf{u}}. \tag{64}$$

The second one is formulated as a linear-quadratic (LQ) tracking problem, and we treat the weighted squared errors as well as the control costs as our objective:

$$J = \min_{\mathbf{u}} \frac{1}{2} \int_0^T p_t^2 (y_t - r_t)^2 + \mathbf{u}^{\mathbf{T}} \mathbf{R} \mathbf{u} dt \tag{65}$$

$$s.t. \quad -\bar{\mathbf{u}} \leq \mathbf{u} \leq \bar{\mathbf{u}}. \tag{66}$$

In the traditional control theory, we need to know the whole trajectory of r_t in $[0, T]$. However, accurately forecasting the wind power production long term, say one day or even several hours, is quite hard. Inaccurate forecasts may cause the controlled outputs to deviate from the desired trajectory in the long run. We apply MPC to handle the problem by doing on-line optimization across a time window at each step with updated states and inputs. At time k, MPC finds number N_c of controllers which

[1] If LSEs own conventional generators and use them to cover the wind power shortage, the opportunity cost is identical to selling power at the wholesale price

minimize the costs across N_p steps. The reference signal during N_p steps is assumed to be constant at r_k. Thus, only the state estimation and wind power forecasts are needed at the step to perform the optimization. Both of them are fairly accurate.

We discrete the system (61)-(62) into:

$$\mathbf{x_{k+1}} = \mathbf{A x_k} + \mathbf{B u_k} \tag{67}$$

$$y_k = \mathbf{C x_k} + \mathbf{D u_k}, \tag{68}$$

and the augmented system is

$$\mathbf{Y_k}_{N_p \times 1} = \mathbf{F}_{N_p \times 2mn} \mathbf{x_k}_{2mn \times 1} + \mathbf{G}_{N_p \times m(N_c+1)} \mathbf{U_k}_{m(N_c+1) \times 1}. \tag{69}$$

The derivation of $\mathbf{F}$ and $\mathbf{G}$ is given in the Appendix B.2.

At time k, the control problem (63)-(64) can be solved by the following linear programming (LP). The derivation and the coefficients are also given in Appendix B.2.

$$J_k = \min_{\mathbf{Z,U}} \mathbf{f_k^T Z_k} \tag{70}$$

$$s.t. \quad \mathbf{H}[\mathbf{Z_k}, \mathbf{U_k}]^{\mathbf{T}} \leq \mathbf{h}. \tag{71}$$

At time k, the control problem (65)-(66) can be solved by the following quadratic programming (QP) with inequality constraints:

$$J_k = \min_{\mathbf{U}} (\mathbf{S_k} - \mathbf{Y_k})^{\mathbf{T}} \mathbf{Q_k} (\mathbf{S_k} - \mathbf{Y_k}) + \mathbf{U_k^T} \bar{\mathbf{R}} \mathbf{U_k} \tag{72}$$

$$s.t. \quad \mathbf{M U_k} \leq \mathbf{m_0}, \tag{73}$$

where $\mathbf{Q_k} = \text{diag}(p_k^2 \Delta t, \cdots p_{k+N_p}^2 \Delta t)_{N_p \times N_p}$, $\bar{\mathbf{R}} = \text{diag}(\mathbf{s^2}, \mathbf{s^2}, \cdots, \mathbf{s^2}) r_w$. Without constraints, we have $\mathbf{U_k} = (\mathbf{G^T Q_k G} + \bar{\mathbf{R}})^{-1} \mathbf{G^T Q_k^T} (\mathbf{S_k} - \mathbf{F x_k}) = -\mathbf{K_x x_k} + \mathbf{K_r r_k}$. Here, we use Active Set method to solve the constrained quadratic programming. So far, we are able to solve the second stage problem which optimizes LSEs' targets given rebate contract offerings and customers' subscription.

3.3.4 Customers' Preference and Participation

At the first stage, LSEs offer a set of rebate/discomfort levels $(\mathbf{s}, \bar{\mathbf{u}}) = (s_j, \bar{u}_j)$, $j = 0, 1, \cdots m$ ($s_0 = 0$ and $\bar{u}_0 = 0$ stand for opt-out of these contracts). They need to estimate the number of customers subscribing to each contract N_j, $j = 0, 1, \cdots, m$. We start to derive some conditions under which the contracts offered are gauranteed to be incentive compatible (IC) and individually rational (IR). For such offerings, we study customers' choices through their utility functions. Based upon this study, LSEs have information to imply the number of customers of each group and to estimate how the subscription changes with respect to the change of contract parameters.

The contracts offered are different pairs of reward associated with a discomfort level. Customers have experiences in choosing from different price and quantity combos of a product. For example, sellers sometimes offer customers different packing sizes of a certain good and charge them different prices. Different types of customers will purchase different sizes. In economic theory, this is called second-degree price discrimination, which states that if a seller does not know customer types, but the inverse demand function of each type, the seller can design a pricing scheme such that each type of customers choose their corresponding price and quantity bundle. Here, customers choose from different levels of discomfort, represented by temperature set-points adjustment ranges. They trade discomfort $\bar{u}_j$ for reward s_j. To analyze customers' choices, we make a few assumptions. 1) We assume a continuum of customer types $\alpha \in [\underline{\alpha}, \overline{\alpha}]$, and a single customer's type α is drawn from a distribution $F(\alpha)$. The density function is denoted as $f(\alpha)$, $\alpha \in [\underline{\alpha}, \overline{\alpha}]$. 2) We define customers' utility functions $V(s, \bar{u}; \alpha)$. In second-degree price discrimination, the utility function is defined as the consumers surplus, which is the integration of the inverse demand function minus the cost. Here, we denote an inverse discomfort function $d(\bar{u}, \alpha)$, $\bar{u} \geq 0$, representing the rewards that a type α customer requires to compensate every unit of change in the temperature set-point adjustment limit $\bar{u}$.

The aggregated discomfort $D(\bar{u}, \alpha)$ is the integration of $d(\bar{u}, \alpha)$:

$$D(\bar{u}, \alpha) = \int_0^{\bar{u}} d(\mu, \alpha) d\mu.$$

Then the utility function of a type α customer $V(s, \bar{u}; \alpha) = s - D(\bar{u}, \alpha)$ depends on the lump sum payment s (rewards), the set-point adjustment limit $\bar{u}$ (discomfort), and the customer's type α. In equilibrium, each customer chooses a contract offer which maximizes his/her utility. We denote the equilibrium utility function $U(\alpha) = \max_j V(s_j, \bar{u}_j; \alpha) = V(s(\alpha), \bar{u}(\alpha); \alpha)$. 3) We assume the inverse discomfort function is positive and increasing, i.e. $d(\bar{u}, \alpha) > 0$ and $\partial d(\bar{u}, \alpha)/\partial \bar{u} > 0$. Moreover, by Spence-Mirrlees condition ([72, 85]), we also assume

$$\frac{\partial^2 D(\bar{u}, \alpha)}{\partial \alpha \partial \bar{u}} > 0.$$

This implies that $\partial D/\partial \bar{u} > 0$ and $\partial D/\partial \alpha > 0$ for all $\bar{u} > 0$. The higher α is, the more discomfort averse the customer is. The bottom line of LSEs' contract offerings is to ensure a customer who is more tolerant to discomfort chooses a larger range of set-point adjustment. This means LSEs need to design a pricing scheme such that a pair $(s(\alpha), \bar{u}(\alpha))$ is preferred to type α customer, i.e. it is IC and IR.

Based on the above assumptions, the following conditions guarantee an IC and IR contract design. The proofs to Lemma 1, Proposition 1 and Theorem 1 are quite standard in the textbook ([8]).

Lemma 3.1. *A necessary condition for a pricing scheme* $(\mathbf{s}, \bar{\mathbf{u}})$ *to be incentive compatible and individually rational is that* $\bar{u}(\cdot)$ *is non-increasing.*

Proposition 3.1. *If a pricing scheme* $(\mathbf{s}, \bar{\mathbf{u}})$ *is incentive compatible and individually rational, we have*

$$U'(\alpha) = -\frac{\partial D(\bar{u}(\alpha), \alpha)}{\partial \alpha} \tag{74}$$

Theorem 3.1. *If a pricing scheme* $(\mathbf{s}, \bar{\mathbf{u}})$ *satisfies (74) and* $\bar{u}(\cdot)$ *is a non-increasing function, then it is incentive compatible and individually rational.*

If we view non-subscription as a contract offer $(0, 0)$, we have $m + 1$ different levels in a pricing scheme $(\mathbf{s}, \bar{\mathbf{u}})$. In our setting, $\bar{u}(\cdot)$ in what LSEs offer is a stepwise non-increasing function, which jumps at α_j:

$$\bar{u}(\alpha) = \bar{u}_j, \alpha_j < \alpha \leq \alpha_{j-1}. \tag{75}$$

It is obviously a special case of an IC and IR scheme. In order for LSEs to estimate customers' subscription to an IC and IR pricing scheme, they need to infer a distribution of customer type $f(\alpha)$, determine the switching points α_j, and then calculate the numbers of customers subscribing to each contract. The switching point happens when a type of customer is indifferent to two consequent contract offers. Theorem 1 implies that the utility function $U(\cdot)$ is continuous in α, which enables LSEs to find the type α's at switching points.

Corollary 3.1. *The utility function $U(\cdot)$ is continuous in α, and at α_j, we have*

$$s_j - D(\bar{u}_j, \alpha_j) = s_{j+1} - D(\bar{u}_{j+1}, \alpha_j). \tag{76}$$

In terms of the distribution of type $f(\alpha)$, LSEs can start with some surveys or pilot programs to get an initial subscription N_j to contracts $(s_j, \bar{u}_j)$, $j = 1, 2, \cdots, l$. After finding the switching type points α_j, LSEs can infer a distribution $f(\alpha)$ from N_j. A distribution with l parameters can be inferred by l contracts (including no subscription). For example, LSEs need 2 contracts in the survey to infer a normal distribution of customer type. If LSEs offer N contracts, they are able to cover the true type distribution, which allows LSEs to easily to compute the subscription $\mathbf{N}$ for other contract offerings.

LSEs are also able to find how α_j and N_j change with respect to s_j. Denote $E(\cdot) = \partial D/\partial \alpha$, we have the following propositions. The derivations are given in Appendix C.

Proposition 3.2. *The increase in reward s_j will have a positive effect on α_{j-1} but a*

negative effect on α_j, for $j = 1, 2, \cdots, m$:

$$\frac{d\alpha_j}{ds_j} = -\frac{1}{E(\bar{u}_{j+1}, \alpha_j) - E(\bar{u}_j, \alpha_j)} < 0, \tag{77}$$

$$\frac{d\alpha_{j-1}}{ds_j} = \frac{1}{E(\bar{u}_j, \alpha_{j-1}) - E(\bar{u}_{j-1}, \alpha_{j-1})} > 0. \tag{78}$$

Proposition 3.3. *The increase in reward s_j will have a positive effect on N_j but a negative effect on N_{j-1} and N_{j+1}, for $j = 1, 2, \cdots, m-1$:*

$$\frac{dN_j}{ds_j} = N\left[\frac{f(\alpha_{j-1})}{E(\bar{u}_j, \alpha_{j-1}) - E(\bar{u}_{j-1}, \alpha_{j-1})} + \frac{f(\alpha_j)}{E(\bar{u}_{j+1}, \alpha_j) - E(\bar{u}_j, \alpha_j)}\right] > 0, \tag{79}$$

$$\frac{dN_{j-1}}{ds_j} = -N\left[\frac{f(\alpha_{j-1})}{E(\bar{u}_j, \alpha_{j-1}) - E(\bar{u}_{j-1}, \alpha_{j-1})}\right] < 0, \tag{80}$$

$$\frac{dN_{j+1}}{ds_j} = -N\left[\frac{f(\alpha_j)}{E(\bar{u}_{j+1}, \alpha_j) - E(\bar{u}_j, \alpha_j)}\right] < 0. \tag{81}$$

For s_m, its change only affects N_m and N_{m-1}:

$$\frac{dN_m}{ds_m} = N\left[\frac{f(\alpha_{m-1})}{E(\bar{u}_m, \alpha_{m-1}) - E(\bar{u}_{m-1}, \alpha_{m-1})}\right] > 0, \tag{82}$$

$$\frac{dN_{m-1}}{ds_m} = -N\left[\frac{f(\alpha_{m-1})}{E(\bar{u}_m, \alpha_{m-1}) - E(\bar{u}_{m-1}, \alpha_{m-1})}\right] < 0. \tag{83}$$

In addition, we compute the marginal utility for s and $\bar{u}$:

$$MU_s = 1, MU_{\bar{u}} = -\frac{\partial D}{\partial \bar{u}} < 0.$$

This indicates that $\bar{u}$ is a "bad", and its marginal utility is also diminishing. The marginal rate of substitution is calculated as well:

$$MRS = -\frac{MU_s}{MU_{\bar{u}}} = \frac{1}{\partial D/\partial \bar{u}} > 0.$$

It decreases when $\bar{u}$ increases, meaning that with a larger range of set-point adjustment, a customer requires a higher rebate level to maintain his/her utility.

We consider a linear inverse discomfort function

$$d(\bar{u}, \alpha) = \bar{u} + \alpha,$$

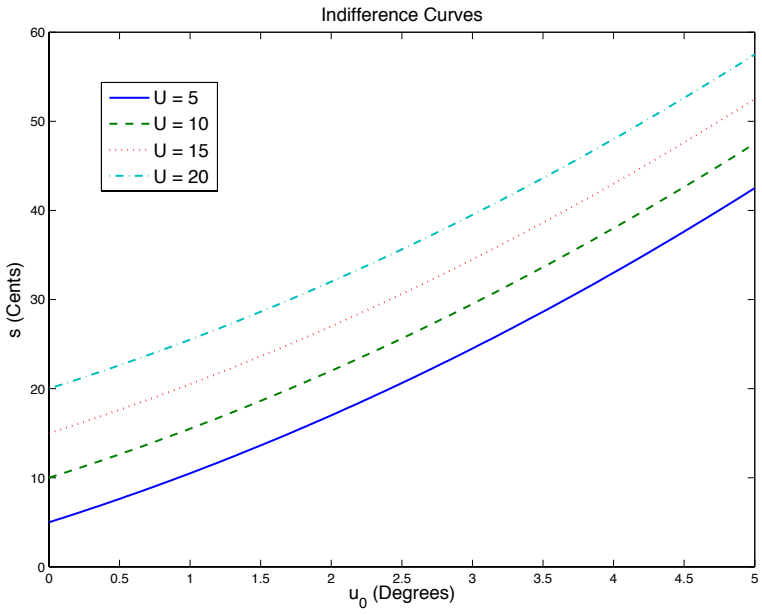

Figure 14: Utility Indifference Curves

Then the utility function is given as follows:

$$U(s, \bar{u}) = s - \frac{1}{2}\bar{u}^2 - \alpha\bar{u},$$

where $\alpha \in [\underline{\alpha}, \overline{\alpha}]$ is the type of customers [2]. Figure 14 plots several indifferent utility curves with $\alpha = 5$.

3.4 A Case Study

In this section, we perform a case study to illustrate how customers subscribe to given TCL contracts, and how LSEs design a control law to meet their targets. At a certain location, we assume a population of $N = 4,000$ potential customers receiving the contract offers. The type of customers α is drawn uniformly from $[1, 75]$. We assume their thermostats are homogeneous with parameters in Table 9. Initially,

[2] In general, LSEs can specify a parametric form of the discomfort function and the utility function, then infer the parameters from customers' feedback through pilot programs. The resulting utility function is more realistic in reflecting customers' tradeoff between bearing discomfort and getting rebates.

Table 9: Thermostat Parameters

Ambient temp.	Thermal capacitance	Thermal resistance	TCL's rated power
θ_a	C	R	P
32°C	10kWh/°C	2°C/kW	14kW
Dead-band width	Temp. set-point	Electrical efficiency	Damping coefficient
δ	θ_0	η	σ
1°C	21, 22, 23°C	2.5	0.002 hr^{-1}

Table 10: Contract Parameters

Regular rate	Rebate I	Rebate II	Temp. change limit I	Temp. change limit II
$\bar{p}$	s_1	s_2	$\bar{u}_1$	$\bar{u}_2$
10¢/kWh	23¢	45¢	0.5°C	1.5°C

customers set their room temperature at three different levels, 21°C, 22°C, and 23°C with an equal probability. The average daily expenses on air-conditioning $b = 480$¢ in the steady state. We first study a case in which a LSE offers two rebate levels to customers. The contract parameters are shown in Table 10. Customers who do not subscribe to any of these contracts pay a fixed regular rate at 10¢/kWh for power consumption, while participators in group I receive a fixed rebate payment 23¢/day, which is approximately 4.8% savings of the regular bills, and those in group II receive 45¢/day, approximately 9.4% savings. With s_1=23¢, s_2 = 45¢, we obtain a subscription, in which each customer maximizes the utility functions. The numbers of customers subscribing to contract I and contract II are $N_1 = 135(3.4\%)$, and $N_2 = 2284(57.1\%)$ respectively. And there are $N_0 = 1581(39.5\%)$ customers who do not participate.

We assume these customers consume wind power. We use the National Renewable Energy Laboratory (NREL) 10 minutes forecasting wind power data of 2006

in Western U.S., and pick the wind power series on a typical day Feb. 26 as our reference signal. This location in the power grid contains 10 wind turbines with capacity of 30MW. Time horizon of tracking is $T = 24$ (hours), and step size $\Delta t = 1/6$ (10 minutes), matching the wind power forecasts. In the following subsection, we apply MPC to solve a control problem with two different performance metrics. One minimizes the electricity purchasing cost in the wholesale market (linear objective), and the other minimizes the cost represented by the wind tracking errors (quadratic objective). We compare the control strategy, tracking errors and total costs under these two objectives. In MPC, we set prediction step $N_p = 7$, control step $N_c = 7$, and weight $r_w = 10^2$ in the quadratic objective.

Linear versus Quadratic Objective under a Two Contracts Case

We generate the optimal output trajectory and the control signal for the linear objective in Figure 15 and for the quadratic objective in Figure 16. The first plots in both figures show TCLs versus wind power outputs versus the electricity wholesale prices. The second plots show the tracking errors, and the third and fourth ones show the control signals of manipulating the set-points of group I and II respectively. We have several observations by comparing Figure 15 and Figure 16. 1) In Figure 15, LSEs minimize the purchasing costs in the wholesale market due to wind shortage. That is why the controlled loads tend to go below the wind power signal to avoid the purchasing costs. In Figure 16, LSEs minimize the tracking errors plus the control costs. We find that the resulting controlled loads tend to fluctuate near the wind power signal to avoid large deviations from the tracking wind power. The total costs which contain the lump sum rebate payments to customers and the purchasing costs in the wholesale market are \$1179.89/day for the linear objective and \$1243.52/day for the quadratic objective (5.39% higher). 2) When the electricity spot prices are high from 5pm to 6pm on this day, the deviations of TCLs from wind power are small in both cases to avoid the high costs during peak hours. The loads are compensated

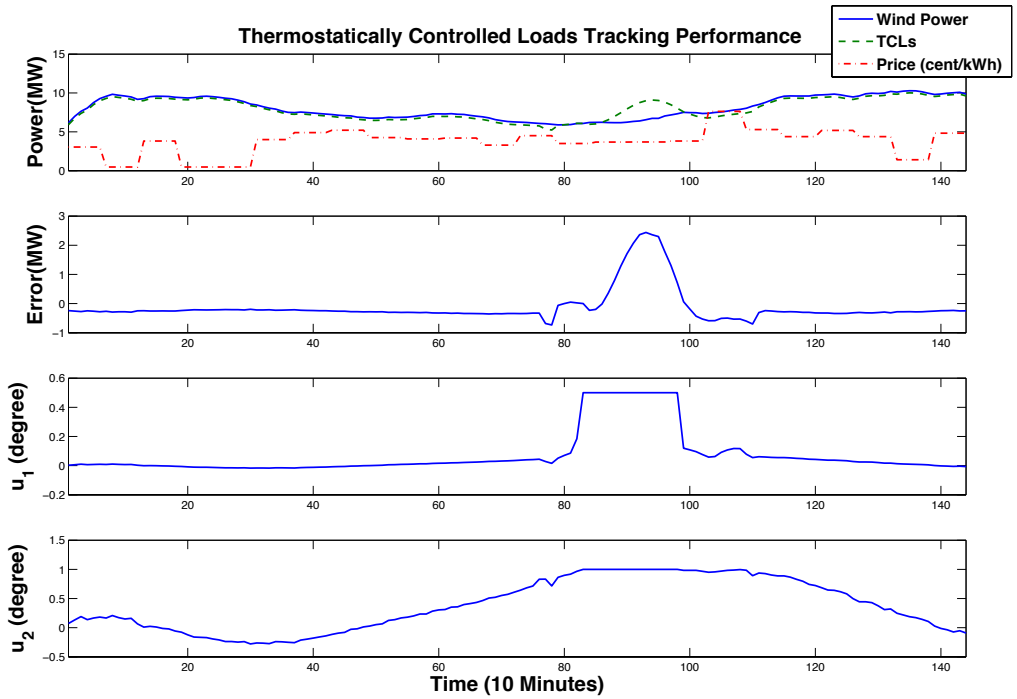

Figure 15: Controlled Loads v.s. Wind Power (Linear)

an hour ago when the prices are low. 3) The maximum error in Figure 16 is higher than it in Figure 15, 3.33 MW versus 2.44 MW. But fortunately, it is negative in Figure 16 , implying no purchases. 4) In Figure 15, both groups reach their set-points change upper limits during 3pm-5pm to lower the aggregated load, while in Figure 16, the second group never reaches their control limits. This is because LSEs also consider the cost of set-points change (stand for customers' discomfort) in the quadratic objective. We list several statistics in Table 11 and Table 12. Figure 17 plots the power outputs of group I and II respectively for the linear objective. The outputs of two groups tend to offset each other to achieve the desired trajectory of the wind power signal.

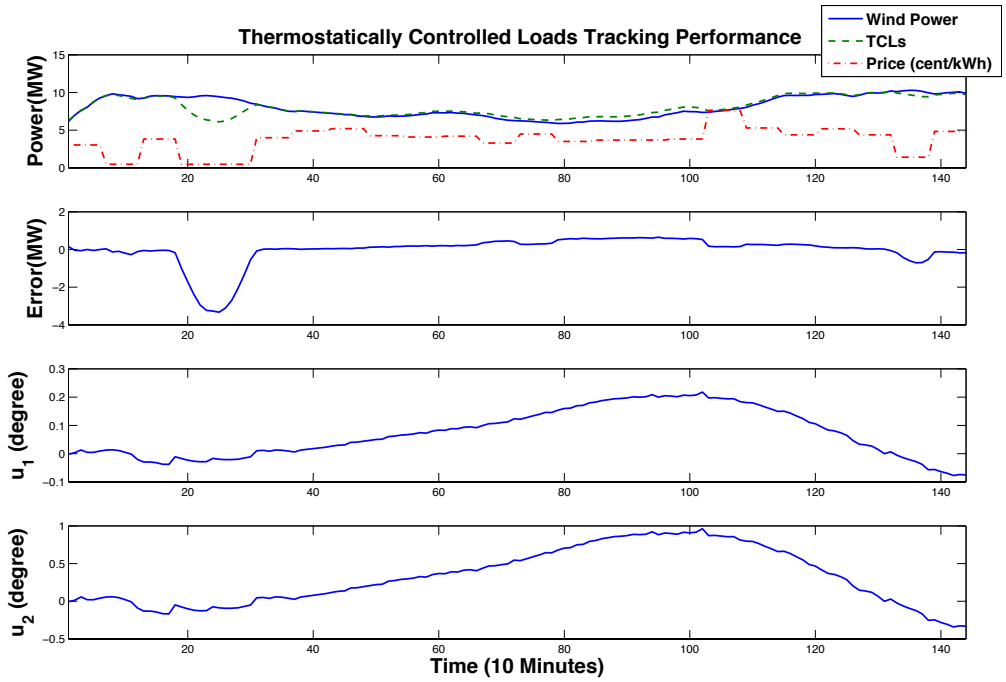

Figure 16: Controlled Loads v.s. Wind Power (Quadratic)

Table 11: Tracking Performance (Linear)

Max Err. (MW)	Percent Err	Min NRMSE (MW)	Max NRMSE (MW)
2.44	37%	6%	10%
Rebate ($/day)	Buying Cost ($/day)	Total Cost ($/day)	Control Cost
1058.85	121.04	1179.89	1.24E8

Table 12: Tracking Performance (Quadratic)

Max Err. (MW)	Percent Err	Min NRMSE (MW)	Max NRMSE (MW)
3.33	35%	8%	13%
Rebate ($/day)	Buying Cost ($/day)	Total Cost ($/day)	Control Cost
1058.85	184.67	1243.52	7.61E7

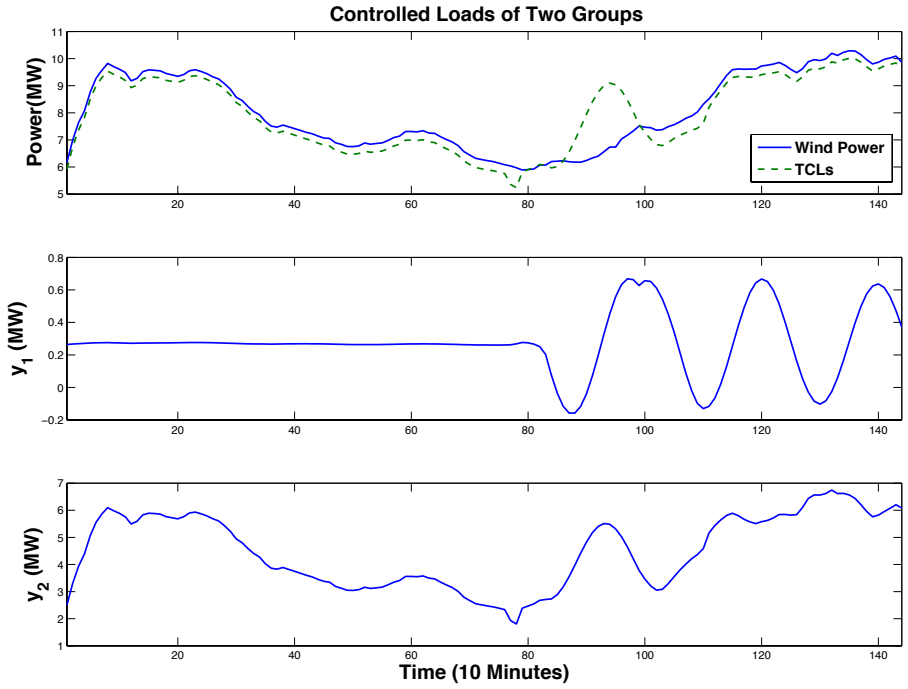

Figure 17: Controlled Loads of Two Groups

Three Levels of Contract Offers

We also investigate the performance under the linear objective with more contract offerings. We assume the LSE adds an extra contract offer at $s_3 = 50¢$, $\bar{u}_3 = 1.2°\text{C}$. The participation becomes $N_1 = 135$, $N_2 = 1046$, $N_3 = 1238$, and $N_0 = 1581$. The performance statistics are given in Table 13. We find that all four metrics of tracking errors are reduced, and it follows the buying costs from the wholesale market is 30.57% lower after introducing a higher rebate level contract. This is because the optimal control strategy under two contracts is always a feasible strategy under extra contract levels. This implies that LSEs can offer more levels of rebate to attract customers in order to create more control flexibility and to further mitigate the mismatch between the controlled loads and the renewable outputs. It is very important especially during extreme events, e.g., very low level of renewable supply. However, LSEs need to pay more to customers as the number of contracts increases. They pay this extra portion

Table 13: Tracking Performance (3 Contracts)

Max Err. (MW)	Percent Err	Min NRMSE (MW)	Max NRMSE (MW)
1.64	23%	4%	7%
Rebate ($/day)	Buying Cost ($/day)	Total Cost ($/day)	Control Cost
1120.75	84.08	1204.83	2.61E8

of money aiming to reduce the risks (uncertainties in renewables). It is worth doing because during such extreme events, the cost of generating power is very high. LSEs can hedge against the risks of renewables by paying this fixed and pre-determined amount of money.

Local Optimum of Rebate Levels

The above analysis shows given contract rebate levels, how customers choose and how LSEs come up with a control law to achieve desired targets. In this subsection, we study how to obtain a set of optimal rebate levels by solving a two-stage stochastic programming problem (55)-(56). For one year NREL wind power data, if we bootstrap a bunch of samples directly, we lose the seasonal patterns. We treat the wind power series as 365 sample curves, each with 144 data points, and then apply block bootstrap to handle this two dimensional data. We pick 100 sample wind power curves and use the sample average approximation to derive a control law for each scenario. Then in the two constracts example, we apply a random search within $s_1 \in [15, 30]$¢/day and $s_2 \in [35, 55]$¢/day. After 39 iterations, we obtain a local optimal rebate level $s_1 = 23$¢/day and $s_2 = 45$¢/day. By offering these levels of rebate to customers, LSEs apply MPC to derive the control law when the wind and price processes are realized, as we did above. We find that customers subscribed to group II (57.1%) is much higher than those of group I (3.4%). LSEs design contracts to encourage more customers to choose higher temperature adjustment ranges, so that LSEs become easier to reduce the loads when wind power supply is extreme low and avoid purchasing in the spot

market.

Finally, we investigate how contract parameters $(\mathbf{s}, \bar{\mathbf{u}})$ affect the subscription, the lump sume payment, the purchasing cost and the total cost. We perform the following sensitivity analysis.

Change the Rebate of Group I ($\mathbf{s_1}$)

We fix the set-point manipulation limits $\bar{u}$ and the rebate s_2 at 45¢/day, but vary the rebate of group I, s_1, from 26¢/day to 30¢/day. The upper chart in Figure 18 illustrates the change of customers subscription versus the change of rebate s_1. We find that one unit increase in rabate s_1 causes 108 customers who opt-out initially will choose contract I, and causes 108 customers switch from contract II to contract I. The lower left plot in Figure 18 illustrates the change of the rebate payment and the buying cost versus the rebate level of contract I. As the rebate of group I increases, the aggregated rebate payment almost increases linearly, and the marginal payment is at around \$20/day. However, the buying cost in the spot market decreases at the beginning and then increases. The lower right plot in Figure 18 illustrates the expected total cost with respect to different levels of rebate s_1. The lowest total cost happens at s_1 =27¢/day. The largest marginal cost is \$312.01/day and the smallest marginal cost is \$28.97/day. The 90% cut off of root mean squared error (RMSE) normalized by the mean power output is 5.42%, meaning that LSEs are 90% confident that the RMSE of tracking the wind power outputs is lower than 5.42%.

Change the Rebate of Group II ($\mathbf{s_2}$)

Then we fix the set-point manipulation limits $\bar{u}$ and the rebate s_1 at 27¢/day, but change the rebate of group II s_1 from 43¢/day to 47¢/day. In the upper chart of Figure 19, we show the change of customers subscription versus the change of rebate s_2. We note that one unit increase in rabate s_2 causes 108 customers switch from contract I to contract II. In the lower left plot of Figure 19, we show the change of the rebate payment and the buying cost change versus the rebate level of contract II.

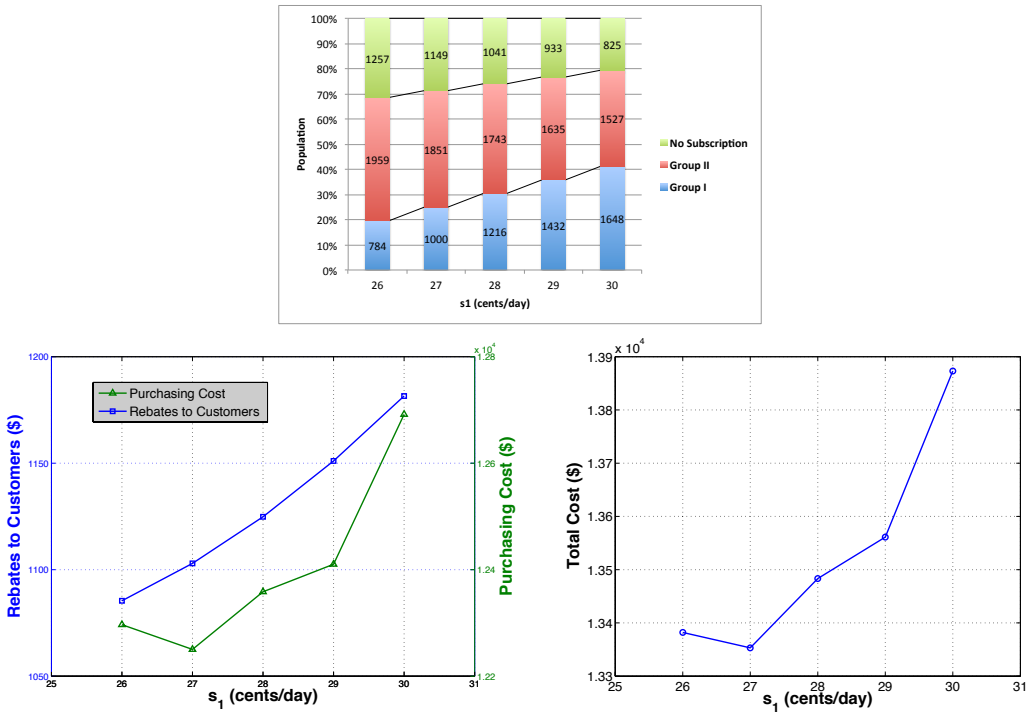

Figure 18: Customers Participation (Upper), Rebates to Customers/Purchasing Cost (Lower Left), and Total Cost (Lower Right) v.s. Rebate Level of Group I

As the rebate of group II increases, the aggregates rebate payment almost increases linearly, and the marginal payment is at around \$38/day. However, the buying cost in the spot market tends to decrease. In the lower right plot in Figure 19, we show the expected total cost with respect to different levels of rebate s_2. It achieves the lowest total cost at s_2 =45¢/day. The largest marginal cost is \$162.60/day and the smallest marginal cost is \$19.16/day. The 90% cut off of RMSE normalized by the mean power output is also 5.42%.

We find that the total cost is more sensitive to the high rebate level (s_2) than to the low rebate level (s_1). This is because high rebate group offers more flexible to LSEs in controlling the loads and LSEs become easier to reduce the total cost. The customers' subscription is more sensitive to the low rebate level than to the high rebate level. This is because the change in the low rebate turns those who opt-out of

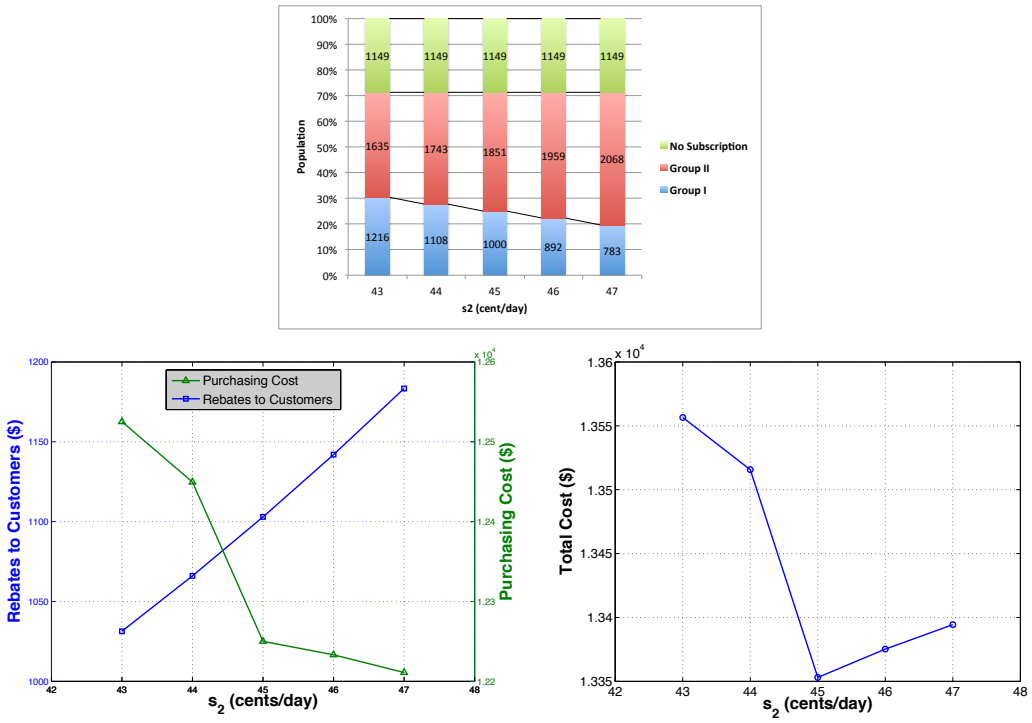

Figure 19: Customers Participation (Upper), Rebates to Customers/Purchasing Cost (Lower Left), and Total Cost (Lower Right) v.s. Rebate Level of Group II

contracts to opt-in.

Change of Setpoint Limits

We also investigate how change in the set-point manipulation limits affect the control. We fix the rebate levels at $s_1 = 27¢$ and $s_2 = 45¢$, but vary the setpoint limits of group I, $\bar{u}_1$ in $[0.3, 0.7]$ degree and then vary that of group II, $\bar{u}_2$ in $[0.8, 1.2]$ degree. The upper charts in Figure 20 and 21 show the change of customers subscription versus the change of manipulation limits. We find that one tenth unit increases in $\bar{u}_1$ causes approximately 1000 customers opt-out from group I, and one tenth unit increases in $\bar{u}_2$ causes approximately 400 customers opt-out from group II. The lower left plots in Figure 20 and 21 show the rebate payments decrease as the manipulation limits increase. This is also because customers opt-out of the their subscription, i.e. the number of participating customers decreases follows the payments decrease. In Figure 20, the increase in group I's set-point reduces the buying cost, because it increases the size of group II and hence adds the control flexibility. However, in Figure 21, the increase in group II's set-point raises the buying cost, because it reduces the size of group II and hence reduces the control flexibility.

3.5 Conclusion

In this chapter, we propose an incentive-based demand response contract design for TCLs to absorb the variability of renewable energy production in a smart grid. LSEs offer different levels of reward and temperature set-points adjustment range for customers to choose from. In this way, LSEs separate customers into several control groups according to their types. Each group offers different degree of directly control ability to LSEs via programmable thermostats. As long as the contracts are IC and IR, customers decide whether to subscribe and which contract to subscribe to depending on their utility functions, which measure a tradeoff between bearing

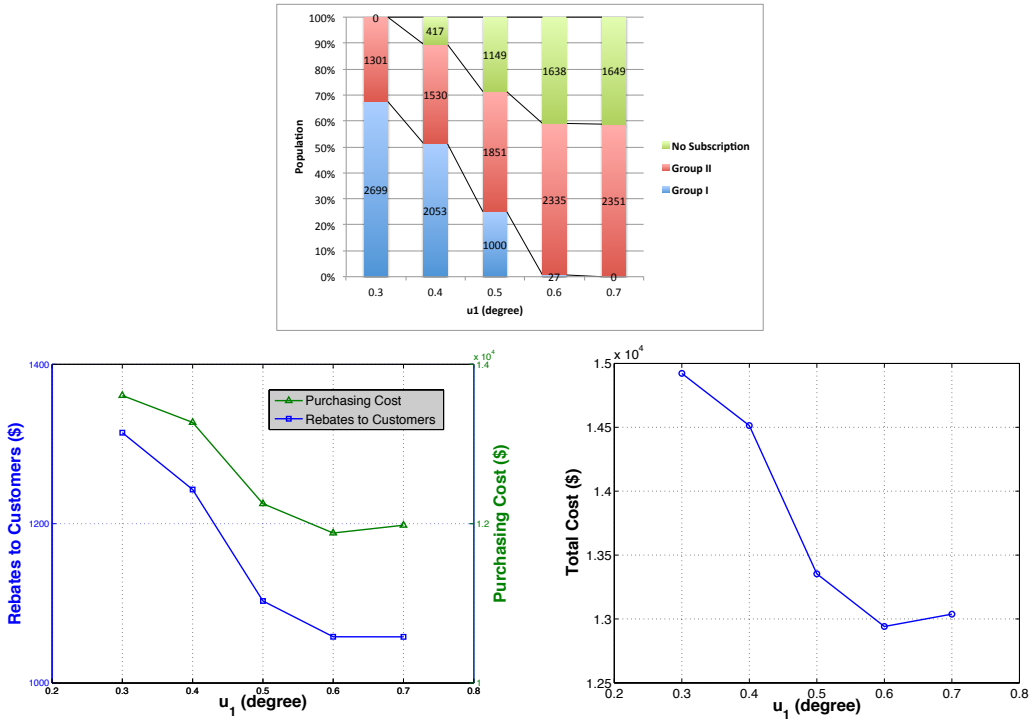

Figure 20: Customers Participation (Upper), Rebates to Customers/Purchasing Cost (Lower Left), and Total Cost (Lower Right) v.s. Set-Point Limit of Group I

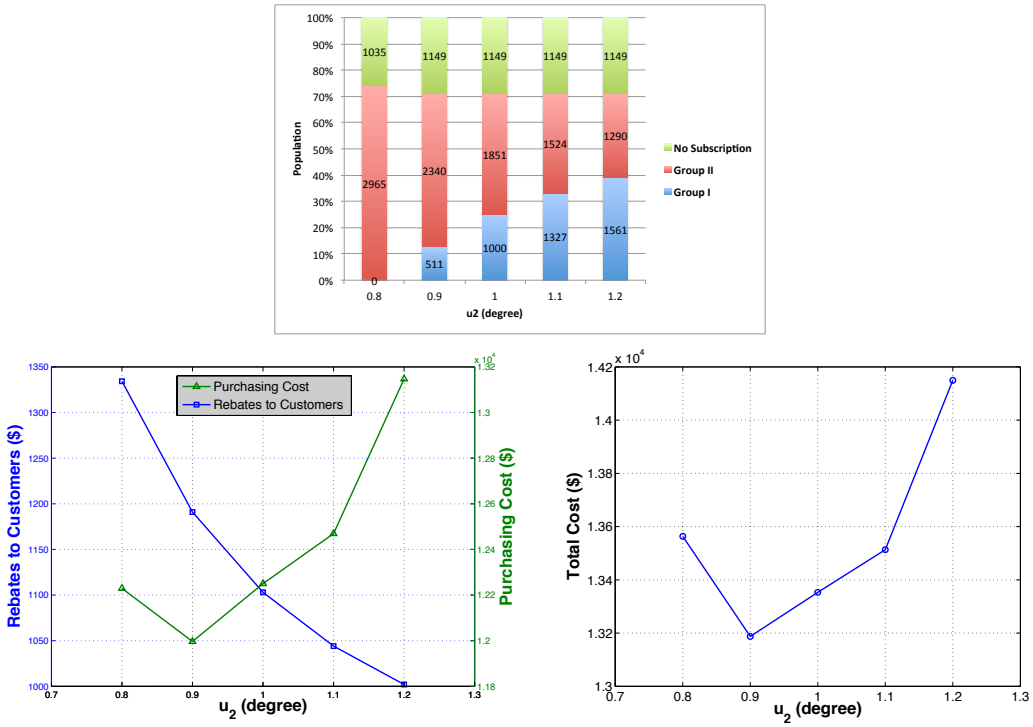

Figure 21: Customers Participation (Upper), Rebates to Customers/Purchasing Cost (Lower Left), and Total Cost (Lower Right) v.s. Set-Point Limit of Group II

discomfort and getting rebates. LSEs then observe the customers' subscription, and design an optimal control law to meet their targets. We discuss two performance metrics: minimizing the cost of integrating the renewable energy outputs, and minimizing the tracking errors. We apply MPC to solve for the optimal control signal due to its nice features. It handles inequality constraints easily, and it only requires one step ahead forecasting of the wind power signal. We formulate a two-stage stochastic programming to find the optimal rebate levels which minimize the total cost among different scenarios.

Through the analysis, we show this contract design mechanism is a very flexible and effective way for LSEs to mitigate the variability of renewable energy resources in the smart grid environment. 1) It greatly increases the availability of customers' TCLs to LSEs, which is essential to reduce the loads as well as the costs during extreme events, e.g., wind power production is very low. LSEs can easily change the subscription distribution by means of varying the contract parameters. Or they can add extra contract offerings to exploit more potentials of accessing TCLs. 2) LSEs can infer customer types and estimate the subscription distribution to an IC and IR pricing scheme. 3) The local optimal rebate levels suggest LSEs to encourage more customers to choose large set-points manipulation ranges. This creates more demand flexibility and lower costs of integrating renewables. 4) This mechanism also obtains a 90% confidence cut for LSEs to understand the NRMSE of tracking renewable signals among all scenarios. 5) The total cost is more sensitive to high rebate levels, but the customers subscription is more sensitive to low rebate levels. As a result, LSEs need to be careful when varying the contract parameters. However, the optimal contract design depends on the choice of customers' utility functions and the distribution of customer types. These information may take LSEs several rounds of pilot problems to find out. The global optimal contract parameters are also hard to find. We left all these issues in a future study.

CHAPTER IV

CARBON EMISSION PERMIT PRICE VOLATILITY REDUCTION VIA FINANCIAL OPTIONS

4.1 Introduction

Cap-and-trade mechanisms are market-based approaches to control pollution. They are used to reduce greenhouse gas emissions in the European Union under the Kyoto Protocol, as well as under the Regional Greenhouse Gas Initiative (RGGI) in ten U.S. states, building on the cap-and-trade experience of US SO_2 and NO_x reduction policies (Napolitano et al. [75]). Allowance trading rewards efficient energy production/consumption and motivates emissions reductions. Thus, cap-and-trade programs provide flexibility to energy producers and consumers in designing their own compliance strategy while ensuring that the overall emissions reductions are achieved, as discussed in [2, 86, 90, 13, 40]. A comprehensive review of emission cap-and-trade mechanism can be found in [6].

The concept of cap-and-trade was first introduced by Dales [29]. He showed that emission trading is able to achieve the emission reduction targets at the lowest social cost, when the marginal abatement cost is the same among all regulated polluters. Montgomery [73] formalized this result. He proposed a static and deterministic model showing that there exists an equilibrium in a competitive permit market without transaction costs. Based upon this work, numerous studies on modeling the emission permit markets have been conducted. Researchers have extended the model of permit prices to dynamic frameworks as well as stochastic settings. Tietenberg [89] and Cronshaw and Kruse [28] developed a discrete-time deterministic model with banking and borrowing allowed. In their models, the permit price rises at the rate of interest.

Rubin [80] further extended the results to a continuous time setting. Furthermore, he obtained that if borrowing is restricted, the growth rate of the marginal abatement cost and the permit price is less than the rate of interest. Schennach [81] explored the consequences of constraints on borrowing. She also attempted to incorporate random emissions into modeling the permit price dynamic. She showed that the expected permit prices grow at the discount rate when the constraint on borrowing is not binding, while the expected prices will rise less than the discount rate when the constraint is binding. The same results were proved in Newell [76] under a stochastic model, and they also showed the cap-and-trade system with banking and borrowing would be largely equivalent to an emissions tax system.

Under a stochastic model of permit markets, it is important to understand not only the path of the expected permit prices, but also its variation from the expected price levels. That means the control of price volatility is a key to design efficient cap-and-trade programs. The issue of permit price volatility has also been investigated in the literature. For example, Celebi and Graves [18] estimated a standard deviation of 50% or more for CO_2 price per year in the U.S. under Americas Climate Security Act proposed by Lieberman and Warner in 2007. As it is argued that a cap-and-trade market mechanism for carbon may offer stronger incentives for carbon reduction technology investment (e.g., [21]), high volatility in CO_2 price could discourage and delay investment in the CO_2 abatement technologies needed to achieve large reductions in carbon emissions.

We contribute to the body of knowledge on the design of mechanisms for reducing carbon permit price volatility by examining the role of trading permit options in influencing the permit price volatility and its implications on carbon emission reduction policy design. Specifically, we show that the trading of properly designed financial options on carbon permits can prevent excessive price volatility in the spot market for permits and reduce overall carbon emission reduction costs.

Several approaches have been proposed to address the price volatility issue in carbon emission trading. Jacoby and Ellerman [58] proposed a safety valve mechanism which includes a slowly evolving price floor and ceiling. They mentioned that this mechanism does reduce price volatility, however, a low price ceiling can lead to extra emissions. As we reviewed, banking is well studied in smoothing permit prices and lowering costs. However, Fell et al. [42] showed that the price volatility remains large with the persistence of baseline emissions shocks. They suggested there may still be motivation for considering price mechanisms in addition to banking. Other authors also addressed the controls of price and price volatility with bankable permits. Maeda [68] studied the linkage between the spot price and the future price of bankable permits. He showed that an increase in the uncertainty in future prices would first lower the spot price and then cause an increase in spot price with the futures price volatility getting too high. He also studied how future spot volatility may affect the current spot level and the banking behavior. Empirically, Alberola [1] showed that the low European Union Allowance (EUA) spot price during Phase I (2005-2007) was partially due to the unlimited intra-period banking and restricted inter-period banking between Phase I and II. The intra-period banking can increase the abatement and spot price in the early phase of a program, but can knock them down at the end of the same period. Seifert et al. [83] showed the price volatility in EU ETS increases when it comes closer to the end of the Phases, while, at the same time, it decreases when the price is close to its bounds. Carmona et al. [16] also showed that this phenomenon is a general result of cap and trade systems without inter-period banking. When inter-period banking is now allowed, Hitzemann and Uhrig-Homburg [53] found that the price of allowances and its volatility depend on upcoming Phases, and identify that each additional Phase leads to an additional component in the current price. Although these studies conclude that banking is able to stabilize the expected permit price level, price variability may remain large. How banking or other

mechanisms may affect the future spot volatility needs further study.

It is well-known from the finance literature that, in a world with complete markets, symmetric information, and no transaction costs, the trading of financial options would have no effect on their underlying assets. However, as most financial markets including carbon permit markets are inherently incomplete and prone to asymmetric information, options can affect their underlying assets in various aspects. In a setting with incomplete markets and transaction costs, Grossman [47] showed the trading of options may indeed affect the price volatility of the underlying assets. In the financial equity markets, research indicates that the magnitude of reduction in the price volatility of underlying assets following the introduction of their options' trading ranges from 4% to 20% [24, 4, 84, 30]. In the commodity markets, for example, the crude oil market, Fleming and Ostdiek [44] found that deep and liquid future markets may reduce the volatility of the underlying market. And the introduction of crude oil options and other energy derivatives has little effect on increasing the price volatility, because they gradually complete the market.

Carbon futures and options are actively traded in the European Emission Trading Scheme (EU ETS), and European Union Allowance (EUA) and Certified Emission Reduction (CER) futures and options are also traded through NYMEX, Nasdaq OMX, and ICE platform in the United States. Leconte and Pagano [63] argued that in the European carbon market, insufficient market regulation drove the market to deviate from its critical functions of price discovery and risk transfer. To ensure a properly functioning derivative market, they as well as Grüll and Taschini [48] suggested a range of actions, such as screening of market participants.

In this chapter, in the context of a properly functioning derivative market, we investigate the trading of financial options on CO_2 permits as an alternative approach for carbon permit price volatility reduction. For emissions permits markets, several papers: [22, 32, 51, 59] have studied options pricing on emission allowances. And

Kijima et al. [59] also showed that price spikes can be reduced with banking. Grüll and Taschini [48] showed that popular price control mechanisms, such as price floor, price collar and allowance reserve, can be replicated by an ordinary scheme with European and American options. This implies that options are efficient and sufficient in permit price management, and their results also hold when banking is allowed. Recently, Chevallier et al. [23] completed an empirical study on the effect of the introduction of options on emission permit price volatility based on data collected from EU ETS. They suggested that the introduction of options may decrease the volatility level of emission permits. However, they did not investigate the mechanism behind this effect in detail. Through a stylized model, this chapter demonstrates that introducing financial options on emission permits increases the price elasticity of demand. We find that the existence of financial options reduces the spot price level, the price volatility of CO_2 permits, and the total cost of achieving emission limits. We also show that the financial option approach works more effectively in a system with banking than in a system without banking. In contrast to the price ceiling approach, the options approach does not result in extra emissions. Furthermore, the existence of option markets enable the regulated sources to hedge the uncertainty of future spot prices and stimulates investment in carbon emission abatement technologies.

The reminder of the chapter is organized as follows. We formulate a two-compliance-time model of a carbon cap and trade system without controls or financial instruments in Section 2. Then we analyze the effect of the following four approaches to price volatility reduction: 1) safety valve, 2) banking/borrowing, 3) financial options, and 4) financial options in a bankable system in Section 3. We follow up with a numerical example for illustration. Finally, we conclude that financial options are potentially effective tools in emission permit price volatility reduction.

4.2 A Two-compliance-time Model

We consider a model in which there are only two compliance times, the present time ($t = 0$) and the future time ($t = 1$). Carbon permits can be traded in the spot market at both times. In this base case model, we assume that there are N regulated sources in the system[1]. For each source i, $i = 1, \cdots, N$, the business-as-usual emissions at time t are denoted as $e_{i,t}$, and the allocated emission allowances at time t are denoted as $a_{i,t}$. We denote P_t as the spot price at time t and $C_{i,t} = C_{i,t}(q_{i,t})$ as the cost function of achieving emissions reduction $q_{i,t}$ for source i at time t. Some papers [16, 52] model these costs explicitly; here we use a stylized model to focus on the price volatility issue. We assume that the emission allowances are initially allocated freely. And business-as-usual emission for time 1, $e_{i,1}$, is uncertain at time 0, which is drawn from a probability space $(\Omega, \mathcal{F}, \mathbb{P})$ with mean $\mu_{i,1}$ and variance $\sigma_{i,1}^2$. This also determines the uncertainty of the spot price P_1 at time 0. Usually the business-as-usual emissions of different emission sources, for example, power plants, are driven by some common factors, so we assume $e_{i,1}$ and $e_{j,1}$ are correlated to each other with correlation ρ_{ij} for any $i, j = 1, \cdots, N$. We also impose a condition that the regulator always allocates less allowances to the individual emitters than their expected business-as-usual emissions, i.e., $a_{i,1} < \mu_{i,1}$, $i = 1, \cdots, N$, to ensure the positive expectations of spot prices.

From the perspective of regulators, the policy goal is to achieve the desired carbon emissions reductions with the lowest costs to the regulated sources during each compliance period. All regulated sources will equate marginal costs with the permit price, which results in lower marginal cost sources to increase their abatement levels relative to others. In this case, the above problem of the regulators can be formulated

[1]In later sections, we extend this model to include unregulated sources which play a role of supplying financial options. In the base case model, there are no banking and no financial instruments involved.

as follows:

$$\begin{aligned} \min_{q_{i,t}} \quad & \sum_{i=1}^{N} C_{i,t}(q_{i,t}) \\ \text{s.t.} \quad & \sum_{i=1}^{N} q_{i,t} = \sum_{i=1}^{N} [e_{i,t} - a_{i,t}],\ t = 0, 1. \end{aligned} \tag{84}$$

The solution to problem (84) implies the lowest social cost for required emissions reductions.

However, from the perspective of emission sources, the goal is to minimize their individual costs. Specifically, at time 1, for any realized spot price $P_1(\omega)$, $\omega \in \Omega$, each source would like to reduce $q_{i,1}(\omega)$ emissions such that $P_1(\omega)$ is equal to its marginal cost, i.e.

$$P_1(\omega) = C'_{i,1}(q_{i,1}(\omega)),\ i = 1, \cdots, N. \tag{85}$$

Here, each source is assumed to be a price taker. If each emission source acts in this way, the outcome is equivalent to the first best solution in problem (84). For simplicity, we assume that the cost function of each source is quadratic: $C_{i,t}(q_{i,t}) = \frac{1}{2} c_{i,t} q_{i,t}^2$, $i = 1, \cdots, N$, where $c_{i,t} > 0$ represents the ability in emissions reductions at time t. Then the spot price P_1 can be determined by imposing the following market clearing condition:

$$\sum_{i=1}^{N} q_{i,1}(\omega) = \sum_{i=1}^{N} [e_{i,1}(\omega) - a_{i,1}],\ \omega \in \Omega. \tag{86}$$

Since everything at time 0 is known, the market clearing condition at time 0 is similarly written as:

$$\sum_{i=1}^{N} q_{i,0} = \sum_{i=1}^{N} [e_{i,0} - a_{i,0}]. \tag{87}$$

By applying equation (85), we have the spot price at time 0 and time 1 as:

$$P_0 = \frac{\sum_{i=1}^{N} [e_{i,0} - a_{i,0}]}{\sum_{i=1}^{N} c_{i,0}^{-1}},\ P_1(\omega) = \frac{\sum_{i=1}^{N} [e_{i,1}(\omega) - a_{i,1}]}{\sum_{i=1}^{N} c_{i,1}^{-1}}, \tag{88}$$

and the minimized total costs of achieving $a_{i,0}$ and $a_{i,1}$ are:

$$TC_{i,0} = P_0[(e_{i,0} - q_{i,0}) - a_{i,0}] + C_{i,0}(q_{i,0}), \tag{89}$$

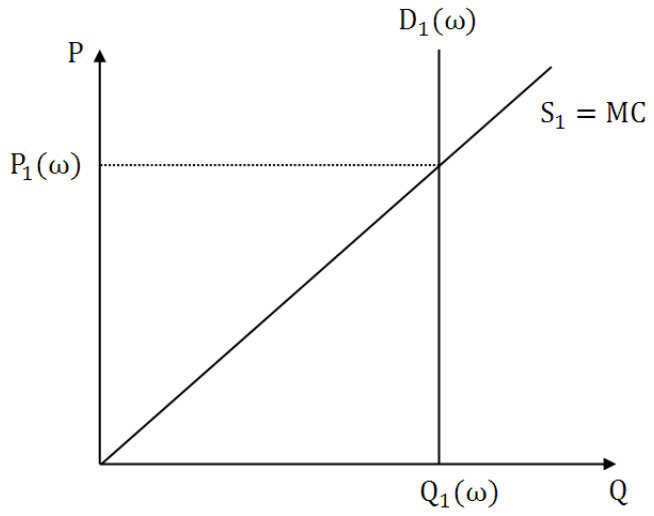

Figure 22: Market Equilibrium in the Base Case

$$TC_{i,1}(\omega) = P_1(\omega)[(e_{i,1}(\omega) - q_{i,1}(\omega)) - a_{i,1}] + C_{i,1}(q_{i,1}(\omega)). \tag{90}$$

Figure 22 illustrates the market equilibrium at time 1 in this case. In this figure, $D_1(\omega) = \sum_{i=1}^{N}[e_{i,1}(\omega) - a_{i,1}]$ stands for the net demand of required emissions reductions at time 1, which is random. S_1 is the aggregate supply curve at time 1, which is equivalent to the aggregate marginal cost curve, $\sum_{i=1}^{N} q_{i,1}(\omega)/\sum_{i=1}^{N} c_{i,1}^{-1} = P_1(\omega)$. The intersection of them determines the carbon permit price at time 1, $P_1(\omega)$, and the total actual emissions reductions at time 1, $Q_1(\omega)$. These notations will be used in the subsequent figures.

For simplicity, we consider that these N regulated sources are symmetric, i.e., $e_{i,1}$ are independent and identically distributed (i.i.d.). So we omit the subscript i in our notation and obtain the following expressions:

$$P_0 = c_0(e_0 - a_0), \tag{91}$$

$$\mathbb{E}[P_1] = c_1(\mu_1 - a_1),\ Var[P_1] = \frac{c_1^2\sigma_1^2}{N}, \tag{92}$$

$$
\begin{aligned}
TC &= TC_0 + \frac{1}{1+r}\mathbb{E}[TC_1] \\
&= \frac{c_0(e_0 - a_0)^2}{2} + \frac{1}{1+r}\left[\frac{c_1(\mu_1 - a_1)^2}{2} + \frac{c_1\sigma_1^2}{2N}\right]. \qquad (93)
\end{aligned}
$$

We find that the variance of carbon permit prices or the price volatility decreases as N becomes larger. This means the uncertainty in business-as-usual emissions and spot prices can be offset as N increases due to the law of large numbers. We also calculate $\mathrm{d}TC/\mathrm{d}c_1$, which equals

$$
\frac{1}{1+r}\left[\frac{(\mu_1 - a_1)^2}{2} + \frac{\sigma_1^2}{2N}\right] > 0. \qquad (94)
$$

This implies that an increase in the ability to reduce emissions will definitely reduce the total discounted cost of achieving the emission limits. Regulated sources have an incentive to invest in carbon abatement technology in the case that the marginal cost for reducing c_1 is less than $\mathrm{d}TC/\mathrm{d}c_1$. In the subsequent sections, these above expressions are used as a benchmark for comparison of different volatility reduction approaches. We summarize the expressions in Table 16 at the end of Section 4 to facilitate the comparison.

4.3 Price Volatility Reduction via Different Approaches

In this section, we study different approaches to permit price volatility reduction in the framework of the above two-compliance-time model. We analyze the following four schemes: 1) safety valve, 2) banking/borrowing, 3) financial options, and 4) financial options in a bankable system, and we also compare their performance.

4.3.1 A Safety Valve Approach

First, we look at the safety valve approach. A safety valve refers to a price limit for confining the spot price to a desired range. With this approach, the regulator puts a floor $\underline{P}$ and a ceiling $\overline{P}$ on the spot price. When the spot price exceeds the price ceiling, market buyers can purchase products from the government at this

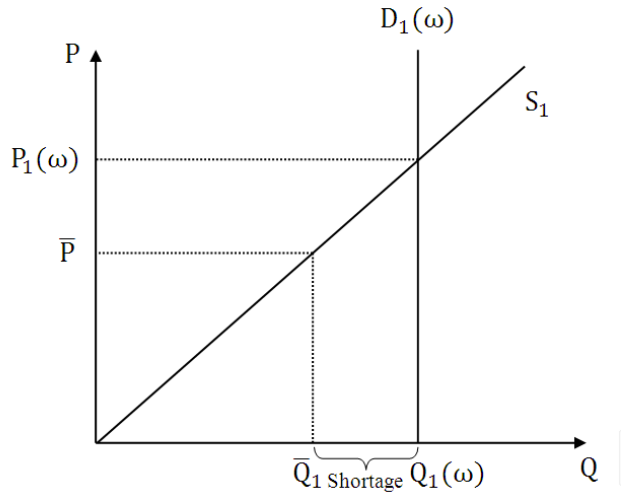

Figure 23: Market Equilibrium in the Safety Valve Case

regulated ceiling. When the spot price falls below the price floor, market sellers can sell products to the government at this floor. In this case, the spot price at time 1, $P_1^v(\omega) = \underline{P} \vee P_1(\omega) \wedge \overline{P}$. This does reduce the variance or the volatility of the spot price, while the change of its expected value depends on the choice of the floor $\underline{P}$ and the ceiling $\overline{P}$. However, if a price ceiling is imposed, an imbalance between supply and demand may occur. In a carbon emission market, when the spot price is higher than $\overline{P}$, the regulator needs to issue new allowances of carbon emissions to buyers at the price ceiling in order to compensate for the supply shortage, resulting in emissions above the policy target. Figure 23 illustrates the market equilibrium at time 1 in the safety valve case. When the price ceiling $\overline{P}$ is lower than the equilibrium price, the supply curve determines the corresponding total emissions reductions $\overline{Q_1}$. The difference between $\overline{Q_1}$ and $Q_1(\omega)$ is shown by the shortage.

4.3.2 Banking and Borrowing Approach

The second approach we discuss is a banking and borrowing mechanism. When banking is allowed, the regulated sources are able to hold their unused allowances for the future compliance period usage, or even purchase allowances from the current spot

market and hold them to hedge against a high future spot price. When borrowing is allowed, the emitters can use the future allowances to cover a shortage in the current period, or even sell them in the current spot market to hedge against a decline in the future spot price. This provides a linkage between the current spot and the future spot. In our two-compliance-time model, each source i can bank or borrow allowances $B_{i,0}$ at time 0. $B_{i,0} > 0$ corresponds to banking, while $B_{i,0} < 0$ represents borrowing. Then the market clearing conditions at time 0 and time 1 are written as:

$$\sum_{i=1}^{N} q_{i,0} = \sum_{i=1}^{N} [e_{i,0} - a_{i,0} + B_{i,0}], \tag{95}$$

$$\sum_{i=1}^{N} q_{i,1}(\omega) = \sum_{i=1}^{N} [e_{i,1}(\omega) - a_{i,1} - B_{i,0}], \ \omega \in \Omega. \tag{96}$$

By equation (85), we have the spot price at time 0 and time 1 as

$$P_0^b = \frac{\sum_{i=1}^{N} [e_{i,0} - a_{i,0} + B_{i,0}]}{\sum_{i=1}^{N} c_{i,0}^{-1}}, \ P_1^b(\omega) = \frac{\sum_{i=1}^{N} [e_{i,1}(\omega) - a_{i,1} - B_{i,0}]}{\sum_{i=1}^{N} c_{i,1}^{-1}}. \tag{97}$$

The total costs of achieving $a_{i,0}$ and $a_{i,1}$ are

$$TC_{i,0}^b = P_0^b[(e_{i,0} - q_{i,0}) - a_{i,0} + B_{i,0}] + C_{i,0}(q_{i,0}), \tag{98}$$

$$TC_{i,1}^b(\omega) = P_1^b(\omega)[(e_{i,1}(\omega) - q_{i,1}(\omega)) - a_{i,1} - B_{i,0}] + C_{i,1}(q_{i,1}(\omega)). \tag{99}$$

Comparing equation (97) with equation (88), we note when $\sum_{i=1}^{N} B_{i,0} > 0$, P_0^b increases and $\mathbb{E}[P_1^b]$ decreases but $Var[P_1^b]$ does not change. This implies banking is able to stabilize the spot price process with the variance or volatility unchanged. The regulators can reduce the price difference between time 0 and time 1 by bankable permits. The left panel of Figure 24 plots the market equilibrium at time 0 in the banking case. It shows that positive net banking $B = \sum_{i=1}^{N} B_{i,0}$ increases the demand for emissions reductions from D_0 to D_0^b, and consequently raises the price level at time 0. The right panel of Figure 24 plots the market equilibrium at time 1. It shows that positive net banking B decreases the demand for emissions reductions from $D_1(\omega)$ to $D_1^b(\omega)$ at time 1, so that the demand curve shifts towards the left. This parallel

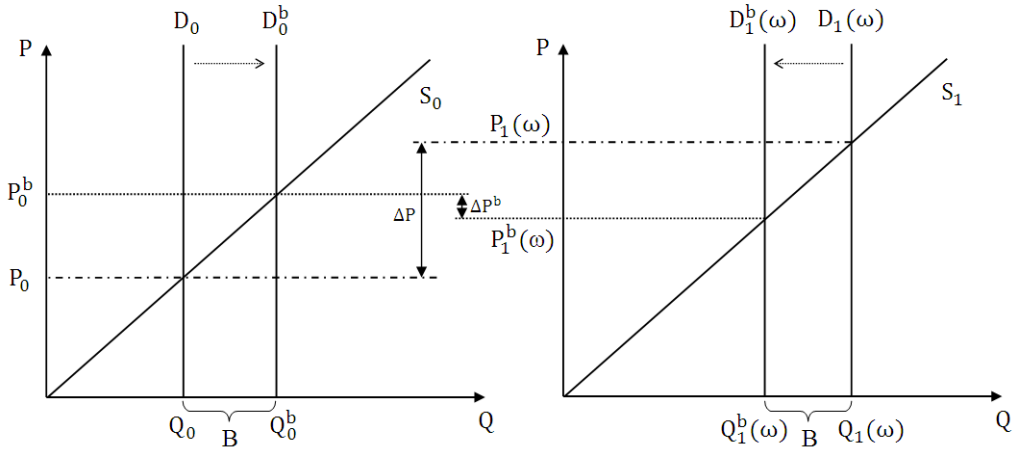

Figure 24: Market Equilibrium in the Banking Case at Time 0 (Left) and at Time 1 (Right)

shifting leads to the decrease in the expected equilibrium price while the variance of the price remains unchanged. We also note in Figure 24 that the price difference between time 0 and time 1 with banking (ΔP^b) is smaller than the one without banking (ΔP).

In order to determine the optimal amount of banking/borrowing $B^*_{i,0}$, we assume each source i needs to minimize the following total discounted cost:

$$TC^b_i = TC^b_{i,0} + \frac{1}{1+r}\mathbb{E}[TC^b_{i,1}],\ i = 1, \cdots, N, \tag{100}$$

where r is the interest rate, and that they make decisions independently and at the same time. This is a game with N players on the amount of $B_{i,0}$. To find the Nash equilibrium of this game, we first solve the best response functions of these players by taking the first order condition to (100). We have the following for each i, $i = 1, \cdots, N$,

$$\begin{aligned} & \frac{(e_{i,0} - a_{i,0} + B_{i,0}) + \sum_{i=1}^N [e_{i,0} - a_{i,0} + B_{i,0}]}{\sum_{i=1}^N c_{i,0}^{-1}} - c_{i,0}^{-1} \frac{\sum_{i=1}^N [e_{i,0} - a_{i,0} + B_{i,0}]}{(\sum_{i=1}^N c_{i,0}^{-1})^2} \\ - & \frac{1}{1+r}\left[\frac{(\mu_{i,1} - a_{i,1} - B_{i,0}) + \sum_{i=1}^N [\mu_{i,1} - a_{i,1} - B_{i,0}]}{\sum_{i=1}^N c_{i,1}^{-1}} - c_{i,1}^{-1} \frac{\sum_{i=1}^N [\mu_{i,1} - a_{i,1} - B_{i,0}]}{(\sum_{i=1}^N c_{i,1}^{-1})^2}\right] \\ = & \ 0. \end{aligned} \tag{101}$$

By summing up (101) in i from 1 to N, we are able to obtain $\sum_{i=1}^{N} B_{i,0}^{*}$ as:

$$\sum_{i=1}^{N} B_{i,0}^{*} = \frac{\sum_{i=1}^{N}(\mu_{i,1} - a_{i,1})/\sum_{i=1}^{N} c_{i,1}^{-1} - (1+r)\sum_{i=1}^{N}(e_{i,0} - a_{i,0})/\sum_{i=1}^{N} c_{i,0}^{-1}}{(1+r)/\sum_{i=1}^{N} c_{i,0}^{-1} + 1/\sum_{i=1}^{N} c_{i,1}^{-1}}. \quad (102)$$

The Nash equilibrium $(B_{1,0}^{*}, B_{2,0}^{*}, \cdots, B_{N,0}^{*})$ can be obtained by plugging (102) into best response functions (101).

In order to study the implications of a banking mechanism, we consider the simplified symmetric case. We obtain the following:

$$P_0^b = c_0(e_0 - a_0 + B_0), \quad (103)$$

$$\mathbb{E}[P_1^b] = c_1(\mu_1 - a_1 - B_0),\ Var[P_1^b] = \frac{c_1^2\sigma_1^2}{N}. \quad (104)$$

Comparing equations (103) (104) with equations (91) (92), we note when $B_0 > 0$, P_0^b increases and $\mathbb{E}[P_1^b]$ decreases, meaning that banking is able to stabilize the spot price process with the variance or volatility unchanged.

In this case, the total discounted cost in (100) is simplified as:

$$\begin{aligned} TC^b &= TC_0^b + \frac{1}{1+r}\mathbb{E}[TC_1^b] \\ &= \frac{c_0(e_0 - a_0 + B_0)^2}{2} + \frac{1}{1+r}\left[\frac{c_1(\mu_1 - a_1 - B_0)^2}{2} + \frac{c_1\sigma_1^2}{2N}\right], \end{aligned} \quad (105)$$

where r is the interest rate. We also simplify equations (101) and (102) to get the explicit form of the optimal amount B_0^{*} for each source,

$$B_0^{*} = \frac{c_1(\mu_1 - a_1) - c_0(1+r)(e_0 - a_0)}{c_0(1+r) + c_1}. \quad (106)$$

To ensure $B_0^{*} > 0$, equation (106) is rewritten as:

$$\frac{\mu_1 - a_1}{e_0 - a_0} > \frac{(1+r)c_0}{c_1}, \quad (107)$$

implying that the regulator needs to impose a cap a_1 such that the ratio of carbon emissions reductions at time 1 to those at time 0 is greater than $(1+r)c_0/c_1$, in which case the price difference of carbon permits between time 0 and 1 is reduced.

The effect of emissions reduction potential on the total discounted cost, $\mathrm{d}TC^{b*}/\mathrm{d}c_1$ is given by:

$$\frac{\mathrm{d}TC^{b*}}{\mathrm{d}c_1} = \frac{1}{1+r}\left[\frac{(\mu_1 - a_1 - B_0^*)^2}{2} + \frac{\sigma_1^2}{2N}\right] > 0, \tag{108}$$

This shows that the increase in emissions reduction potential will definitely reduce the total discounted cost of achieving the emission limits. But compared with equation (94), as long as the regulator chooses $B_0^* > 0$ to stabilize the price, we have $\mathrm{d}TC^{b*}/\mathrm{d}c_1 < \mathrm{d}TC/\mathrm{d}c_1$, meaning that the regulated sources do not have more incentive to invest in carbon abatement technology than in the base case. This is because investment in carbon abatement technology is the only way to reduce the total discounted cost in the base case, while in the banking case, the bankable permits offset the cost reduction benefits of increasing carbon emissions reduction potential. Moreover, the banked allowances will be used in the following compliance period, which means there are no extra emission allowances issued in a whole control period. Furthermore, as B_0^* minimizes TC^b, while the total discounted cost in the base case equals TC^b when setting $B_0 = 0$, we conclude the total discounted cost of achieving the emission target is reduced when banking and borrowing are allowed compared with the base case. Finally, we plug B_0^* into equation (103) and (104), and obtain:

$$P_0^{b*} = \frac{c_0 c_1(e_0 - a_0 + \mu_1 - a_1)}{c_0(1+r) + c_1} \tag{109}$$

$$\mathbb{E}[P_1^{b*}] = \frac{c_0 c_1(1+r)(e_0 - a_0 + \mu_1 - a_1)}{c_0(1+r) + c_1} = (1+r)P_0^{b*}. \tag{110}$$

We find that expected permit prices rise at the interest rate, which is consistent with the result obtained in [76].

Based on all the calculations above, we summarize the findings in the following propositions.

Proposition 4.1 (Banking only)**.** *For symmetric regulated emitters, if the ratio of carbon emissions reductions at time 1 to those at time 0 is greater than* $(1+r)c_0/c_1$*,*

the emitters will bank permits for future usage, i.e., the optimal banking/borrowing B_0^* is positive. This stabilizes the spot price process with the variance or volatility unchanged.

Remark: If the marginal cost is not linear, but a general convex function, banking is able to reduce the price volatility.

Proposition 4.2 (Banking only)**.** *For symmetric regulated emitters, if the ratio of carbon emissions reductions at time 1 to those at time 0 is greater than $(1+r)c_0/c_1$, the change of total discounted cost with respect to carbon abatement ability is less than in the base case, and the total discounted cost of achieving required emissions reductions is always less than in the base case.*

4.3.3 Financial Options Approach

In this section, we investigate a financial options approach for reducing carbon price volatility. A call option on a carbon emission permit gives the holder the right but not obligation to purchase the underlying permit at the predetermined strike price in a pre-specified maturity time. This offers a way to hedge the risk of high future permit prices.

In the financial equity markets, researchers suggest that there are several reasons why volatility reduction in a stock price return can be expected following the introduction of trading of derivatives on the stock. In the context of futures contracts, Stein [87] showed that volatility reduction can be achieved when the benefit of risk sharing by the derivative securities outweighs the possible volatility-increasing effect due to speculative trading. For options markets, both improved risk-sharing (in the case of options extending the hedging contingency set) and the lowered transaction costs (due to leverage offered by options) attract more informed trading activities in the options markets, making the underlying price reflect more information about the underlying assets [15]. This improves information sharing and reduces the risk

of investing in the underlying assets, and in turn tends to raise the underlying asset prices and make them less volatile [24, 79].

Augmenting the base-case model, we introduce markets for trading carbon permit call options. We assume that carbon permit options with all strike prices are traded and there exist M unregulated sources participating in the emission options markets. These unregulated sources could be companies which can provide carbon offsets that meet verification requirements of the market regulator. At time 0, options are traded among these regulated and unregulated sources, and the maturity of these options is time 1.

We consider an option instrument written on carbon emission permits which has a payoff defined as that of a portfolio of call options on carbon permits with strike price spanning all possible permit price levels (a bundle of call options with strike prices uniformly distributed from zero to a large price cap). We term it as an option bundle, or a bundle (the use of such options in the context of electricity reserve capacity market was proposed in [20]). If a market participant purchases a bundle at time 0, then, as P_1 gets higher, the holder will exercise more call options (those with strikes lower than P_1) at time 1, that is, the number of permits settled via options at time 1 are positively correlated to the spot price P_1. Here we simply assume one permit can be purchased from exercising the option bundle at each strike price level[2]. At time 1, the permits settled via options equals $\int_0^{P_1} \mathrm{d}P = P_1$ for such a bundle, and the payoff of this bundle is $\int_0^{P_1} P\mathrm{d}P = \frac{1}{2}P_1^2$. We denote θ_i and γ_j as the number of bundles purchased or sold by regulated source i and unregulated source j, where $i = 1, \cdots, N$ and $j = 1, \cdots, M$. Here the positive numbers correspond to buy and the negative ones correspond to sell. The price of such a bundle is denoted as λ.

The regulated sources can be natural buyers of option contracts, because these contracts offer them a way to hedge the risk of high permit prices at time 1. When

[2]This corresponds to a proportional factor with value 1 in ton^2/\$.

spot price P_1 is realized at time 1, holding θ_i bundles of option portfolio allows them to acquire $\theta_i P_1$ units of permits at cost $\frac{1}{2}\theta_i P_1^2$ versus $\theta_i P_1^2$ if purchasing in the spot market directly. In addition, unregulated sources can be natural sellers in the option market. For example, companies with carbon reducing capabilities can generate income by selling option contracts and use this income for investment and development of their carbon reducing technologies. We assume each source j has its own cost structure for carbon abatement. In order to sequester or store q units of emissions, they are assumed to pay $\frac{1}{2}h_j q^2$, $j = 1, \cdots, M$. The unregulated sources with carbon reducing potential can be viewed as if they own carbon permits. When option portfolios are exercised, they do not need to buy from the spot market at price P_1. Instead, they use their facilities to reduce carbon emissions. Thus, the company j is willing to participate as an option seller if the following condition is satisfied:

$$-\frac{1}{2}\gamma_j P_1^2 \geq \frac{1}{2}h_j(\gamma_j P_1)^2, j = 1, \cdots, M. \tag{111}$$

This means that the benefits of settling $-\gamma_j P_1$ units of emissions from options are sufficient to cover the cost of reducing them. Then we have $0 \leq -\gamma_j \leq \frac{1}{h_j}$, $j = 1, \cdots, M$. Here γ_j is negative by definition, because these companies are selling options. In this case, when h_j is low enough, there will be sufficient sellers willing to clear the option market.

The market clearing conditions for spot and options at time 0 are written as:

$$\sum_{i=1}^{N} q_{i,0} = \sum_{i=1}^{N}[e_{i,0} - a_{i,0}],\ \sum_{i=1}^{N}\theta_i = -\sum_{j=1}^{M}\gamma_j. \tag{112}$$

The market clearing condition for spot at time 1 is written as:

$$\sum_{i=1}^{N}[q_{i,1}(\omega) + \theta_i P_1^o(\omega)] = \sum_{i=1}^{N}[e_{i,1}(\omega) - a_{i,1}],\ \omega \in \Omega. \tag{113}$$

By equation (85), we have the spot price at time 0 and time 1 as

$$P_0^o = \frac{\sum_{i=1}^{N}[e_{i,0} - a_{i,0}]}{\sum_{i=1}^{N} c_{i,0}^{-1}},\ P_1^o(\omega) = \frac{\sum_{i=1}^{N}[e_{i,1}(\omega) - a_{i,1}]}{\sum_{i=1}^{N}[c_{i,1}^{-1} + \theta_i]}. \tag{114}$$

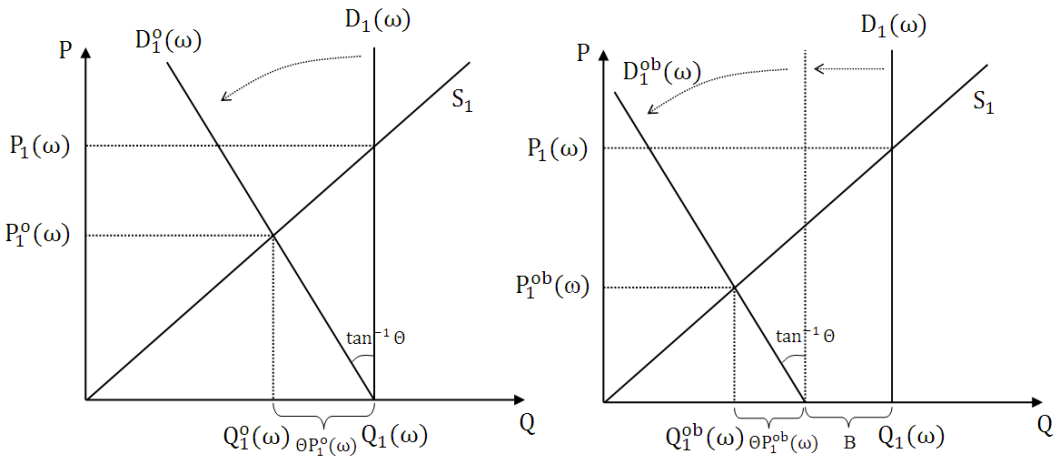

Figure 25: Market Equilibrium in the Financial Option Case (Left) and the Combined Case (Right)

The total cost of achieving $a_{i,0}$ and $a_{i,1}$ are

$$TC_{i,0}^o = P_0^o[(e_{i,0} - q_{i,0}) - a_{i,0}] + \lambda\theta_i + C_{i,0}(q_{i,0}), \tag{115}$$

$$TC_{i,1}^o(\omega) = P_1^o(\omega)[(e_{i,1}(\omega) - q_{i,1}(\omega)) - a_{i,1}] - \frac{1}{2}\theta_i P_1^{o2}(\omega) + C_{i,1}(q_{i,1}(\omega)). \tag{116}$$

Comparing equation (114) with equation (88), we note that when $\sum_{i=1}^N \theta_i > 0$, both $\mathbb{E}[P_1^o]$ and $Var[P_1^o]$ decrease. This implies that call options can reduce the spot price level and the variance or volatility simultaneously. The left panel of Figure 25 plots the market equilibrium at time 1 in the financial option case. It shows the positive net purchase of call options $\Theta = \sum_{i=1}^N \theta_i$ tilts the demand curve from $D_1(\omega)$ to $D_1^o(\omega)$, i.e., increases the price elasticity of demand. The angle of tilting is $\tan^{-1}\Theta$ and it corresponds to $\Theta P_1^o(\omega)$ units of emission permits settled via option purchase. This non-parallel movement results in the reduction in both the expected equilibrium price and the price volatility.

In order to determine the optimal amount of options θ_i^*, we assume each source i needs to minimize the following total discounted cost:

$$TC_i^o = TC_{i,0}^o + \frac{1}{1+r}\mathbb{E}[TC_{i,1}^o],\ i = 1, \cdots, N, \tag{117}$$

where r is the interest rate, and each makes decisions independently and at the same time. This is again a game with N players on the amount of θ_i. To find the Nash equilibrium of this game, we first solve the best response functions of these players by taking the first order condition to (117).

If one imposes the no-arbitrage condition on the price of this bundle of options, λ becomes a function of θ_i, $i = 1, \cdots, N$. We have

$$\lambda = \lambda(\theta_1, \cdots, \theta_N) = \frac{1}{1+r}\mathbb{E}[\frac{1}{2}P_1^{o2}], \tag{118}$$

which is the discounted expectation of the payoff at maturity. Then terms $\lambda\theta_i$ and $\frac{1}{1+r}\mathbb{E}[\frac{1}{2}\theta_i P_1^{o2}]$ are cancelled in (117). From the first order condition, we have the following for each i, $i = 1, \cdots, N$

$$\begin{aligned} & - \frac{(\mu_{i,1} - a_{i,1})\sum_{i=1}^N(\mu_{i,1} - a_{i,1}) + \sigma_{i,1}^2 + \sum_{j\neq i}\rho_{ij}\sigma_{i,1}\sigma_{j,1}}{[\sum_{i=1}^N(c_{i,1}^{-1} + \theta_i)]^2} \\ & + \frac{c_{i,1}^{-1}\{[\sum_{i=1}^N(\mu_{i,1} - a_{i,1})]^2 + \sum_{i=1}^N\sigma_{i,1}^2 + \sum_{i=1}^N\sum_{j\neq i}\rho_{ij}\sigma_{i,1}\sigma_{j,1}\}}{[\sum_{i=1}^N(c_{i,1}^{-1} + \theta_i)]^3} \\ & = 0. \end{aligned} \tag{119}$$

By summing up (119) for i from 1 to N, we are able to obtain $\sum_{i=1}^N \theta_i^* = 0$. This means that if arbitrage opportunities are ruled out in the market, the regulated sources' aggregate purchase or selling of bundles of options are zero. This is because such bundles of options can be replicated using spot permits at any price level. So, as a whole, there is no difference between before and after introducing financial options.

However, if the price λ is assumed to be an exogenous parameter[3], then the participants in the option market are price takers, and λ is taken as a constant. Discussion of pricing option contracts on tradable permits can be found in [32, 59, 19]. In this case, we can show the optimal choice of θ_i will also lead to arbitrage free in the market. From the first order condition to equation (117), we have the following

[3]One justification for this assumption is that these option bundles cannot be exactly replicated by trading carbon permits. The introduction of such options indeed makes the markets more complete.

for each i, $i = 1, \cdots, N$

$$\begin{aligned}
\lambda &+ \frac{1}{1+r}\Big[- \frac{(\mu_{i,1} - a_{i,1}) \sum_{i=1}^{N} (\mu_{i,1} - a_{i,1}) + \sigma_{i,1}^2 + \sum_{j \neq i} \rho_{ij} \sigma_{i,1} \sigma_{j,1}}{[\sum_{i=1}^{N} (c_{i,1}^{-1} + \theta_i)]^2} \\
&- \frac{1}{2} \frac{[\sum_{i=1}^{N} (\mu_{i,1} - a_{i,1})]^2 + \sum_{i=1}^{N} \sigma_{i,1}^2 + \sum_{i=1}^{N} \sum_{j \neq i} \rho_{ij} \sigma_{i,1} \sigma_{j,1}}{[\sum_{i=1}^{N} (c_{i,1}^{-1} + \theta_i)]^2} \\
&+ (c_{i,1}^{-1} + \theta_i) \frac{[\sum_{i=1}^{N} (\mu_{i,1} - a_{i,1})]^2 + \sum_{i=1}^{N} \sigma_{i,1}^2 \sum_{i=1}^{N} \sum_{j \neq i} \rho_{ij} \sigma_{i,1} \sigma_{j,1}}{[\sum_{i=1}^{N} (c_{i,1}^{-1} + \theta_i)]^3} \Big] \\
&= 0. \qquad (120)
\end{aligned}$$

By summing up (120) in i from 1 to N, we are able to obtain $\sum_{i=1}^{N} \theta_i^*$ as:

$$\sum_{i=1}^{N} \theta_i^* = \sqrt{\frac{[\sum_{i=1}^{N} (\mu_{i,1} - a_{i,1})]^2 + \sum_{i=1}^{N} \sigma_{i,1}^2 + \sum_{i=1}^{N} \sum_{j \neq i} \rho_{ij} \sigma_{i,1} \sigma_{j,1}}{2\lambda(1+r)}} - \sum_{i=1}^{N} c_{i,1}^{-1}. \quad (121)$$

The Nash equilibrium $(\theta_1^*, \theta_2^*, \cdots, \theta_N^*)$ can be obtained by plugging (121) into the best response functions (120). If such $(\theta_1^*, \theta_2^*, \cdots, \theta_N^*)$ are chosen, it is easy to compute the discounted expectation of payoff:

$$\frac{1}{1+r} \mathbb{E}[\frac{1}{2} P_1^{o2}] \equiv \lambda, \quad (122)$$

implying that the optimal choice of θ_i still ensures there is no arbitrage in the option market. The chosen θ_i guarantees a partial equilibrium in the option market. In this case, $\sum_{j=1}^{M} \gamma_j$ needs to equal $-\sum_{i=1}^{N} \theta_i^*$ to clear the option market. To ensure price and volatility reduction, $\sum_{j=1}^{M} \gamma_j$ is negative, meaning the unregulated sources sell options aggregately.

For simplicity, we again consider the symmetric case to study the implications of the options approach. We obtain the following:

$$P_0^o = c_0(e_0 - a_0), \quad (123)$$

$$\mathbb{E}[P_1^o] = \frac{\mu_1 - a_1}{c_1^{-1} + \theta}, \; Var[P_1^o] = \frac{\sigma_1^2}{N(c_1^{-1} + \theta)^2}. \quad (124)$$

Comparing equations (123) and (124) with equations (91) and (92), we note that when $\theta > 0$, both $\mathbb{E}[P_1^o]$ and $Var[P_1^o]$ decrease, meaning that, as was shown in the

general case, call options can reduce the spot price level and the variance or volatility simultaneously.

In this case, the total discounted cost in (117) is simplified as:

$$\begin{aligned} TC^o &= TC_0^o + \frac{1}{1+r}\mathbb{E}[TC_1^o] \\ &= \frac{c_0(e_0-a_0)^2}{2} + \lambda\theta + \frac{1}{1+r}\frac{N(\mu_1-a_1)^2+\sigma_1^2}{2N(c_1^{-1}+\theta)}, \end{aligned} \tag{125}$$

where r is interest rate. We also simplify equations (120) and (121) to get the explicit form of the optimal amount θ^* for each source,

$$\theta^* = \sqrt{\frac{N(\mu_1-a_1)^2+\sigma_1^2}{2N\lambda(1+r)}} - c_1^{-1}, \tag{126}$$

which is a local minimum point.

Similarly, to ensure $\theta^* > 0$, equation (126) is rewritten as:

$$\begin{aligned} \lambda &< \frac{c_1}{1+r}\left[\frac{c_1(\mu_1-a_1)^2}{2} + \frac{c_1\sigma_1^2}{2N}\right] \\ &= \frac{c_1\mathbb{E}[TC_1]}{1+r}, \end{aligned} \tag{127}$$

or

$$\mu_1 - a_1 > \frac{\sqrt{2\lambda(1+r) - Var[P_1]}}{c_1}, \tag{128}$$

implying that the regulator needs to impose a sufficiently tight cap a_1 such that the emissions reductions are greater than the lower bound specified in equation (128), in which case both the spot price and price volatility are controlled. In this case, the regulated sources are the buyers in the option market, while the unregulated sources are the sellers. In addition, we investigate the change of total discounted cost with respect to the ability of emissions reductions. We compute $\mathrm{d}TC^{o*}/\mathrm{d}c_1 = \lambda c_1^{-2} > 0$, meaning that the increase in ability of emissions reduction will definitely reduce the total discounted cost of achieving the emission limits. But compared with equation (94), as long as the regulator chooses $\theta^* > 0$ to reduce the price and price volatility (equation (127) holds), we have $\mathrm{d}TC^{o*}/\mathrm{d}c_1 < \mathrm{d}TC/\mathrm{d}c_1$, meaning that the regulated

sources do not have more incentive to invest in carbon abatement technology than in the base case. However, comparing with equation (108), the regulated sources may have more incentive to invest in the option case than in the banking case, if we have $\mathrm{d}TC^{o*}/\mathrm{d}c_1 > \mathrm{d}TC^{b*}/\mathrm{d}c_1$, which implies

$$\lambda > \frac{c_1 \mathbb{E}[TC_1^{b*}]}{1+r}. \tag{129}$$

Thus, we can write down the lower bound and upper bound of λ to ensure the benefits of financial options:

$$\frac{c_1 \mathbb{E}[TC_1^{b*}]}{1+r} < \lambda < \frac{c_1 \mathbb{E}[TC_1]}{1+r}. \tag{130}$$

In this case, regulated sources don't have additional incentives to carbon abatement technology investment over base case is because their risks in high permit prices are partially hedged by entering option contracts. However, these allowance permits coming from option contracts are created by unregulated sources, which could be companies with carbon capture and sequestration technologies. They have incentives to invest in carbon reduction technologies. With option trading, investment in carbon technology is reallocated among regulated and unregulated sources, i.e., partially transferred from regulated sources to unregulated sources. In the long-run, the total emission reduction targets will still be guaranteed.

Moreover, there are no extra emission allowances issued in a whole control period after introducing financial options. Furthermore, as θ^* minimizes TC^o while the total discounted cost in the base case equals TC^o when setting $\theta = 0$, we conclude the that the total discounted cost of achieving the emission target is reduced by introducing options compared with the base case. Of course, the existence of such an option market requires new regulation. The cost for encouraging selling options, the operations cost and transaction cost should also be taken into account. Finally, we plug θ^* into equation (124) and obtain:

$$\mathbb{E}[P_1^{o*}] = \sqrt{\frac{2N\lambda(1+r)(\mu_1 - a_1)^2}{N(\mu_1 - a_1)^2 + \sigma_1^2}}, Var[P_1^{o*}] = \frac{2\lambda(1+r)\sigma_1^2}{N(\mu_1 - a_1)^2 + \sigma_1^2}. \tag{131}$$

Based on all the calculations above, we summarize the findings in the following propositions.

Proposition 4.3 (Options only)**.** *For symmetric regulated emitters, if condition (128) is satisfied, the regulated emitters would purchase financial options, i.e., the optimal option portfolio position θ^* is positive. This reduces both the expected spot price and the price volatility.*

Remark: If the marginal cost is not linear, but a general convex function, options are able to reduce the price volatility more than banking does.

Proposition 4.4 (Options only)**.** *For symmetric regulated emitters, the optimal choices of option portfolio θ^*, which minimizes the total discounted costs, ensure that the price of the option portfolio λ equals $\frac{1}{1+r}\mathbb{E}[\frac{1}{2}P_1^{o2}]$, i.e., there is no arbitrage in the option market.*

Proposition 4.5 (Options only)**.** *For symmetric regulated emitters, if condition (130) is satisfied, the change of total discounted cost with respect to the ability in carbon abatement is less than in the base case but greater than in the banking case, and the total discounted cost of achieving required emissions reductions is always less than in the base case.*

4.3.4 Financial Options in a Bankable System

From the analysis in the previous sections, we conclude that both banking and financial options are able to reduce price volatility in carbon permits markets. They also reduce the total discounted cost of achieving the emission target without extra emission allowances issued in a whole control period. Due to the popularity of banking in the recent cap-and-trade proposals, we are interested in studying the impact of introducing financial options on price volatility when carbon permits are bankable.

Following the framework of the previous sections, we still assume there are only two compliance times 0 and 1. Each regulated source i can bank or borrow allowances

and trade bundles of options at time 0. The same notation is used in this two-compliance-time model with both financial options and bankable permits. Then the market clearing conditions for spot and options at time 0 are written as:

$$\sum_{i=1}^{N} q_{i,0} = \sum_{i=1}^{N} [e_{i,0} - a_{i,0} + B_{i,0}],\ \sum_{i=1}^{N} \theta_i = -\sum_{j=1}^{M} \gamma_j. \tag{132}$$

The market clearing condition for spot at time 1 is written as:

$$\sum_{i=1}^{N} [q_{i,1}(\omega) + \theta_i P_1^{ob}(\omega)] = \sum_{i=1}^{N} [e_{i,1}(\omega) - a_{i,1} - B_{i,0}],\ \omega \in \Omega. \tag{133}$$

By equation (85), we have the spot price at time 0 and time 1 as

$$P_0^{ob} = \frac{\sum_{i=1}^{N} [e_{i,0} - a_{i,0} + B_{i,0}]}{\sum_{i=1}^{N} c_{i,0}^{-1}},\ P_1^{ob}(\omega) = \frac{\sum_{i=1}^{N} [e_{i,1}(\omega) - a_{i,1} - B_{i,0}]}{\sum_{i=1}^{N} [c_{i,1}^{-1} + \theta_i]}. \tag{134}$$

The total cost of achieving $a_{i,0}$ and $a_{i,1}$ are

$$TC_{i,0}^{ob} = P_0^{ob}[(e_{i,0} - q_{i,0}) - a_{i,0} + B_{i,0}] + \lambda\theta_i + C_{i,0}(q_{i,0}), \tag{135}$$

$$TC_{i,1}^{ob}(\omega) = P_1^{ob}(\omega)[(e_{i,1}(\omega) - q_{i,1}(\omega)) - a_{i,1} - B_{i,0}] - \frac{1}{2}\theta_i P_1^{ob2}(\omega) + C_{i,1}(q_{i,1}(\omega)). \tag{136}$$

The right panel of Figure 25 plots the market equilibrium at time 1 in this combined case. It shows that the positive net banking B shifts the demand curve $D_1(\omega)$ towards the left, and at the same time, the positive net purchase of call options Θ tilts the demand curve to $D_1^{ob}(\omega)$, i.e., increases the price elasticity of demand. The angle of tilting is $\tan^{-1}\Theta$ and it corresponds to $\Theta P_1^{ob}(\omega)$ units of emission permits settled via option purchase. This movement also results in the reduction in both the expected equilibrium price and the price volatility.

In the symmetric case, we get the following results:

$$P_0^{ob} = c_0(e_0 - a_0 + B_0), \tag{137}$$

$$\mathbb{E}[P_1^{ob}] = \frac{\mu_1 - a_1 - B_0}{c_1^{-1} + \theta},\ Var[P_1^{ob}] = \frac{\sigma_1^2}{N(c_1^{-1} + \theta)^2}. \tag{138}$$

Comparing equations (137) and (138) with equations (91) and (92), we note that when $B_0 > 0$ and $\theta > 0$, P_0^{ob} increases and both $\mathbb{E}[P_1^{ob}]$ and $Var[P_1^{ob}]$ decrease.

In this combined mechanism, even $B_0 < 0$, i.e., the regulated sources choose to borrow permits from future periods, their purchase of financial options may still reduce both $\mathbb{E}[P_1^{ob}]$ and $Var[P_1^{ob}]$, meaning that introducing options is still effective in reducing the spot price level and the variance or volatility simultaneously in a banking environment.

The total discounted cost is simplified as:

$$\begin{aligned} TC^{ob} &= TC_0^{ob} + \frac{1}{1+r}\mathbb{E}[TC_1^{ob}] \\ &= \frac{c_0(e_0 - a_0 + B_0)^2}{2} + \lambda\theta + \frac{1}{1+r}\frac{N(\mu_1 - a_1 - B_0)^2 + \sigma_1^2}{2N(c_1^{-1} + \theta)}, \end{aligned} \tag{139}$$

where r is the interest rate. In this case, the optimal B_0^* and θ^* for each source are determined by solving the simplified equation system:

$$c_0(e_0 - a_0 + B_0) - \frac{1}{1+r}\frac{\mu_1 - a_1 - B_0}{c_1^{-1} + \theta} = 0, \tag{140}$$

and

$$\lambda - \frac{1}{1+r}\frac{N(\mu_1 - a_1 - B_0)^2 + \sigma_1^2}{2N(c_1^{-1} + \theta)^2} = 0. \tag{141}$$

We recall that the regulator needs to impose a sufficiently tight cap a_1 so that $B_0^* > 0$ and $\theta^* > 0$ to control the spot price and price volatility in the banking only or option only case. However, in this case, when both financial options and banking exist, the regulator may choose a relatively looser cap such that B_0^* may be negative, while the spot price and price volatility are still controlled. This suggests that combining financial options with banking/borrowing is more flexible in potentially allowing borrowing or choosing a cap while managing the permit price process. In addition, we also have $\mathrm{d}TC^{ob*}/\mathrm{d}c_1 = \lambda c_1^{-2} > 0$, indicating that these regulated sources have at least the same incentive to invest in carbon abatement technologies as in the option case. Furthermore, there are no extra emission allowances issued in a whole control period after introducing financial options. Finally, we note that the total discounted cost of achieving the emission target is further reduced by combining

options and banking. Thus, this combined mechanism provides all the advantages of banking and financial options.

4.4 Numerical Example

In this section, we develop a numerical example to illustrate the above mechanisms, based on the U.S. carbon emissions profile. U.S. CO_2 emissions in 2008 were about 6,000 million metric tons (Mt) [93]. Although climate regulation may not regulate all CO_2 emissions, for this example we work with 6,000 Mt. In the U.S. there are about 3000 total electric utilities, although the roughly 200 investor-owned electric utilities provide 40 percent of total electric generation. In addition, petroleum refiners might under certain circumstances be regulated emitters, as well as industrial sources of CO_2 and other greenhouse gases. In a more detailed climate regulation scenario, there might be several hundred large regulated sources and more than a thousand smaller regulated sources. For development of a simple numerical example, we here approximate the emission sources as 1000 equal-sized regulated emitters. Let the number of regulated emitters be $N = 1000$, the initial business-as-usual emissions for each emitter be $e_0 = 6$ Mt CO_2, and the permit allocations at the beginning of the period be $a_0 = 5.9$ Mt. A 15% reduction target over the modeled period, which might be 10 years or more, would correspond to allowances at the end of the period of $a_1 = 5.1$ Mt. Let the expected business-as-usual emissions at the end of the period be $\mu_1 = 5.5$ Mt, with a standard deviation $\sigma_1 = 0.5$ Mt. EPA [92] estimates an allowance price of about \$11 per metric ton (t) for 2012, and with a 15% cut in emissions allowances, estimates that the price would rise to about 23 \$/t in 2027. Accordingly, for the base case we let $P_0 = 11$ \$/t and $\mathbb{E}[P1] = 23$ \$/t. By equation (91) and (92), we estimate $c_0 = 1.1 \times 10^{-4}$ \$/t^2 and $c_1 = 0.6 \times 10^{-4}$ \$/t^2. We set the interest rate $r = 0.02$ and by equation (122), we estimate the price of a bundle of options $\lambda = \$100$. All the parameters used in this numerical example are summarized

Table 14: Summary of Parameters in the Numerical Example

N	e_0	μ_1	σ_1	a_0	a_1
1000	6 Mt	5.5 Mt	0.5 Mt	5.9 Mt	5.1 Mt
c_0	c_1	P_0(base)	$\mathbb{E}[P_1]$(base)	r	λ
1.1×10^{-4} \$/t^2	0.6×10^{-4} \$/t^2	11 \$/t	23 \$/t	0.02	\$100

in Table 14.

For a system with combined banking and options, we solve (140) and (141) numerically, and get the optimal banked quantity $B_0^{ob*} = 0.03$ Mt for each emitter, $\theta^{ob*} = 8509$ units and the total discounted cost for each regulated source $TC^{ob*} =$ \$4.45 million. With the same parameters, we solve $B_0^{b*} = 0.07$ Mt for the banking only case and $\theta^{o*} = 11361$ units for the option only case. And the total discounted costs for each regulated emitter under the base case, banking case and option case are \$5.26 million, \$4.80 million and \$4.49 million respectively. This illustrates that the combination of banking and options offers the lowest cost to achieve the carbon emissions limits. We show the total discounted cost for the entire system of N emitters in Figure 26 for emission limits ranging from 5,050 to 5,150 Mt. The figure shows that if the reductions target is 15% (at 5,100 Mt level), introducing financial options provides greater cost savings than banking. The slight difference between the options case and the combined options plus banking case shows the cost reductions mainly come from option contracts rather than from banking.

Based on the above numbers, we show the performance of different approaches in reducing price difference, price volatility and total discounted cost in Table 15. The numbers in the brackets stand for the differences compared to the base case. We note that bankable permits can reduce more price difference than financial options, and that the combined approach is the best here in reducing price difference. Banking does nothing to reduce price volatility; the financial options approach performs the

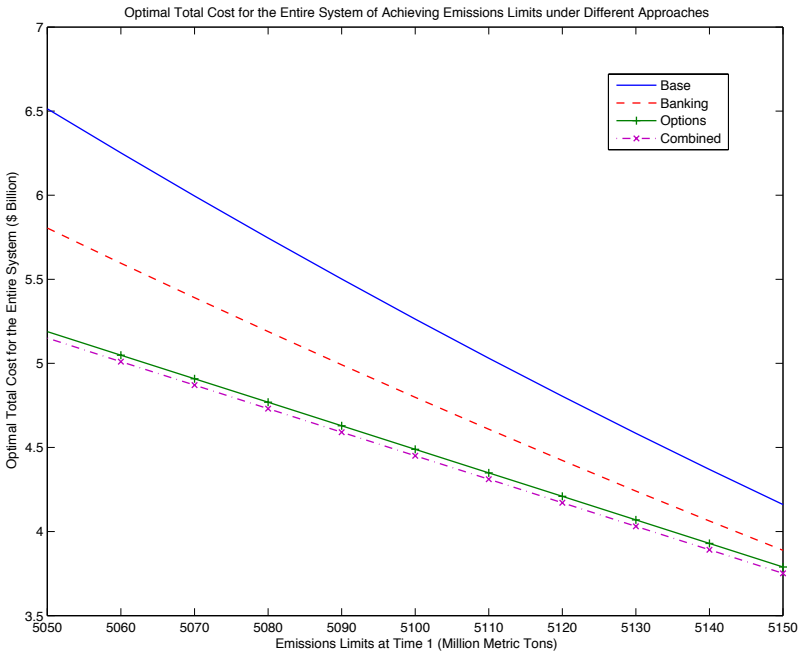

Figure 26: Numerical Example of Optimal Total Cost for the Entire System of Achieving Emissions Limits under Different Approaches

best in reducing volatility. The lowest total discounted cost of the entire system is achieved in the combined case.

A comparison of spot prices, variances, total discounted costs and changes of total discounted costs with respect to c_1 in the base case, banking case, financial option case, and combined case is provided in Table 16. The main findings are as follows. In the banking case, the positive net banking makes the price difference between time 0

Table 15: Numerical Example of Performance of Different Price Management Approaches

	Base	Banking/Borrowing	Financial Options	Combined
$P_0, \mathbb{E}[P_1]$ (\$/t)	11, 23	19.16, 19.54	11, 14.27	14.38, 14.67
Price difference: $\mathbb{E}[P_1] - P_0$ (\$/t)	12	0.38 (-11.62)	3.27 (-8.73)	0.29 (-11.71)
Price volatility (\$/t)	0.95	0.95 (0.00)	0.56 (-0.39)	0.63 (-0.32)
Total discounted cost (\$ billion)	5.26	4.80 (-0.46)	4.49 (-0.77)	4.45 (-0.81)

Table 16: A Summary Comparison of Price Management Approaches

	Base	Banking/Borrowing
P_0	$c_0(e_0 - a_0)$	$c_0(e_0 - a_0 + B_0)$
$\mathbb{E}[P_1]$	$c_1(\mu_1 - a_1)$	$c_1(\mu_1 - a_1 - B_0)$
$Var[P_1]$	$\frac{c_1^2\sigma_1^2}{N}$	$\frac{c_1^2\sigma_1^2}{N}$
$\mathbb{E}[TC_1]$	$\frac{c_1(\mu_1-a_1)^2}{2} + \frac{c_1\sigma_1^2}{2N}$	$\frac{c_1(\mu_1-a_1-B_0)^2}{2} + \frac{c_1\sigma_1^2}{2N}$
TC	$\frac{c_0(e_0-a_0)^2}{2} + \frac{1}{1+r}\left[\frac{c_1(\mu_1-a_1)^2}{2} + \frac{c_1\sigma_1^2}{2N}\right]$	$\frac{c_0(e_0-a_0+B_0)^2}{2} + \frac{1}{1+r}\left[\frac{c_1(\mu_1-a_1-B_0)^2}{2} + \frac{c_1\sigma_1^2}{2N}\right]$
$\mathrm{d}TC^*/\mathrm{d}c_1$	$\frac{1}{1+r}\left[\frac{(\mu_1-a_1)^2}{2} + \frac{\sigma_1^2}{2N}\right]$	$\frac{1}{1+r}\left[\frac{(\mu_1-a_1-B_0^*)^2}{2} + \frac{\sigma_1^2}{2N}\right]$
	Financial Options	**Combined**
P_0	$c_0(e_0 - a_0)$	$c_0(e_0 - a_0 + B_0)$
$\mathbb{E}[P_1]$	$\frac{\mu_1-a_1}{c_1^{-1}+\theta}$	$\frac{\mu_1-a_1-B_0}{c_1^{-1}+\theta}$
$Var[P_1]$	$\frac{\sigma_1^2}{N(c_1^{-1}+\theta)^2}$	$\frac{\sigma_1^2}{N(c_1^{-1}+\theta)^2}$
$\mathbb{E}[TC_1]$	$\frac{N(\mu_1-a_1)^2+\sigma_1^2}{2N(c_1^{-1}+\theta)}$	$\frac{N(\mu_1-a_1-B_0)^2+\sigma_1^2}{2N(c_1^{-1}+\theta)}$
TC	$\frac{c_0(e_0-a_0)^2}{2} + \lambda\theta + \frac{1}{1+r}\frac{N(\mu_1-a_1)^2+\sigma_1^2}{2N(c_1^{-1}+\theta)}$	$\frac{c_0(e_0-a_0+B_0)^2}{2} + \lambda\theta + \frac{1}{1+r}\frac{N(\mu_1-a_1-B_0)^2+\sigma_1^2}{2N(c_1^{-1}+\theta)}$
$\mathrm{d}TC^*/\mathrm{d}c_1$	λc_1^{-2}	λc_1^{-2}

and time 1 smaller than the base case, but the variance or the volatility is unchanged. The total discounted cost is lower than the base case, while the marginal cost with respect to c_1 is larger. In the financial options case, the positive net purchase of call options makes both the price difference and variance smaller than the base case. The total discounted cost is also reduced, while the marginal cost with respect to c_1 is larger than the base case. If we choose λ appropriately, we have lower total discounted cost and marginal cost in the option case than in the banking case. Finally, in the combined case, there is more flexibility to choose the amount of banking or borrowing to reduce both the price difference and the variance. The combined case has the lowest total discounted cost among the four schemes, providing the benefits of both the simple banking case and the option case.

4.5 Conclusion

In this chapter, we investigate the role of option contracts in managing the spot price risk such as price volatility in the carbon emission permit market under a cap-and-trade system. Through a two-compliance-time model, we show that with a tight cap imposed by the regulator, the trading of bundles of call options can reduce both the spot price level and the price volatility, regardless of whether banking is allowed in the system or not[4]. In addition, option contracts enable regulators to achieve some other important benefits simultaneously: providing incentives for the regulated emitters to invest more in carbon abatement technologies given appropriate prices of options, providing incentives for unregulated emission sources to develop carbon reduction opportunities, and reducing the total discounted cost of achieving the emission target.

We also compare the option contracts mechanism with its alternatives: a safety valve approach and a banking approach. While a price ceiling can indeed reduce the price volatility in the spot market, it may result in more carbon emissions than the desired cap level. Banking, when a tight emission cap is imposed, can stabilize the expected price levels of carbon permits and reduce the total discounted cost of achieving the emission cap. However, it does not necessarily reduce the volatility of carbon price at any future time nor provides sufficient incentives for investments in carbon abatement technologies.

Finally, we show when combining banking and financial options, all the advantages of both approaches get kept. Moreover, it offers the regulator with more flexibility in determining the desired emission target, and this target can be achieved at lower cost. Although the introduction of such an option market requires new regulations and

[4]While it appears that the options bundles proposed in our approach have an impractical feature of covering a continuum of strike prices, the insight of such financial instruments can reduce the carbon permit price volatility through increasing the carbon permits' demand elasticity remains true when we consider options bundles with a set of properly chosen discrete strike price levels in a practical design to approximate the theoretical ones.

induces extra operations and transactions costs, we conclude that it is a potentially promising market-based approach to reduce carbon permit price volatility and manage the emission market. The design of such an option market requires careful study and can be left for future work.

CHAPTER V

CONCLUSION

The electric power industry in the United States is being restructured and several major trends are happening towards the future electricity markets. These include establishing cap-and-trade systems to reduce greenhouse-gas emissions, continuous integration of renewable energy resources, and adoption of smart grid technologies. Various types of risks associated with the newly established emission markets as well as the traditional electricity markets with emerging elements present significant new challenges to all industry participants. On the LSE side, the uncertainty and intermittency of renewable energy resources drive the LSEs to enhance demand-side management, which poses challenges in managing volumetric risks as well as the positively correlated price risks in the electricity markets. On the generation side, in the carbon emission markets, permit prices turn out to be volatile, bringing additional uncertainties to conventional fossil-fuel generators' operational costs.

This dissertation is dedicated to study the design and utilization of financial contracts and pricing mechanisms for managing the demand/price risks in electricity markets and the price risks in carbon emission markets from different perspectives. We address the issues pertaining to the efficient computational algorithms for pricing complex financial options which include many structured energy financial contracts and the design of economic mechanisms for managing the risks associated with increasing penetration of renewable energy resources and with trading emission allowance permits in the restructured electric power industry. To address the computational challenges arising from pricing exotic energy derivatives designed for various hedging purposes in electricity markets, we develop a generic computational

framework based on a fast transform method, which attains asymptotically optimal computational complexity and exponential convergence. For the purpose of absorbing the variability and uncertainties of renewable energy resources in a smart grid, we propose an incentive-based contract design for thermostatically controlled loads (TCLs) to encourage end users participation as a source of DR. Finally, we propose a market-based approach to mitigate the emission permit price risks faced by generation companies in a cap-and-trade system. Through a stylized economic model, we illustrate that the trading of properly designed financial options on emission permits reduces permit price volatility and the total emission reduction cost.

The results of this dissertation are summarized as follows. In the first part, we propose a fast algorithm to compute a convolution which reduces the computational complexity from $\mathcal{O}(N \log N)$ to asymptotically $\mathcal{O}(N)$, where N is the number of discretized price levels in computing the convolution. The computational complexity of our method in pricing path-dependent options and Bermudan options is $\mathcal{O}(MN)$, where M is the number of monitoring/exercise dates. The algorithm is general to a broad class of stochastic electricity price models, including AJD processes and Lévy processes, because it takes the characteristic function of the underlying electricity price distribution as an input, which is known in closed-form for such price models. The proposed fast convolution algorithm is applicable to non-uniform grids instead of uniform grids in FFT. This feature allows us to take advantage of the double-exponential integration formula to speed up the rate of convergence in option pricing. Theoretically, the error of our method decreases faster than any negative power of N. Our computational framework can also handle lookback and Asian options due to the use of non-uniform grids. We also extend the fast convolution algorithm to two dimensions in order to price spread options with path-dependent and early exercise features. Numerical examples show the fast convolution method is flexible and efficient pricing different types of exotic options in electricity markets.

In the second part, we propose an incentive-based demand response contract design for TCLs to absorb the variability of renewable energy production in a smart grid. Through the analysis, we show this contract design mechanism is a very flexible and effective way for LSEs to mitigate the variability of renewable energy resources in the smart grid environment. 1) It greatly increases the availability of customers' TCLs to LSEs, which is essential to reduce the loads as well as the costs during extreme events, e.g., wind power production is very low. LSEs can easily change the subscription distribution by means of varying the contract parameters. Or they can add extra contract offerings to exploit more potentials of accessing TCLs. 2) LSEs can infer customer types and estimate the subscription distribution to an IC and IR pricing scheme. 3) The local optimal rebate levels suggest LSEs to encourage more customers to choose large set-points manipulation ranges. This creates more demand flexibility and lower costs of integrating renewables. 4) This mechanism also obtains a 90% confidence cut for LSEs to understand the NRMSE of tracking renewable signals among all scenarios. 5) The total cost is more sensitive to high rebate levels, but the customers subscription is more sensitive to low rebate levels. As a result, LSEs need to be careful when varying the contract parameters. However, the optimal contract design depends on the choice of customers' utility functions and the distribution of customer types. The global optimal contract parameters are also hard to find. We left all these issues in a future study.

In the thrid part, we investigate the role of option contracts in managing the spot price risk such as price volatility in the carbon emission permit market under a cap-and-trade system. Through a two-compliance-time model, we show that with a tight cap imposed by the regulator, the trading of bundles of call options can reduce both the spot price level and the price volatility, regardless of whether banking is allowed in the system or not. In addition, option contracts enable regulators to achieve some other important benefits simultaneously: providing incentives for the

regulated emitters to invest more in carbon abatement technologies given appropriate prices of options, providing incentives for unregulated emission sources to develop carbon reduction opportunities, and reducing the total discounted cost of achieving the emission target. We also show when combining banking and financial options, all the advantages of both approaches get kept. Moreover, it offers the regulator with more flexibility in determining the desired emission target, and this target can be achieved at lower cost. Although the introduction of such an option market requires new regulations and induces extra operations and transactions costs, we conclude that it is a potentially promising market-based approach to reduce carbon permit price volatility and manage the emission market. The design of such an option market requires careful study and can be left for future work.

APPENDIX A

DERIVATION OF THE CHARACTERISTIC FUNCTION OF A 2D AJD PROCESS

We derive the characteristic function of the following 2D AJD process used in Chapter 2:

$$d\begin{bmatrix} x_t \\ y_t \end{bmatrix} = \begin{bmatrix} \kappa_1(\theta_1 - x_t) \\ \kappa_2(\theta_2 - y_t) \end{bmatrix} dt + \begin{bmatrix} \sigma_1 & 0 \\ \rho\sigma_2 & \sqrt{1-\rho^2}\sigma_2 \end{bmatrix} dW_t + \sum_{i=1}^{2} \Delta Z_t^i. \tag{142}$$

Its conditional characteristic function at T given x_t, y_t is given in the following form (see [34]):

$$\phi(u, v; x_t, y_t) = \exp(\alpha(t, u, v) + \beta_1(t, u)x_t + \beta_2(t, v)y_t) \tag{143}$$

where

$$\begin{aligned} \beta_1(t,u) &= iu\exp(-\kappa_1(T-t)) \\ \beta_2(t,v) &= iv\exp(-\kappa_2(T-t)) \\ \alpha(t,u,v) &= \int_t^T([\kappa_1\theta_1\beta_1(s,u) + \tfrac{1}{2}\sigma_1^2\beta_1^2(s,u)] \\ &\quad +[\kappa_2\theta_2\beta_2(s,v) + \tfrac{1}{2}\sigma_2^2\beta_2^2(s,v)] \\ &\quad +\rho\sigma_1\sigma_2\beta_1(s,u)\beta_2(s,v) \\ &\quad +\sum_{j=1}^{2}\lambda_j(\phi_j(\beta,s)-1))ds \end{aligned} \tag{144}$$

and $\phi_j(\beta, s) = \frac{1}{1-\mu_j\beta_1}, j = 1, 2.$

The integrand of $\alpha(t, u, v)$ can be divided into five parts:

$$\kappa_1\theta_1\beta_1(s,u) + \frac{1}{2}\sigma_1^2\beta_1^2(s,u)$$

$$\kappa_2\theta_2\beta_2(s,v) + \frac{1}{2}\sigma_2^2\beta_2^2(s,v)$$

$$\rho\sigma_1\sigma_2\beta_1(s,u)\beta_2(s,v)$$

$$\lambda_1(\frac{1}{1-\mu_1\beta_1}-1)=\frac{\lambda_1\mu_1\beta_1}{1-\mu_1\beta_1}$$

$$\lambda_2(\frac{1}{1-\mu_2\beta_1}-1)=\frac{\lambda_2\mu_2\beta_1}{1-\mu_2\beta_1}$$

We compute the integral for each of them:

1. **The first part:**

$$\begin{aligned}&\int_t^T \kappa_1\theta_1 iue^{-\kappa_1(T-s)}-\frac{1}{2}\sigma_1^2u^2e^{-2\kappa_1(T-s)}ds\\&=\kappa_1\theta_1 iu\int_t^T e^{-\kappa_1(T-s)}ds-\frac{\sigma_1^2u^2}{2}\int_t^T e^{-2\kappa_1(T-s)}ds\\&=(\theta_1-\theta_1e^{-\kappa_1(T-t)})iu-(\frac{\sigma_1^2}{4\kappa_1}-\frac{\sigma_1^2}{4\kappa_1}e^{-2\kappa_1(T-t)})u^2\end{aligned}$$

2. **The second part**:

$$\begin{aligned}&\int_t^T \kappa_2\theta_2 ive^{-\kappa_2(T-s)}-\frac{1}{2}\sigma_2^2v^2e^{-2\kappa_2(T-s)}ds\\&=\kappa_2\theta_2 iv\int_t^T e^{-\kappa_2(T-s)}ds-\frac{\sigma_2^2v^2}{2}\int_t^T e^{-2\kappa_2(T-s)}ds\\&=(\theta_2-\theta_2e^{-\kappa_2(T-t)})iv-(\frac{\sigma_2^2}{4\kappa_2}-\frac{\sigma_2^2}{4\kappa_2}e^{-2\kappa_2(T-t)})v^2\end{aligned}$$

3. **The third part:**

$$\begin{aligned}\int_t^T \rho\sigma_1\sigma_2\beta_1(s,u)\beta_2(s,v)ds&=-\int_t^T \rho\sigma_1\sigma_2uve^{-(\kappa_1+\kappa_2)(T-s)}ds\\&=-(\frac{\rho\sigma_1\sigma_2}{\kappa_1+\kappa_2}-\frac{\rho\sigma_1\sigma_2}{\kappa_1+\kappa_2}e^{-(\kappa_1+\kappa_2)(T-t)})uv\end{aligned}$$

4. **The forth part**:

$$\begin{aligned}\int_t^T \frac{\lambda_1\mu_1\beta_1(s,u)}{1-\lambda_1\mu_1\beta_1(s,u)}ds&=\int_t^T \frac{\lambda_1\mu_1e^{-\kappa_1(T-s)}iu}{1-\lambda_1\mu_1e^{-\kappa_1(T-s)}iu}ds\\&=\frac{\lambda_1}{\kappa_1}\ln(1-\mu_1iue^{-\kappa_1(T-t)})-\frac{\lambda_1}{\kappa_1}\ln(1-\mu_1iu)\end{aligned}$$

5. **The fifth part**:

$$\int_t^T \frac{\lambda_2\mu_2\beta_1(s,u)}{1-\lambda_2\mu_2\beta_1(s,u)}ds = \int_t^T \frac{\lambda_2\mu_2 e^{-\kappa_1(T-s)}iu}{1-\lambda_2\mu_2 e^{-\kappa_1(T-s)}iu}ds$$
$$= \frac{\lambda_2}{\kappa_1}\ln(1-\mu_2 iue^{-\kappa_1(T-t)}) - \frac{\lambda_2}{\kappa_1}\ln(1-\mu_2-iu)$$

Putting the above parts into (143), the final form of the conditional charatertistic function of the AJD process (54) is given by:

$$\begin{aligned}\phi(u,v;x_t,y_t) &= e^{-Au^2-Bv^2-Cuv+iDu+iEv+H(u)} \\ &= (\frac{1-iH_1u}{1-iH_2u})^{\frac{\lambda_1}{\kappa_1}}(\frac{1-iH_3u}{1-iH_4u})^{\frac{\lambda_2}{\kappa_1}}e^{-Au^2-Bv^2-Cuv+iDu+iEv}, \qquad (145)\end{aligned}$$

where

$$A = \frac{\sigma_1^2}{4\kappa_1} - \frac{\sigma_1^2}{4\kappa_1}e^{-2\kappa_1(T-t)},$$
$$B = \frac{\sigma_2^2}{4\kappa_2} - \frac{\sigma_2^2}{4\kappa_2}e^{-2\kappa_2(T-t)},$$
$$C = \frac{\rho\sigma_1\sigma_2}{\kappa_1+\kappa_2}(1-e^{-(\kappa_1+\kappa_2)(T-t)})$$
$$D = \theta_1 + (x_t-\theta_1)e^{-\kappa_1(T-t)},$$
$$E = \theta_2 + (y_t-\theta_2)e^{-\kappa_2(T-t)},$$
$$H_1 = \mu_1 e^{-\kappa_1(T-t)}, H_2 = \mu_1, H_3 = \mu_2 e^{-\kappa_1(T-t)}, H_4 = \mu_2.$$

APPENDIX B

NOTATIONS AND PARAMETERS IN CHAPTER III

B.1 Notations

Contract and Population Parameters:

N:	Number of customers
m:	Number of contract offerings
n:	Number of initial set-points
$\mathbf{s_{m\times 1}}$:	Vector of rebates, $\mathbf{s} = (s_1, s_2, \cdots, s_m)$
$\bar{\mathbf{u}}_{\mathbf{m}\times\mathbf{1}}$:	Vector of set-point adjustment limits, $\bar{\mathbf{u}} = (\bar{u}_1, \bar{u}_2, \cdots, \bar{u}_m)$
$\mathbf{u_{m\times 1}}$:	Vector of set-point controller, $\mathbf{u} = (u_1, u_2, \cdots, u_m)$
$\mathbf{N_{m\times 1}}$:	Customers' subscription to contract pair $(\mathbf{s}, \bar{\mathbf{u}})$, $\mathbf{N} = (N_1, N_2, \cdots, N_m)$
$\theta_\mathbf{0}$:	Initial set-points temperature, $\theta_\mathbf{0} = (\theta_0^1, \theta_0^2, \cdots, \theta_0^n)$
N_j	Number of customers subscribing to contract j
N_{ij}	Number of customers with initial set-point θ_0^i subscribing to contract j

Thermostats Parameters:

θ_a:	Ambient temperature
C:	Thermal capacitance
R:	Thermal resistance
P:	TCL's rated power
θ_+^i:	Temperature upper bound of group i
δ:	Dead-band width
η:	Electrical efficiency
σ:	Damping coefficient

T^i_{c0}: Total cooling time of group i
T^i_{h0}: Total heating time of group i

State Space and Control Parameters:

$\mathbf{x_{ij}}$:	States of thermostats with initial temperature θ^i_0 and subscribing to contract j
y_{ij}:	Loads of customers with initial temperature θ^i_0 and subscribing to contract j
$\mathbf{A_i}, \mathbf{B_{ij}}, \mathbf{C_0}, D_j$:	States space coefficients of $\mathbf{x_{ij}}$ and y_{ij}
$\mathbf{x}$:	States of thermostats for all groups
$y(y_t)$:	Aggregated controlled loads at time t
$\mathbf{A}, \mathbf{B}, \mathbf{C}, \mathbf{D}$:	States space coefficients of $\mathbf{x}$ and y
p_t:	Wholesale electricity price at time t
r_t:	Reference renewable power outputs at time t
$\mathbf{R}$:	Weights on control costs, $\mathbf{R} = \text{diag}(r_w s_1^2, r_w s_2^2, \cdots, r_w s_m^2)$
r_w:	Weight coefficient

Customers' Preferences:

α:	Customer's type
$F(\alpha), f(\alpha)$:	Distribution function and density function of type α
$V(s, \bar{u}; \alpha)$:	Utility function of type α customer
$U(\alpha)$:	Equilibrium utility function of type α customer
$d(\bar{u}, \alpha)$:	Inverse discomfort function
$D(\bar{u}, \alpha)$:	Aggregated discomfort

B.2 Parameters and Matrices

The state space coefficients in (59)-(60) are given as follows:

$$\mathbf{A_i} = \begin{bmatrix} -2\sigma & -\omega_i \\ \frac{\sigma^2+\omega_i^2}{\omega_i} & 0 \end{bmatrix}, \mathbf{B_{ij}} = \begin{bmatrix} \omega_i \Delta_{ij} \\ 0 \end{bmatrix}, \mathbf{C_0} = \begin{bmatrix} -1 & 0 \end{bmatrix}, \text{ and } D_j = -d_j.$$

$$\Delta_{ij} = \frac{5\sqrt{15}C(\theta_a - \theta_+^i)(PR - \theta_a + \theta_+^i)}{\eta(P^2R^2 + 3PR(\theta_a - \theta_+^i) - 3(\theta_a - \theta_+^i)^2)^{3/2}} \cdot \frac{(3PR - \theta_a + \theta_+^i)N_{ij}}{(T_{c0}^i + T_{h0}^i)},$$

$$\omega_i = \frac{2\sqrt{15}C(\theta_a - \theta_+^i)(PR - \theta_a + \theta_+^i)}{CR\delta\sqrt{P^2R^2 + 3PR(\theta_a - \theta_+^i) - 3(\theta_a - \theta_+^i)^2}},$$

$$d_j = \frac{N_j}{\eta R}.$$

The state space coefficients to equation (61)-(62) are given as follows:

$$\mathbf{x} = \begin{bmatrix} \mathbf{x_1} & \cdots & \mathbf{x_n} \end{bmatrix}^T_{2mn\times 1}, \mathbf{x_i} = \begin{bmatrix} \mathbf{x_{i1}} & \cdots & \mathbf{x_{im}} \end{bmatrix}^T_{2m\times 1}, \mathbf{u} = \begin{bmatrix} u_1 \\ \vdots \\ u_m \end{bmatrix}_{m\times 1},$$

$$\mathbf{A} = \text{diag}\begin{bmatrix} \overbrace{\mathbf{A_1}\cdots\mathbf{A_1}}^{m} & \cdots & \overbrace{\mathbf{A_n}\cdots\mathbf{A_n}}^{m} \end{bmatrix}_{2mn\times 2mn},$$

$$\mathbf{B} = \begin{bmatrix} \mathbf{B_1} & \cdots & \mathbf{B_n} \end{bmatrix}^T_{2mn\times m}, \mathbf{B_i} = \text{diag}\begin{bmatrix} \mathbf{B_{i1}} & \cdots & \mathbf{B_{im}} \end{bmatrix}_{2m\times m},$$

$$\mathbf{C} = \begin{bmatrix} \overbrace{\mathbf{C_0}\cdots\mathbf{C_0}}^{2mn} \end{bmatrix}_{1\times 2mn},$$

$$\mathbf{D} = \begin{bmatrix} -d_1 & \cdots & -d_m \end{bmatrix}_{1\times m}.$$

By equation (67)-(68), we rewrite the linear system as:

$$\begin{aligned} y_{k+1} &= \mathbf{CAx_k} + \mathbf{CBu_k} + \mathbf{Du_{k+1}}; \\ y_{k+2} &= \mathbf{CA^2x_k} + \mathbf{CABu_k} + \mathbf{CBu_{k+1}} + \mathbf{Du_{k+2}}; \\ &\cdots \\ y_{k+N_p} &= \mathbf{CA^{N_p}x_k} + \mathbf{CA^{N_p-1}Bu_k} + \cdots + \mathbf{CA^{N_p-N_c}Bu_{k+N_c-1}} + \mathbf{Du_{k+N_p}}. \end{aligned}$$

Let $\mathbf{Y_k} = [y_{k+1}, y_{k+2}, \cdots, y_{k+N_p}]^T$ and $\mathbf{U_k} = [\mathbf{u_k}, \mathbf{u_{k+1}}, \cdots, \mathbf{u_{k+N_c-1}}, \mathbf{u_{k+N_p}}]^\mathbf{T}$, we have

$$\mathbf{Y_k} = \mathbf{F x_k} + \mathbf{G U_k},$$

where

$$\mathbf{F} = \begin{bmatrix} CA \\ CA^2 \\ \vdots \\ CA^{N_p} \end{bmatrix}, \mathbf{G} = \begin{bmatrix} CB & D & & & \\ CAB & CB & D & & \\ \cdots & \cdots & \cdots & \ddots & \\ CA^{N_p-1}B & CA^{N_p-2}B & CA^{N_p-N_c}B & \cdots & D \end{bmatrix}.$$

This control problem (70)-(71) is equivalent to the following:

$$\begin{aligned} J &= \min_{\mathbf{u}} \int_0^T p_t z_t dt && (146) \\ s.t. &\ -\bar{\mathbf{u}} \le \mathbf{u} \le \bar{\mathbf{u}}, && (147) \\ &\ z_t \ge y_t - r_t, && (148) \\ &\ z_t \ge 0. && (149) \end{aligned}$$

In the discrete system, we plug in $\mathbf{Y_k} = \mathbf{F x_k} + \mathbf{G U_k}$, then the above formulation can be rewritten as the following linear programming:

$$\begin{aligned} J_k &= \min_{\mathbf{Z},\mathbf{U}} \mathbf{f_k^T Z_k} \\ s.t. &\ \mathbf{H}[\mathbf{Z_k}, \mathbf{U_k}]^\mathbf{T} \le \mathbf{h}, \end{aligned}$$

where $\mathbf{f_k^T} = (p_k \Delta t, \cdots p_{k+N_p} \Delta t)_{1 \times N_p}$,

$$\mathbf{H} = \begin{bmatrix} -\mathbf{I} & \mathbf{G} \\ -\mathbf{I} & \mathbf{0} \\ \mathbf{0} & \mathbf{M} \end{bmatrix}_{[2N_p+2m(N_c+1)] \times [N_p+m(N_c+1)]}, \mathbf{h} = \begin{bmatrix} \mathbf{S_k} - \mathbf{F x_k} \\ \mathbf{0} \\ \mathbf{m_0} \end{bmatrix}_{[2N_p+2m(N_c+1)] \times 1},$$

$$\mathbf{S_k} = r_k \mathbf{1}_{N_p \times 1}, \mathbf{M} = \begin{bmatrix} I_{m(N_c+1) \times m(N_c+1)} \\ -I_{m(N_c+1) \times m(N_c+1)} \end{bmatrix},$$

$$\mathbf{m_0} = \mathbf{L}\bar{\mathbf{u}}_{m\times 1}, \mathbf{L} = \begin{bmatrix} I_{m\times m} \\ \vdots \\ I_{m\times m} \end{bmatrix}_{2m(N_c+1)\times m}.$$

APPENDIX C

DERIVATION OF PROPOSITIONS IN CHAPTER III

Derivation of Proposition 3.2:

By Corollary 3.1, for $j = 0, 1, \cdots, m-1$, $s_j - s_{j+1} = D(\bar{u}_j, \alpha_j) - D(\bar{u}_{j+1}, \alpha_j)$. Differentiating it on both sides gives

$$\begin{aligned} d(s_j - s_{j+1}) &= \left[\frac{\partial D(\bar{u}_j, \alpha_j)}{\partial \alpha} - \frac{\partial D(\bar{u}_{j+1}, \alpha_j)}{\partial \alpha}\right] d\alpha_j \\ &= \left[E(\bar{u}_j, \alpha_j) - E(\bar{u}_{j+1}, \alpha_j)\right] d\alpha_j. \end{aligned}$$

Thus, we have

$$\begin{aligned} \frac{d\alpha_j}{ds_j} &= -\frac{1}{E(\bar{u}_{j+1}, \alpha_j) - E(\bar{u}_j, \alpha_j)}, \\ \frac{d\alpha_j}{ds_{j+1}} &= \frac{1}{E(\bar{u}_{j+1}, \alpha_j) - E(\bar{u}_j, \alpha_j)}, \end{aligned}$$

which follows for any $j = 1, 2, \cdots, m$,

$$\begin{aligned} \frac{d\alpha_j}{ds_j} &= -\frac{1}{E(\bar{u}_{j+1}, \alpha_j) - E(\bar{u}_j, \alpha_j)}, \\ \frac{d\alpha_{j-1}}{ds_j} &= \frac{1}{E(\bar{u}_j, \alpha_{j-1}) - E(\bar{u}_{j-1}, \alpha_{j-1})}. \end{aligned}$$

Derivation of Proposition 3.3:

The number of customers to contract j is $N_j = N \int_{\alpha_j}^{\alpha_{j-1}} f(\alpha) d\alpha$, $j = 1, 2, \cdots, m-1$. $N_0 = N \int_{\alpha_0}^{+\infty} f(\alpha) d\alpha$, and $N_m = N \int_{-\infty}^{\alpha_{m-1}} f(\alpha) d\alpha$.

As s_0 is always 0, we analyze how s_j change will affect the subscription, for $j = 1, 2, \cdots, m$.

For s_m, it only affects the number of customers to contract m and $m-1$, N_m and

N_{m-1}.

$$\begin{aligned}\frac{dN_m}{ds_m} &= Nf(\alpha_{m-1})\frac{d\alpha_{m-1}}{ds_m} \\ &= N\left[\frac{f(\alpha_{m-1})}{E(\bar{u}_m,\alpha_{m-1})-E(\bar{u}_{m-1},\alpha_{m-1})}\right].\end{aligned}$$

$$\begin{aligned}\frac{dN_{m-1}}{ds_m} &= -Nf(\alpha_{m-1})\frac{d\alpha_{m-1}}{ds_m} \\ &= -N\left[\frac{f(\alpha_{m-1})}{E(\bar{u}_m,\alpha_{m-1})-E(\bar{u}_{m-1},\alpha_{m-1})}\right].\end{aligned}$$

For s_j, $j = 1, 2, \cdots, m-1$,

$$\begin{aligned}\frac{dN_j}{ds_j} &= N\left[f(\alpha_{j-1})\frac{d\alpha_{j-1}}{ds_j} - f(\alpha_j)\frac{d\alpha_j}{ds_j}\right] \\ &= N\left[\frac{f(\alpha_{j-1})}{E(\bar{u}_j,\alpha_{j-1})-E(\bar{u}_{j-1},\alpha_{j-1})} + \frac{f(\alpha_j)}{E(\bar{u}_{j+1},\alpha_j)-E(\bar{u}_j,\alpha_j)}\right]. \\ \frac{dN_{j-1}}{ds_j} &= -Nf(\alpha_{j-1})\frac{d\alpha_{j-1}}{ds_j} \\ &= -N\left[\frac{f(\alpha_{j-1})}{E(\bar{u}_j,\alpha_{j-1})-E(\bar{u}_{j-1},\alpha_{j-1})}\right]. \\ \frac{dN_{j+1}}{ds_j} &= Nf(\alpha_j)\frac{d\alpha_j}{ds_j} \\ &= -N\left[\frac{f(\alpha_j)}{E(\bar{u}_{j+1},\alpha_j)-E(\bar{u}_j,\alpha_j)}\right].\end{aligned}$$

REFERENCES

[1] Alberola, E. and Chevallier, J., "European carbon prices and banking restrictions: Evidence from Phase I (2005-2007)," *The Energy Journal*, vol. 30, no. 3, pp. 51–79, 2009.

[2] Aldy, J. E., Krupnick, A. J., Newell, R. G., Parry, I. W., and Pizer, W. A., "Designing climate mitigation policy." RFF DP 08-16, 2009.

[3] Asmussen, S., Glynn, P., and Pitman, J., "Discretization error in simulation of one-dimensional reflecting brownian motion," *The Annals of Applied Probability*, pp. 875–896, 1995.

[4] Bansal, V., Pruitt, S., and Wei, K., "An empirical reexamination of the impact of cboe option initiation on the volatility and trading volume of the underlying equities: 1973-1986," *Financial Review*, vol. 24, pp. 19–29, 1989.

[5] Benhamou, E., "Fast Fourier transform for discrete Asian options," *Journal of Computational Finance*, vol. 6, no. 1, pp. 49–68, 2002.

[6] Bertrand, V., "Modeling of emission allowance markets: a literature review." Working Paper Series, Climate Economics Chair, 2013.

[7] Black, F., S. M., "The pricing of option and corporate liabilities," *Journal of Political Economy*, vol. 81, no. 637-659, 1973.

[8] Bolton, P. and Dewatripont, M., *Contract Theory*. MIT Press, 2005.

[9] Boyle, P., "Options: a Monte Carlo approach," *Journal of Financial Economics*, vol. 4, pp. 323–338, 1977.

[10] Boyle, P. P. and Tian, Y., "An explicit finite difference approach to the pricing of barrier options," *Applied Mathematical Finance*, vol. 5, no. 1, pp. 17–43, 1998.

[11] Broadie, M. and Yamamoto, Y., "A double-exponential fast gauss transform algorithm for pricing discrete path-dependent options," *Operations Research*, vol. 53, no. 5, pp. 764–779, 2005.

[12] Broadie, M. and Yamamoto, Y., "Application of the fast gauss transform to option pricing," *Management Science*, vol. 49, no. 8, pp. 1071–1088, 2003.

[13] Bushnell, J. B. and Chen, Y., "Regulation, allocation, and leakage in cap-and-trade markets for CO2," paper csemwp-183, Center for the Study of Energy Markets, 2009.

[14] Callaway, D. S., "Tapping the energy storage potential in electric loads to deliver load following and regulation, with application to wind energy," *Energy Conversion & Management*, vol. 50, no. 9, pp. 1389–1400, 2009.

[15] Cao, H., "The effect of derivative assets on information acquisition and price behavior in a dynamic rational expectations model," *Review of Financial Studies*, vol. 12, pp. 131–163, 1999.

[16] Carmona, R., Fehr, M., Hinz, J., and Porchet, A., "Market design for emission trading schemes," *SIAM Review*, vol. 52, no. 3, pp. 403–452, 2010.

[17] Carr, P., M. D., "Option valuation using the fast Fourier transform," *Journal of Computational Finance*, vol. 2, no. 4, pp. 61–73, 1999.

[18] Celebi, M. and Graves, F., "CO2 price volatility: Consequences and cures," tech. rep., The Brattle Group, 2009.

[19] Chao, H.-P. and Wilson, R., "Option value of emission allowances," *Journal of Regulatory Economics*, vol. 5, no. 3, pp. 233–249, 1993.

[20] Chao, H.-P. and Wilson, R., "Resource adequacy and market power mitigation via option contracts," tech. rep., Electric Power Research Institute and Stanford University, 2004.

[21] Chen, Y. and Tseng, C.-L., "Inducing clean technology in the electricity sector: Tradable permits or carbon tax policies?," *The Energy Journal*, vol. 32, no. 3, pp. 149–174, 2011.

[22] Chesney, M. and Taschini, L., "The endogenous price dynamics of the emission allowances: An application to co2 option pricing," research paper series n °08 – 02, Swiss Finance Institute, 2008.

[23] Chevallier, J., Pen, Y. L., and Sévi, B., "Options introduction and volatility in the eu ets," *Resource and Energy Economics*, vol. 33, pp. 855–880, 2011.

[24] Conrad, J., "The price effect of option introduction," *Journal of Finance*, vol. 44, pp. 487–498, 1989.

[25] Cont, R. and Tankov, P., *Financial Modelling with Jump Processes*. Chapman and Hall/CRC, 2004.

[26] Cont, R., "Empirical properties of asset returns: stylized facts and statistical issues," *Quantitative Finance*, vol. 1, no. 223–236, 2001.

[27] Cox, J. C., Ross, S. A., and Rubinstein, M., "Option pricing: A simplified approach," *Journal of Financial Economics*, vol. 7, pp. 229–263, 1979.

[28] Cronshaw, M. and Kruse, J., "Regulated firms in pollution permit markets with banking," *Journal of Regulatory Economics*, vol. 9, pp. 179–189, 1996.

[29] Dales, J., *Pollution property and prices*. University of Toronto Press, 1968.

[30] Damadoran, A. and Lim, J., "The effects of option listing on the underlying stocks' return processes," *Journal of Banking and Finance*, vol. 15, pp. 647–664, 1991.

[31] Darrell Duffie, J. P. and Singleton, K., "Transform analysis and asset pricing transform analysis and asset pricing for affine jump-diffusions," *Econometrica*, vol. 68, pp. 1343–1376, November 2000.

[32] Daskalakis, G., Psychoyios, D., and Markellos, R., "Modeling CO2 emission allowance prices and derivatives: Evidence from the european trading scheme," *Journal of Banking and Finance*, vol. 33, no. 7, pp. 1230–1241, 2009.

[33] Dempster, M. and Hong, S., "Spread option valuation and the fast fourier transform," technical report wp 26/2000, The Judge Institute of Management Studies, University of Cambridge, 2000.

[34] Deng, S.-J., "Stochastic models of energy commodity prices and their applications: Mean-reversion with jumps and spikes," tech. rep., University of California Energy Institute, PWP 073, 2000.

[35] Deng, S.-J. and Oren, S. S., "Electricity derivatives and risk management," *Energy*, vol. 31, no. 6, pp. 940–953, 2006.

[36] Deng, S.-J. and Xu, L., "Mean-risk efficient portfolio analysis of demand response and supply resources," *Energy*, vol. 34, pp. 1523–1529, 2009.

[37] Department of Energy, "Smart grid/department of energy," 6 2012.

[38] EIA, "Annual energy outlook 2012," tech. rep., U.S. Energy Information Administration, 2012.

[39] EIA, "Electric power annual 2011." U.S. Energy Information Administration, 2013.

[40] Eshel, D. M. D., "Optimal allocation of tradable pollution rights and market structures," *Journal of Regulatory Economics*, vol. 28, pp. 205–223, 2005.

[41] Fang F, O. C., "Pricing early-exercise and discrete barrier options by fourier-cosine series expansions," *Numerische Mathematik*, vol. 114, pp. 27–52, 2009.

[42] Fell, H., MacKenzie, I. A., and Pizer, W. A., "Prices versus quantities versus bankable quantities," tech. rep., Resources for the Future, 2008.

[43] Feng, L. and Linetsky, V., "Pricing discretely monitored barrier options and defaultable bonds in lévy process models: a fast hilbert transform approach," *Mathematical Finance*, vol. 18, no. 3, pp. 337–384, 2008.

[44] Fleming, J. and Ostdiek, B., "The impact of energy derivatives on the crude oil market," *Energy Economics*, vol. 21, pp. 135–167, 1999.

[45] for Commercialization of Electric Technologies, C., "Demand response pilot projects." Final report, 2009.

[46] Fox-Penner, P. and Bishop, H., "Mission, structure, and governance in future electric markets: Some observations," *Or. L. Rev.*, vol. 89, p. 1107, 2010.

[47] Grossman, S., "An analysis of the implications for stock and futures price volatility of program trading and dynamic trading strategies," *Journal of Business*, vol. 61, pp. 275–298, 1988.

[48] Grüll, G. and Taschini, L., "Cap-and-trade properties under different hybrid scheme designs," *Journal of Environmental Economics and Management*, vol. 61, pp. 107–118, 2011.

[49] Harrison, J. M. and Pliska, S. R., "Martingales and stochastic integrals in the theory of continuous trading," *Stochastic Processes and their Applications*, vol. 11, pp. 215–260, 1981.

[50] Heston, S., "A closed-form solution for options with stochastic volatility with applications to bond and currency options," *Review of Financial Studies*, vol. 6, pp. 327–343, 1993.

[51] Hintermann, B., "An option pricing approach for CO2 allowances in the EU ETS." Working Paper, University of Zurich, 2013.

[52] Hintermann, B., "Allowance price drivers in the first phase of the EU ETS," *Journal of Environmental Economics and Management*, vol. 59, pp. 43–56, 2010.

[53] Hitzemann, S. and Uhrig-Homburg, M., "Understanding the price dynamics of emission permits: A model for multiple trading periods." Working Paper, Karlsruhe Institute of Technology, 2010.

[54] Hurd, T.R., Z. Z., "A fourier transform method for spread option pricing," *SIAM Journal on Financial Mathematics*, vol. 1, pp. 142–157, 2010.

[55] Husen, S. A., Pandharipande, A., Tolhuizen, L., Wang, Y., and Zhao, M., "Lighting systems control for demand response," in *Innovative Smart Grid Technologies (ISGT), 2012 IEEE PES*, pp. 1–6, 2012.

[56] Ihara, S. and Schweppe, F., "Physically based modelling of cold load pickup," *IEEE Trans Power App Syst*, vol. 100, no. 9, pp. 4142 – 4150, 1981.

[57] Jackson, K.R., J. S. S. V., "Fourier space time-stepping for fourier space time-stepping for option pricing with levy models," *Journal of Computational Finance*, vol. 12, no. 2, pp. 1–29, 2008.

[58] Jacoby, H. D. and Ellerman, A. D., "The safety valve and climate policy," *Energy Policy*, vol. 32, no. 4, pp. 481–491, 2004.

[59] Kijima, M., Maeda, A., and Nishide, K., "Equilibrium pricing of contingent claims in tradable permit markets," *Journal of Futures Markets*, vol. 30, no. 6, pp. 559–589, 2010.

[60] Koch, S., Mathieu, J., and Callaway, D., "Modeling and control of aggregated heterogeneous thermostatically controlled loads for ancillary services," in *Proceedings of 17th Power Systems Computation Conference*, (Stockholm, Sweden), 2011.

[61] Kou, S. G. and Wang, H., "Option pricing under a double exponential jump diffusion model," *Management science*, vol. 50, no. 9, pp. 1178–1192, 2004.

[62] Kundu, S., Sinitsyn, N., Backhaus, S., and Hiskens, I., "Modeling and control of thermostatically controlled loads." arXiv:1101.2157v1, Jan 2011.

[63] Leconte, A. and Pagano, T., "Carbon derivatives: A destabilizing or a virtuous mechanism to build a carbon-free economy? The example of the European CO2 trading scheme." Working Paper, 2010.

[64] Longstaff, F. A. and Schwartz, E. S., "Valuing american options by simulation: A simple least-squares approach," *Review of Financial Studies*, vol. 14, no. 1, pp. 113–147, 2001.

[65] Lord, R., Fang, F., Bervoets, F., and Oosterlee, C., "A fast and accurate fft-based method for pricing early-exercise options under levy processes," *SIAM Journal on Scientific Computing*, vol. 30, pp. 1678–1705, 2008.

[66] Lovins, A., "Three major energy trends to watch." 103rd Annual Conference of the International District Energy Association (IDEA), Chicago, Illinois, July 1 2012.

[67] Lu, N., Chassin, D., and Widergren, S., "Modeling uncertainties in aggregated thermostatically controlled loads using a state queueing model," *IEEE Transactions on Power Systems*, vol. 20, no. 2, pp. 725–733, 2005.

[68] Maeda, A., "Impact of banking and forward contracts on tradable permit markets," *Environmental Economics and Policy Studies*, vol. 6, no. 2, pp. 81–102, 2004.

[69] Malhame, R. and Chong, C., "Electric-load model synthesis by diffusion approximation of a high-order hybrid-state stochastic system," *IEEE Trans Automat Contr,*, vol. 30, pp. 854–860, 1985.

[70] Mayer, K., Schmid, T., and Weber, F., "Modeling electricity spot prices: combining mean reversion, spikes, and stochastic volatility," *The European Journal of Finance*, no. ahead-of-print, pp. 1–24, 2012.

[71] Merton, R., "Theory of rational option pricing," *Bell Journal of Economics and Management Sciences*, vol. 4, pp. 141–183, 1973.

[72] Mirrlees, J. A., "An exploration in the theory of optimal income taxation," *Review of Economic Studies*, vol. 38, pp. 175–208, 1971.

[73] Montgomery, W., "Markets in licenses and efficient pollution control programs," *Journal of Economic Theory*, vol. 5, pp. 395–418, 1972.

[74] Mori, M., "Quadrature formulas obtained by variable transformation and the de-rule," *Journal of Computational and Applied Mathematics*, vol. 12, pp. 119–130, 1985.

[75] Napolitano, S., LaCount, M., and Chartier, D., "SO2 and NOx trading markets: Providing flexibility and results," *EM Magazine, Air & Waste Management Association*, pp. 22–26, 2007.

[76] Newell, R., "Managing permit markets to stabilize prices," *Environmental & Resource Economics*, vol. 31, pp. 133–157, 2005.

[77] Ooura, T. and Mori, M., "The double exponential formula for oscillatory functions over the half infinite interval," *Journal of Computational and Applied Mathematics*, vol. 38, no. 1, pp. 353–360, 1991.

[78] Papavasiliou, A. and Oren, S. S., "Large-scale integration of deferrable demand and renewable energy sources." submitted to IEEE Transactions on Power Systems Special section on Electricity Market Operations, 2011.

[79] Roll, R., Schwartz, E., and Subrahmanyam, A., "Options trading activity and firm valuation," *Journal of Financial Economics*, vol. 94, pp. 345–360, 2009.

[80] Rubin, J., "A model of intertemporal emission trading, banking, and borrowing," *Journal of Environmental Economics and Management*, vol. 31, pp. 269–286, 1996.

[81] Schennach, S., "The economics of pollution permit banking in the context of title IV of the 1990 Clean Air Act amendments," *Journal of Environmental Economics and Management*, vol. 40, pp. 189–210, 2000.

[82] Schoutens, W., *Lévy Processes in Finance: Pricing Financial Derivatives (Wiley Series in Probability and Statistics)*. Wiley, May 2003.

[83] Seifert, J., Uhrig-Homburg, M., and Wagner, M., "Dynamic behavior of CO2 spot prices," *Journal of Environmental Economics and Management*, vol. 56, pp. 180–194, 2008.

[84] Skinner, D., "Options markets and stock return volatility," *Journal of Financial Economics*, vol. 23, pp. 61–78, 1989.

[85] Spence, M., "Competitive and optimal responses to signals: An analysis of efficiency and distribution," *Journal of Economic Theory*, vol. 7, pp. 296–332, 1974.

[86] Stavins, R. N., "Addressing climate change with a comprehensive us cap-and-trade system," *Oxford Review of Economic Policy*, vol. 24, no. 2, pp. 298–321, 2008.

[87] Stein, J., "Informational externalities and welfare-reducing speculation," *Journal of Political Economy*, vol. 95, pp. 1123–1145, 1987.

[88] Takahasi, H. and Mori, M., "Double exponential formulas for numerical integration," *Publications of the Research Institute for Mathematical Sciences*, vol. 9, no. 3, pp. 721–741, 1973.

[89] Tietenberg, T., "Emission trading: An exercise in reforming pollution policy." Resources for the Future, 1985.

[90] Tietenberg, T. H., *Emissions Trading: Principles and Practice*. RFF Press, 2 ed., 2006.

[91] Ucak, C. and Dokuyucu, G., "Investigation of thermostat-set control as a new direct load control method." Department of Electrical Engineering, Electrical & Electronics Faculty, Istanbul Technical University, 2010.

[92] U.S. EPA, "EPA supplemental analysis of the american clean energy and security act of 2009 (H.R. 2454)." Data Annex, 2010.

[93] U.S. EPA, "Inventory of U.S. greenhouse gas emissions and sinks: 1990-2008." U.S. EPA # 430-R-10-006, 2010.

[94] Waldvogel, J., "Towards a general error theory of the trapezoidal rule," in *Approximation and computation*, pp. 267–282, Springer, 2011.

[95] Wilmott, P., Howison, S., and Dewynne, J., *The Mathematics of Financial Derivatives: A Student Introduction*. Cambridge University Press, September 1995.

[96] Xu, L., "Nonequispaced fourier transform for option pricing," Master's thesis, University of Calgary, 2008.